PREPARATION OF POLYPYRROLE-METAL SULFIDES NANOCOMPOSITES FOR GAS SENSING

Thesis Submitted for the Award of the Degree of

DOCTOR OF PHILOSOPHY

In

CHEMISTRY

By

Yuvika Sood

11919676

Supervised By

Dr. Anil Kumar (22056)

Assistant Professor

Department of Chemistry,

Lovely Professional University,

Jalandhar, (P.B), India

Co-Supervised by

Dr. Harish Mudila (19331)

Associate Professor

Department of Chemistry,

Lovely Professional University,

Jalandhar, (P.B), India

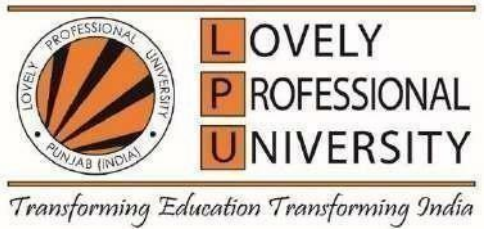

LOVELY PROFESSIONAL UNIVERSITY,PUNJAB

2025

DECLARATION

I, hereby declared that the presented work in the thesis entitled **"Preparation of Polypyrrole-Metal Sulfides Nanocomposites for Gas Sensing"** in fulfilment of degree of **Doctor of Philosophy (Ph. D.)** is outcome of research work carried out by me under the supervision of **Dr Anil Kumar and Dr. Harish Mudila**, Department of Chemistry of Lovely Professional University, Punjab, India. In keeping with general practice of reporting scientific observations, due acknowledgements have been made whenever work described here has been based on findings of other investigator. This work has not been submitted in part or full to any other University or Institute for the award of any degree.

(Signature of Research Scholar)
Yuvika Sood
Registration No: 11919676
Department of Chemistry,
School of Chemical Engineering
and Physical Sciences,
Lovely Professional University,
Punjab, India

CERTIFICATE

This is to certify that the work reported in the Ph. D. thesis entitled "**Preparation of Polypyrrole- Metal Sulfides Nanocomposites for Gas Sensing**" submitted in fulfillment of the requirement for the reward of degree of **Doctor of Philosophy (Ph.D.)** in the **Department of Chemistry** , is a research work carried out by **Yuvika Sood, 11919676**, is bonafide record of her original work carried out under my supervision and that no part of thesis has been submitted for any other degree, diploma or equivalent course.

Signature of Supervisor

Dr. Anil Kumar
Assistant Professor
Department of Chemistry,
School of Chemical Engineering,
and Physical Sciences,
Lovely Professional University,
Punjab, India

Signature of Co-Supervisor

Dr. Harish Mudila
Associate Professor
Department of Chemistry,
School of Chemical Engineering,
and Physical Sciences,
Lovely Professional University,
Punjab, India

ABSTRACT

As the global population surges and various industries flourish, the quest for innovation escalates daily. Similarly, polymers characterized by elongated, chain-like structures serve as highly effective insulators against heat and electricity. However, a novel process now enables these polymers to conduct heat more efficiently, unlike metals, which uniformly conduct heat in all directions. This unique property designates them as conducting polymers. Early investigations into conducting polymers (CPs) were sparked by the remarkable discovery that the conductivity of polyacetylene. However, due to the challenges in assembling and maintaining stability of polyacetylene, the demand for more conductive polymers surged, leading to the emergence of polyheterocycles as a family of highly stable conductive polymers. In 2000, the Nobel Prize in Chemistry honoured MacDiarmid, Heegar, and Shirakawa for their pioneering work on polyacetylene, recognizing its significance as a conducting polymer. Among various CPs, polypyrrole (PPy) is considered to be best due to their intrinsic properties like thermal, electrical and morphological properties which are further used in various applications like sensors, batteries and capacitors. The properties of PPy can be improved by adding various fillers like CNT, metal oxides and metal sulfides.

Recently, there has been a notable surge in attention towards hazardous gas sensors, both within industry and academia. This surge is attributed to their integral role in intelligent systems, particularly due to the pervasive presence of hazardous gases in the air we breathe, posing threats to human health. Researchers are increasingly focusing on the well-being of not just humans, but also animals and plants, underscoring the imperative to detect CO, C_2H_5OH, H_2, and NH_3 in our environment. These pollutants, originating from a variety of roots including natural phenomena, stationary sources, moving vehicles, and thermal power plants. To regulate the air quality of our environment, it is essential to continuously monitor the concentration of various gases or volatile organic compounds (VOCs). Hence, the critical necessity lies in detecting these detrimental gases or VOCs at minimal concentration levels, serving as the fundamental requirement for employing sensors in air quality maintenance.

The proposed research addresses the synthesis of PPy and Metal sulfides (MoS_2, SnS_2, WS_2) chalcogens as matrix and fillers, respectively by in-situ chemical oxidative polymerization route for good dispersion of fillers in the matrix of PPy at different wt % of fillers (1 wt%, 5 wt%, 10 wt%, 20 wt%, and 30 wt%). The key goal is to develop highly selective and response for different gases. To study about structural, morphological and electrical properties of PPy based nanocomposites various physiochemical techniques were done using SEM, TEM, XRD, FTIR and I-V measurements. Finally, sensing activity of PPy and its nanocomposites with metal sulfides were performed at room temperature to detect gases such as H_2, C_2H_5OH, CO, CO_2 and NH_3. The proposed research work achieved good sensing response at low weight percent with high sensitivity and stability.

ACKNOWLEDGEMENTS

I begin by expressing my heartfelt gratitude to the Almighty for bestowing his blessings upon my research endeavors, enabling the successful completion of this academic journey. Special appreciation is extended to my esteemed research supervisors**,** Dr. Anil Kumar and Dr. Harish Mudila, Department of Chemistry, Lovely Professional University, Punjab. His invaluable guidance, unwavering support, and patience played a pivotal role in the successful culmination of my Ph.D. research. I am deeply indebted to him for sharing his immense knowledge and vast experience, which greatly inspired my academic pursuits.

I extend my thanks to the Centre Instrumentation Facility of Lovely Professional University for helping in characterization of samples. I also express my gratitude to Dr. Kamlendra Awasthi from Department of Physics, MNIT Jaipur and Shiv Dutta Lawaniya for their consistent support in gas sensing of samples. I would like to extend thanks to Dr. D. P Singh from School of Physics and Materials Science, Thapar university Patiala for providing current-voltage measurement facility and Dr. Akash Katoch from Centre for Nanoscience and Nanotechnology, Panjab university Chandigarh for providing TEM characterization and pellet making facility. A special acknowledgment goes to the library and administrative staff at Lovely Professional University for their punctual and outstanding library services, which significantly contributed to the success of my research.

My love and gratitude to my parents and all family members for their prayers, caring and sacrifices for educating and preparing me for my future. I am very much thankful to my friend Mr. Shivan and my sisters Yoshita and Dr. Mrinali Sood for their love, understanding, prayers and continuing support to complete this research work. Without their tremendous understanding, sacrifices and encouragement in the past few years, it would have not been impossible to complete my research work.

Ms. Yuvika Sood

Research Scholar

TABLE OF CONTENTS

LIST OF FIGURES

LIST OF TABLES

LIST OF ABBREVATIONS

WHO	World Health Organization
NCDs	non-communicable diseases
VOCs	Volatile organic compound
ICPs	Intrinsically conducting polymers
PPy	Polypyrrole
PANI	Polyaniline
PTh	Polythiophene
$FeCl_3$	Ferric Chloride
APS	Ammonium Persulfate
CNT	Carbon Nanotubes
TMDs	Transition Metal Dichalcogenides
WS_2	Tungsten Disulfide
MoS_2	Molybdenum Disulfide
SnS_2	Tin Disulfide
RH	Relative Humidity
XRD	X-ray diffractometry
FT-IR	Fourier transform infrared spectroscopy
I-V	Current-Voltage measurements
TEM	Transmission electron microscopy
SEM	Scanning electron microscopy
IDEs	Interdigitated Electrodes
LOD	Limit of Detection

CHAPTER ONE

Introduction

This chapter provides a comprehensive overview of gas sensing, conducting polymers, and the research conducted within the scope of the Ph.D. thesis. It delves into the fundamentals of gas sensors, conducting polymers, as well as their composites and nanocomposites, elucidating their respective advantages. Notably, particular emphasis is placed on exploring the application of PPy and its nanocomposites in gas sensing. The chapter concludes with a concise presentation of the motivation behind the research and its objectives.

1.1 Overview of Gas Sensor

Balancing the escalating energy needs due to a growing population and sustaining economic growth poses a significant challenge for humanity. Achieving this without causing irreversible harm to the environment is crucial. The ongoing release of a multitude of chemical pollutants such as NH_3, CH_4, NOx, CO, SO_X and fluorocarbons from industrial activities, vehicle emissions, and domestic waste significantly exacerbates environmental challenges, including acid rain, climate change, indoor air pollution, and ozone depletion [1]. To mitigate environmental damage caused by air pollution, there is a requirement for monitoring systems capable of promptly detecting and identifying pollutants within specified standards [2].

Air pollution poses a significant environmental health challenge, profoundly impacting life on earth. An air pollutant is any substance in the air capable of causing harm to living beings and the environment. Various sources contribute to this issue, including solid particles, household stoves, smoke from tobacco, vehicles, industrial amenities, construction, and flames in forests or agriculture. These pollutants are categorized into two types: primary and secondary. Primary pollutants encompass toxic gases like NO_x and CO emitted directly from vehicle exhausts and SO_x released from industrial factories. In contrast, secondary pollutants are not emitted directly but form in the air through reactions or interactions among primary pollutants. Ground-level ozone, a significant concern, is an example of a secondary pollutant [3]. As per "WHO" pollution significantly exacerbates asthma and heightens the risk of respiratory infections, especially among children. Air pollution is additionally associated with increased rates of illness and death, contributing to conditions such as stroke, chronic respiratory diseases, and various forms of cancer. In 2019, " air pollution" was recognized as the greatest environmental threat to health, underscoring its status as the foremost global environmental health risk.

Moreover, the importance of indoor air quality is underscored, given the substantial time spent indoors in places such as homes, hospitals, and schools. Monitoring various hazardous gases (NH_3, CO_2, CO, Benzene, toluene, etc.) and volatile organic compounds (VOCs) with humidity is crucial. Prolonged exposure to these pollutants indoors can lead to respiratory infections, lung cancer, and heart diseases. Moreover, the importance of

indoor air quality is underscored, given the substantial time spent indoors in places such as homes, hospitals, and schools. Prolonged exposure to these pollutants indoors can lead to respiratory infections, lung cancer, and heart diseases. Consequently, detecting both indoor and outdoor air pollution is equally vital. For this, gas sensors play a crucial role in safeguarding safety and well-being across various industries and applications, providing invaluable advantages such as instant monitoring and timely identification of gas leaks or hazardous concentrations. The gas sensor stands out as the paramount and economical technology embraced by the scientific community for the sensitive, selective and rapid detection of volatile organic compounds, as well as toxic and combustible gases. Every day, the global demand for gas sensors is on the rise, driven by their essential role in health and environmental surveillance, industrial safety measures, and various other applications. Gas sensors empower us to observe and comprehend the unseen and rapid molecular dynamics in our surroundings, enabling proactive measures to anticipate, prepare, and mitigate unforeseen occurrences which includes air quality monitoring, industrial safety and detecting fires.

1.2 Basic Characteristics of gas sensor

Gas sensors are characterized by their response to gas molecules, quantified by transfer function, sensitivity, repeatability, linearity, speed of response, and their susceptibility to environmental effects. This response is often manifested as a change in resistance upon exposure to gas molecules on the sensor's surface. Some of these parameters which are relevant to present work are defined here:

- **Sensitivity**- In context of gas sensor, refers its ability to detect changes in gas concentration. It essentially quantifies how much the sensor's output signal varies in response to a change in gas level.

  R_a/R_g = reducing gases

  R_g/R_a = oxidizing gases

  Where R_a denotes resistance of gas sensors in the reference gas (usually the air) and R_g denotes resistance in the reference gas containing target gases.

- **Response time-** It is defined as the time it takes for the sensor's output to reach a certain percentage (usually 90%) of its final stable value when exposed to a specific gas concentration**.** In essence, a faster response time indicates a more reactive

sensor that can detect changes in gas concentration quickly. This is crucial for applications where rapid detection is vital, such as leak detection systems or safety alarms.

- **Selectivity-** In the realm of gas sensor, it refers to its ability to distinguish between the target gas it's designed for and other gases present in the surrounding environment**.** It is important due to several reasons:

  Accurate Measurements: If a sensor is not selective, its output signal will be a combination of the target gas and interfering gases. This can lead to inaccurate measurements of the target gas concentration.

  False Alarms: In safety applications like CO detectors, poor selectivity can trigger false alarms if the sensor responds to other common gases in the environment.

  Specificity: Many applications require the detection of a specific gas amidst a mixture. Good selectivity ensures the sensor focuses on the target gas of interest.

- **Long term stability-** It refers to its ability to maintain consistent and reliable performance over an extended period of time. This translates to the sensor's output signal remaining relatively unchanged when exposed to the same gas concentration under constant operating conditions.
- **Repeatability-** It refers to the consistency of a sensor's response when measuring the same gas concentration under identical conditions on multiple occasions. It essentially quantifies how closely the sensor's output signal matches itself across repeated measurements.

1.3 Conducting polymers as gas sensor

Researchers have recently made numerous efforts to enhance the features of gas sensors, including “sensitivity”, “repeatability”, fast “response-recovery time”, “selectivity”, and “stability”. CPs display electrical, electronic, magnetic, and optical characteristics resembling those of metals or semiconductors, they are frequently termed "synthetic metals." Researchers are increasingly drawn to the semiconductor behaviour of conducting polymers, acknowledging them as promising materials for gas sensor applications. The demand for innovation is increasing day by day due to rise in population and various industrial facilities. Similarly, polymers made of long, series-like molecules act as excellent

insulators for heat and electricity. But the new process allows the polymer to conduct heat more efficiently on the other side, unlike metals, which conduct equally well in all directions called conducting polymers. The initial research on CPs originated from the discovery that the conductivity of polyacetylene, typically a semiconductor at best, surged by a staggering 10 million-fold upon oxidation with iodine vapor. This phenomenon, termed "doping," proved essential for polymer conductivity as it facilitated the attainment of high conductivity levels. However, due to challenges in assembling polyacetylene and its instability in air, there emerged a need for more conductive polymer alternatives [4]. CPs possess an extended p-orbital system that facilitates electron mobility throughout the polymer structure, enabling electrons to traverse from one end to the other. Recent research classifies intrinsically conducting polymers (ICPs) as one of the interest growing research for synthetic polymeric material from the last century due to its excellent electrical, mechanical, thermal, morphological properties of metal and semiconducting materials [5,6]. The intrinsic conducting polymers (ICPs) are interesting material having π- conjugated system in the polymeric chains [7]. Well-studied conducting polymers like "Polypyrrole," "Polyaniline," "Poly(3,4-ethylenedioxythiophene)," "Polythiophene," along with their composites, have garnered significant attention as highly promising options for sensor applications. Among all the ICPs, Polypyrrole is found to be the best because of its excellent environmental monitoring [8], easy synthesize [9] process, reversible doping/dedoping character, and high electrical conductivity [10,11]. Due to these properties, it has many applications such as batteries [12], sensors [13], capacitors [14], electrodes [15,16] and thus there is growing interest in PPy composites due to their combination of desirable properties including electrical conductivity, thermal stability [17], and well-defined morphologies [18] as well as their ease of fabrication at low cost [19,20]. Experimentally synergy between individual components imparts nanocomposites enhanced characteristics, thus extending its scope of applications [21,22]. Next-generation sensors crafted from 2D/3D materials are promising a best future, potentially replacing traditional metal oxide sensors that require high operating temperatures (200-400°C). Moreover, certain commercial sensors exhibit diminished activity at room temperature. Consequently, the scientific community is delving into novel material categories, including carbon-based materials such as CNTs, graphene and metal sulfides, owing to their reduced resistance and operational temperature requirements. Furthermore, there's a growing demand for materials with lower power consumption, which carbon materials offer compared to semiconductor materials. Hence, the properties of PPy can be improved by incorporating various fillers

like carbon nanotubes (CNT), metal oxide nanoparticles, graphene, and metal sulfides [23]. 2D layered transition metal dichalcogenides (TMDs) have emerged as highly appealing materials for a diverse array of applications in gas sensors [24–26]. TMDs, denoted as MX_2 (where M represents a transition metal and X signifies a chalcogen), exhibit a layered structure wherein the metal atoms coordination can adopt either trigonal or octahedral configurations, resulting in hexagonal or rhombohedral structural symmetries [27,28]. These materials exhibit both a considerable specific surface area and covalently bonded layers united by weak van der Waals forces, resulting in significant interplanar distances. Consequently, the intercalation of small moieties between the layers becomes feasible, rendering such structures suitable for interactions with the environment. TMDs such as WS_2, MoS_2 and SnS_2 are popular choices for gas sensing applications due to their unique properties and advantages:

1. **Large Surface area:**
    - **2D Structure:** These materials exhibit a layered, 2D structure with a high surface-to-volume ratio. This large surface area allows for increased interaction with gas molecules, enhancing sensitivity and response time.
2. **Tunable bandgap:**
    - **Semiconducting Nature:** WS_2, MoS_2, and SnS_2 are semiconductors with tunable bandgaps. This means their electrical conductivity can be adjusted by varying the number of layers. This tunability enables selective detection detection of different gases.
3. **High Sensitivity and Selectivity:**
    - **Surface Reactions:** The large surface area and active sites on these materials facilitate strong interactions with gas molecules, leading to significant changes in electrical conductivity. This results in high sensitivity, allowing detection of even low concentration of gases.
    - **Selective Adsorption:** The unique electronic and chemical properties of these materials enable selective adsorption of specific gas molecules, improving selectivity and reducing interference from other gases.
4. **Stability and Durability:**
    - **Resistance to Degradation:** WS_2, MoS_2, and SnS_2 are relatively resistant to degradation by moisture and other environmental factors, ensuring reliable performance over time.

Based on the aforementioned context, the current research endeavors to fabricate nanocomposite materials based on PPy, aiming to enhance their electrical characteristics. For the selection of better oxidants, PPy has been synthesized by "chemical oxidative polymerization" method using oxidants ammonium persulfate and ferric chloride. These PPy were dried and designated as PPy/APS and PPy/$FeCl_3$ having globular morphology. Pyrrole as a matrix and $FeCl_3$ as an oxidant were selected for developing hybrid nanocomposite, as $FeCl_3$ has better electrical conductivity. Metal sulfides like WS_2, MoS_2 and SnS_2 were selected as a filler material with easily tunable electronic, physical and chemical properties which makes them attractive for gas sensing applications. "In-situ chemical oxidative polymerization" method was adopted to prepare nanocomposite with matrix pyrrole as formation of polymers occurs directly at the interface between the matrix and reinforcing material which results in better adhesion and homogeneity leading to improved properties and overall performance of the composite.

The composition and structure of the matrix, filler, and final nanocomposites were investigated using a range of techniques: X-ray diffractometry (XRD) for crystallographic analysis, Fourier transform infrared (FTIR) spectroscopy for chemical bonding information, current-voltage (I-V) measurements for electrical properties, transmission electron microscopy (TEM) for high-resolution imaging, and scanning electron microscopy (SEM) for morphology analysis. Meanwhile, the electrical properties were assessed utilizing an electrometer. PPy and its nanocomposites like WS_2, MoS_2 and SnS_2 showed different values of electrical conductivity. According to the findings thus far, gas sensing utilizing PPy-based composites such as WS_2, MoS_2, and SnS_2 has been investigated.

1.4 Various Objectives of the Research Work

Specific objectives of research topic are:

- To synthesize of PPy by Chemical oxidative Polymerization method.
- To prepare PPy and its composites with metal disulfides such as WS_2, MoS_2, SnS_2 etc.
- Characterization of PPy and its composites such as WS_2, MoS_2, SnS_2 using FE-SEM, HR-TEM, XRD, EDX, FTIR spectral techniques and I-V measurements.
- Structure-Properties-Sensing correlation of PPy based composites.
- To explore the sensing activity of PPy and its composites with metal sulfides (WS_2, MoS_2, SnS_2).

CHAPTER TWO

Literature Review

An extensive "literature review" is presented on various synthesis methods utilized for the production of conducting polymer PPy, including electrochemical polymerization, photo-induced polymerization, enzymatic polymerization, chemical polymerization, in- situ polymerization, and plasma polymerization in this chapter. Additionally, detailed discussions are provided on the production of conducting polymer composites/nanocomposites combining different fillers. Lastly, the chapter thoroughly explores the utilization of PPy-based nanocomposites to enhance sensing applications.

2.1 Method for synthesis of polypyrrole composites

Overview of all the proposed research methodology for the synthesis of polypyrrole composites is presented in this section.

2.1.1 Electrochemical polymerization

The small amount of monomer required makes this method for studying material growth on electrodes in real-time. It unlocks a powerful platform for analysis, allowing researchers to probe the process using both electrochemical and spectroscopic techniques directly on the electrode [29–31]. This technique enables the creation of electroactive/conductive films, with their properties finely tuned through adjustments to electrolysis conditions like electrode potential, current density, solvent choice, and electrolyte composition. [30,32]. The electrochemical method of synthesis is a simple method to produce conducting polymers as free-standing films and colloids due to its purity and high rate of accuracy [31,33]. **Figure 2.1** shows a general scheme for electrochemical polymerization [34]. The primary factor influencing the efficiency of these sensing materials is the type of dopant utilized. **Table 2.1** illustrates the extensive efforts focused on enhancing gas detection capabilities through the development of PPy films as the basis for gas sensors targeting a range of gases.

Table 2.1 Electrochemically synthesized polymers for gas sensing applications

Polymeric material	D- Dopant	Analyte	References
PPy	D: tetrafluoroborate (BF^{-4})	CO_2	[34]
PPy	12 different dopants with sulfonated anions'	C_6H_6, $C_6H_5CH_3$	[35]
PPy	D: perchlorate	NH_3	[36]
PPy	Perchlorate as dopant	NH_3	[37]
PPy	lithium perchlorate and toluenesulfonic acid as dopant	NH_3	[38]

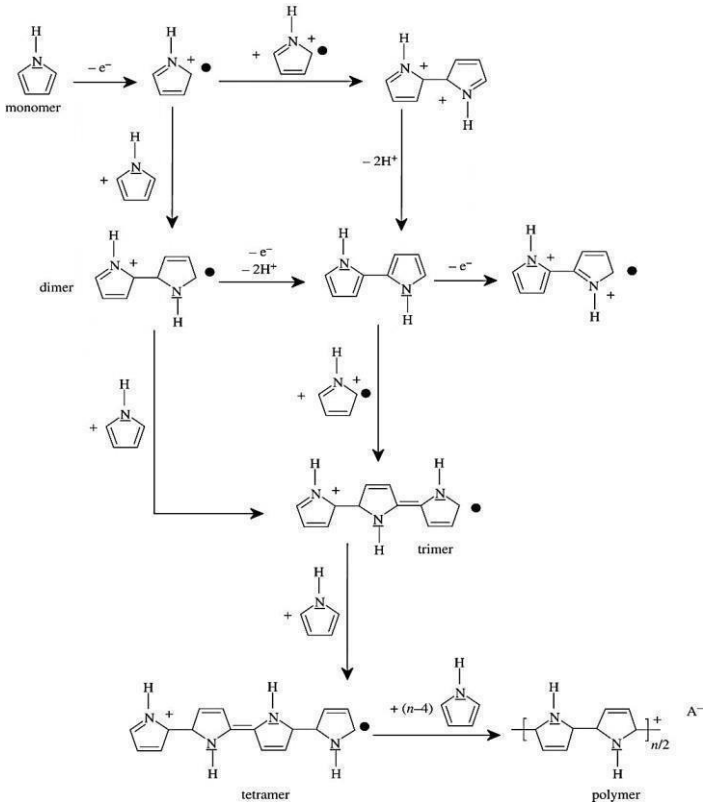

Figure 2.1 Electro polymerization mechanism of polypyrrole [34].

A study by Dunst *et al.* [39] investigated the use of electrochemically polymerized polypyrrole (PPy) films on gold electrodes for ammonia gas sensing. The PPy film exhibited an improved sensor performance, with the normalized resistance (R/R_0) increasing from 1.0 – 1.1 as the NH_3 conc. rise from 10 ppm - 200 ppm at RT. The long- term performance of the PPy sensor for detecting NH_3 gas was monitored over a period of 35 days. The researchers observed a gradual change in the sensor's response to ammonia over time, with the data following a linear trend. This suggests that the sensor's sensitivity to ammonia may slowly decrease over extended use. While PPy sensors suffer from a decrease in sensitivity (normalized response) over time due to aging effects this particular sensor exhibited remarkable stability for 35 days [40]. Despite a drop from a maximum normalized response of 39% to 20% for 100 ppm ammonia, this represents a significant achievement in long-term stability for PPy-based sensors. Patois and his co-workers [41] investigated using a high applied potential (2V vs. SCE) during electrochemical polymerization to enhance the ammonia sensitivity of PPy films. Their work highlights the importance of both the electrolyte solution and its salt concentration in influencing sensor sensitivity. Using a lithium perchlorate ($LiClO_4$) solution at a conc. of 0.1 M as the electrolyte led to a gas sensor with impressive features: it could detect ammonia at 3 ppm (low conc.) and responded quickly [42].

Research approach of Kwon *et al.* was to find the effect of particle size of PPy nanoparticles to detect volatile organic compounds (VOCs) and toxic gases on behaviors of chemical sensing with 20nm, 60nm and 100nm different diameter ranges produced at a rate of 11% changing range from 6 ppm - 200 ppm comparable to the others [43]. PPy nanoparticles of different diameters are chemically synthesized using the soft template method in an aqueous solution and found that the conductivity and volume ratio increase with a decrease in size of nanoparticles. Chemical sensors made from very small polypyrrole nanoparticles (20 nm), as seen in the FE-SEM images of **Figure 2.2**, exhibit excellent performance. These sensors offer high sensitivity, meaning they can detect tiny amounts of gas, along with good reversibility, allowing them to return to their original state after exposure, and a rapid response time.

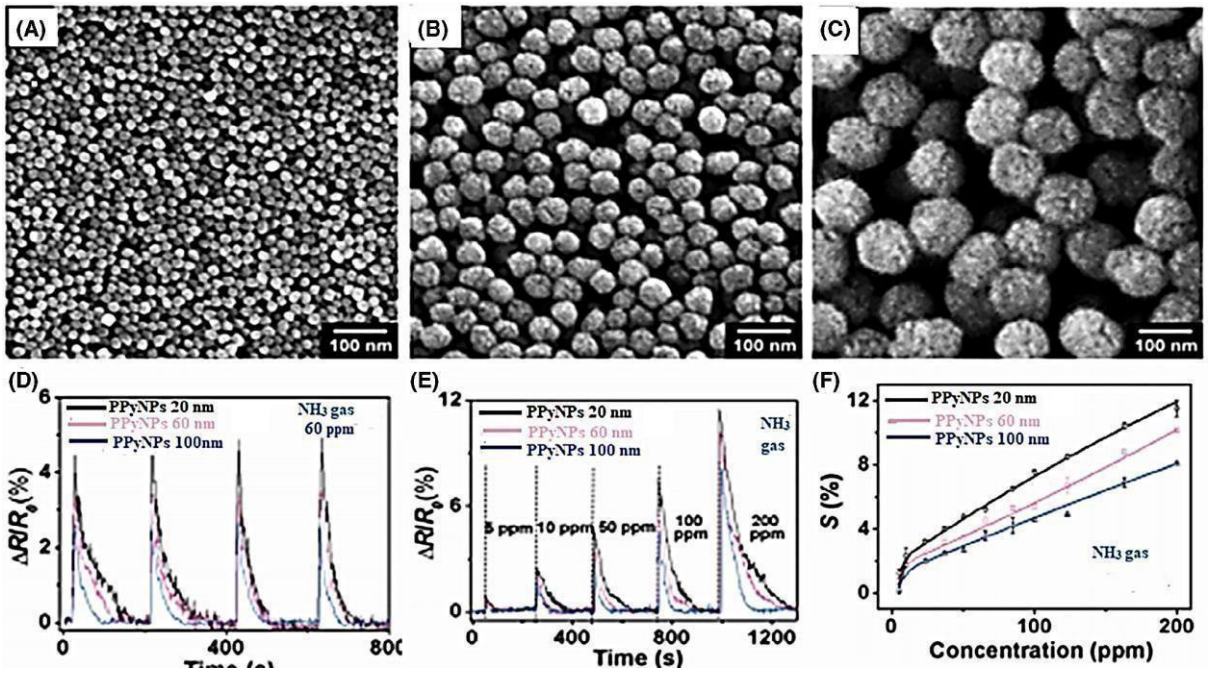

Figure 2.2 SEM micrographs of Polypyrrole NPs (a) 20 nm, (b) 60 nm, and (c) 100 nm PPy NPs. (d, e and f) present data on how the electrical resistance of these nanoparticles is affected by ammonia gas Part (d) focuses specifically on a 50 ppm ammonia concentration, while part (e) explores how resistance changes with different particle diameters (5 nm to 200 nm). Finally, part (f) investigates the relationship between increasing ammonia concentration and the sensor's sensitivity (S) [43]. Reproduced with permission from American Chemical Society

In 2007, Tai [46] team developed TiO_2/PPy nanocomposites ultrathin film showing highly sensitive as well as selective NH_3, CO, and NO_2 sensor. The sensor showed a high response

rate (~2.73%~7.95%) when there were different NH_3 concentrations ranges from 23-141 ppm with recovery time (~60 s) and average response (~17 s). The gas sensor of TiO_2/PPy thin film was defined on interdigited electrodes of gold on SiO_2-coated silicon wafer. The ultrathin TiO_2/PPy film sensor **(Figure 2.3a and 2.3b)** shows a positive response to ammonia (NH_3) with increasing sensitivity as the NH_3 concentration rises. However, the sensor also exhibits cross-sensitivity to carbon monoxide (CO), meaning it can respond to CO gas as well. **Figure 2.4a and 2.4b** illustrate how the sensor's sensitivity varies with different CO concentrations. The data indicates a clear distinction in sensitivity and response time for the sensor when exposed to 23 ppm of NH_3 and CO gas compared to air. Hence, sensors shows NH_3 with high sensitivity, and gases such as CO and NO_2 do not interact with the detection.

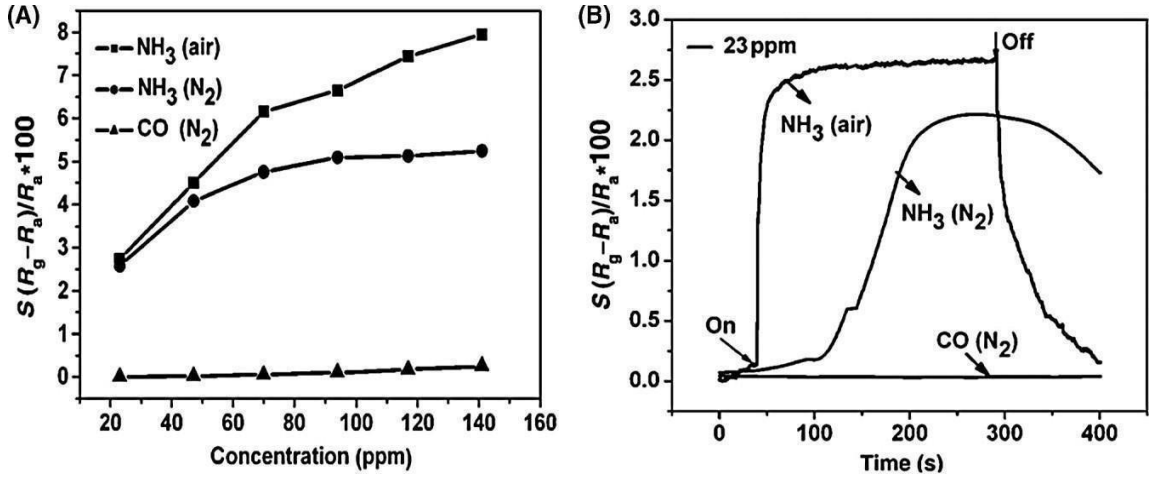

Figure 2.3 focus on (a) Sensitivity of ultrathin-film gas sensor with increasing NH_3 and CO concentrations. (b)Response-recovery of ultrathin-film gas sensor for 23 ppm NH_3 and CO [46]. Reproduced with permission from Taylor and Francis

This method stands out for its simplicity and directness. It allows for the deposition of intrinsically conducting polymers onto electrode surfaces without the requirement for a subsequent doping process [47]. While this method offers several advantages, several factors can influence the film's quality and yield. These factors include the type and concentration of the monomer and electrolyte solution, the solvent used, and the properties of the electrode itself. Certain modification is required on these factors to enhance the applications of electrochemical polymerization.

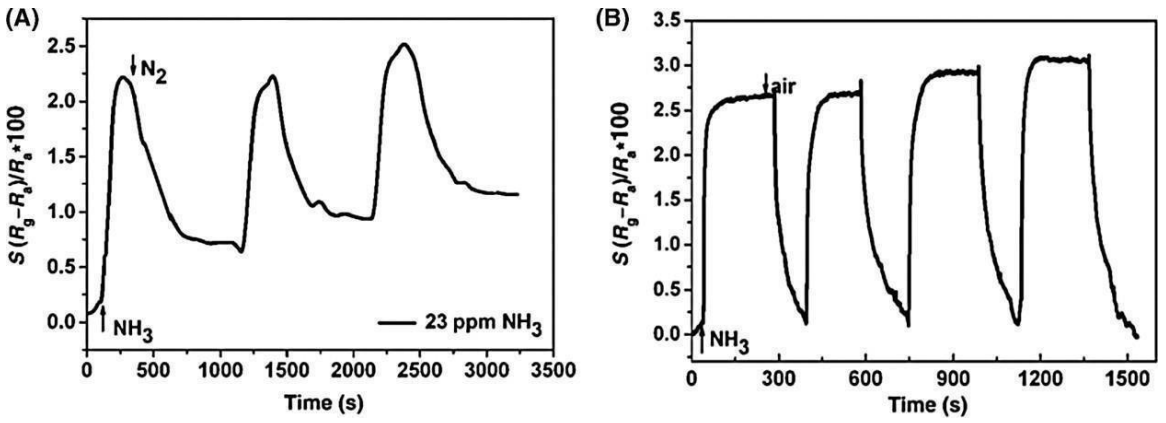

Figure 2.4 Reproducibility features of TiO_2 based polypyrrole ultrathin film gas sensor on addition or removal of 23 ppm NH_3 at N_2 (a) and air (b) [46]. Reproduced with permission from Taylor and Francis

2.1.2 Photo-induced polymerization

This method uses UV light or visible light to pass on cross-linked polymer structures at particular pH and room temperature as this method is free from radial photo polymerization due to the use of hydrogels. This class of materials is made from the manufacture of polymers and semiconductors of oxide metal which is sometimes known as hybrid material. This category of products provides superior properties as compared to their original form. Pyrrole undergoes photoinitiated polymerization, where light excites the pyrrole monomers, leading to their subsequent polymerization and formation of PPy.

Su *et al.* created a humidity sensor by combining titanium dioxide nanoparticles (TiO_2), polypyrrole (PPy), and a special polymer called poly-[(3-methacrylamino)propyl] trimethyl ammonium chloride (PMAPTAC) into a composite film on a polyester sheet [48]. In order to assess the humidity sensing capabilities and electrical properties of thin films made from TiO_2 nanoparticles and PPy, researchers first investigated these films using FTIR spectroscopy. To enhance the film's flexibility, they then introduced a polymer electrolyte called PMAPTAC, which permeated the TiO_2NPs/PPy films. The modified films were subsequently characterized again using FTIR spectroscopy. **Figure 2.5a** focuses on the humidity sensing properties of TiO_2 nanoparticles/polypyrrole (TiO_2 NPs/PPy) films. It presents an Arrhenius plot, which is a graph of resistance data plotted against the inverse of temperature (1/T). This plot is used to determine the activation energy of the sensor. The data shows that for sensors on both PET and alumina substrates, the activation energy for humidity sensing at 30% relative humidity (RH) is different. The activation energy is 0.32

eV for the sensor on the PET substrate and 0.56 eV for the sensor on the alumina substrate**.** Thus the difference in activation energy leads to ion migration and diffusion. To optimize the flexibility of the composite film for humidity sensing, researchers investigated the effect of different concentrations of TiO_2 nanoparticles. They focused on finding the concentration that offered the best balance between sensitivity (ability to detect changes in humidity) and linearity (how consistently the sensor's response reflects humidity changes) within a relevant humidity range (30-90% RH)**. Figure 2.5b** included image shows the flexible sensor bending, demonstrating its capability. **Figure 2.5c** represents changes in electrical response and measurements at 25 ℃ and ac voltage of 1V which increases sensitivity and linearity on adding MAPTAC. The sensor on TiO_2 nanocomposite films shows "better flexibility", "linearity", "faster response" (30s) and "short recovery time".

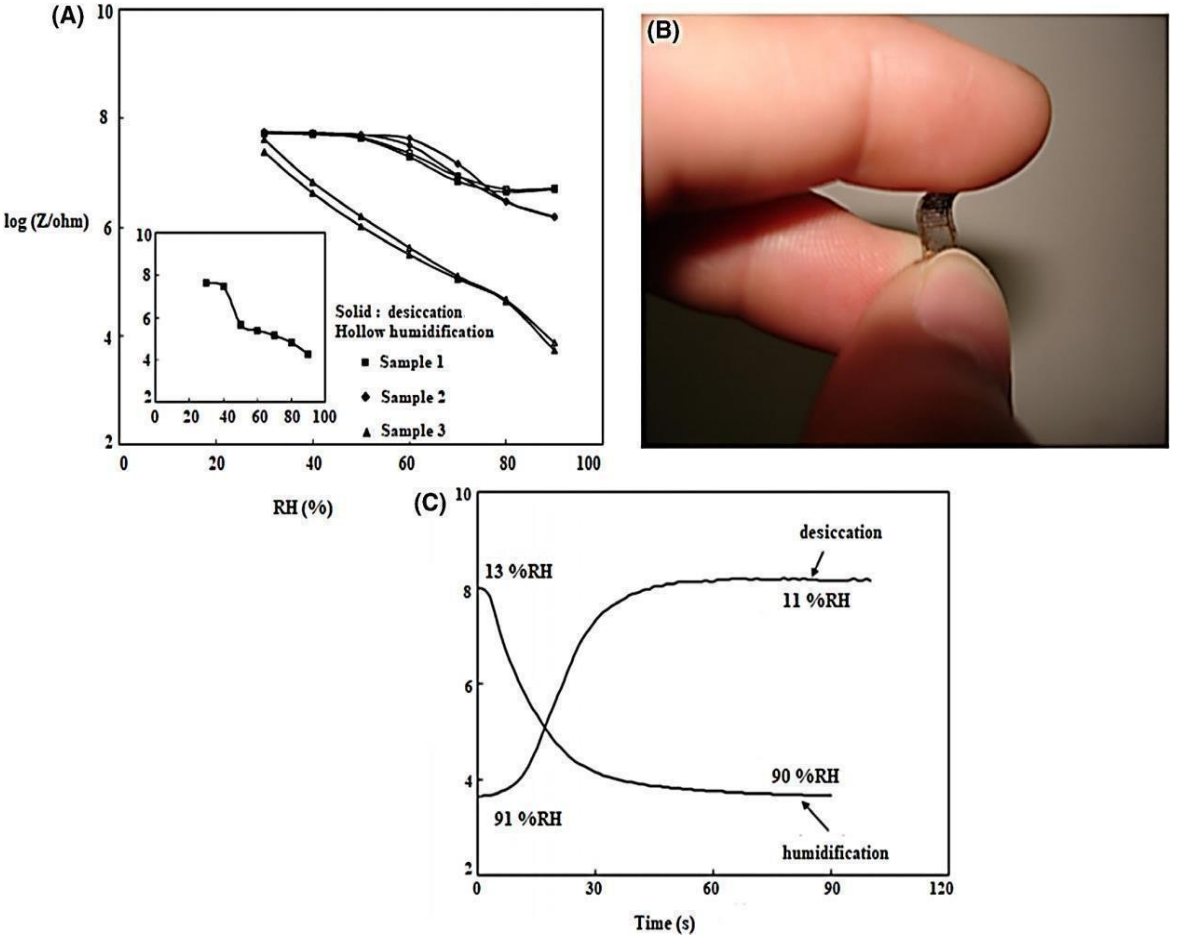

Figure 2.5 (a) Impedance as well as relative humidity for samples at 1V. (b) Image of flexible sensor on TiO_2 nanocomposites on bending (c) Response as well as recovery time of sample at 1V (d) Impedance as well as relative humidity for sample sensor at different temp. at 1 V [48]. Reproduced with permission from Elsevier

Singh *et al.* [49] created PPy-silver nanocomposite films with a core-shell structure. They achieved this by photo-initiating the polymerization of pyrrole monomers on a specially treated BOPET substrate using silver nitrate ($AgNO_3$). This process generates pyrrole radicals and metallic silver nanoparticles [50]. The pyrrole radicals then undergo chain growth and dimerization, forming the polypyrrole (PPy) shell around the silver core.

The researchers prepared films using a constant concentration of pyrrole (0.5 M) and varied the amount of silver nitrate ($AgNO_3$) from 0.05 M to 0.7 M. They also experimented with different ultraviolet (UV) exposure times, ranging from 15 to 180 minutes. Interestingly, they observed a change in the film's structure (morphology) as these conditions changed. Initially, the films exhibited a layered or plate-like structure (two-dimensional lamellar). However, with increasing $AgNO_3$ concentration or longer UV exposure, the structure transitioned to a more granular form**.** SEM images of PPy-silver nanocomposite films prepared with a fixed UV exposure time of 120 minutes but varying $AgNO_3$ concentrations (0.05 M to 0.7 M). These images allow for the observation of how the film morphology changes with increasing $AgNO_3$ concentration. The obtained films are small and show a small amount of PPy grains in the lowest range of concentration 0.5. On increasing the $AgNO_3$ solution to 0.1M, the film becomes larger in 2-D lamellar structures**.** As the concentration of the solution continuously increases up to 0.5 M, plate-like crystals gradually cover the entire BOPET surface. This clearly shows the growth of polypyrrole directed by Py salts in the plane of the substrate. When identical conditions were used (pyrrole and silver nitrate concentrations both at 0.5 M, and UV exposure time of 120 minutes) on a BOPET substrate, a granular film was formed. In this film, the layer of PPy is believed to be responsible for the sensor's response to various gases. The researchers tested the sensor's ability to detect different gases at a concentration of 20 ppm, including ammonia (NH_3), hydrogen sulfide (H_2S), chlorine (Cl_2), nitric oxide (NO), nitrogen dioxide (NO_2), carbon monoxide (CO), and methane (CH_4). Across all the samples investigated, the PPy-Ag films containing approximately 0.1M silver exhibited a chemiresistive response to NH_3 and H_2S gases. The response curve for NH_3 and H_2S (30 ppm exposure) shows response and recovery time of NH_3 as 8 sec and 130 min but H_2S shows an increase in conductance and compares response times for NH_3 and H_2S gas.

This study compares the performance of the developed PPy-Ag nanocomposite film sensor with previously reported PPy-based sensors and their nanocomposites for gas sensing applications. **Table 2.2** summarizes the results of this comparison across different materials. The PPy-Ag nanocomposite film sensor stands out with several advantages: Lowest detection limit: It can detect ammonia gas at concentrations as low as 5 ppm. Good sensitivity: The sensor's electrical response effectively reflects changes in gas concentration. Very fast response time: The sensor reacts to gas exposure within approximately 6 seconds (at 20 ppm ammonia). However, there's also a drawback to consider: High recovery time: The sensor takes a relatively long time (around 80 minutes at 20 ppm ammonia) to return to its baseline state after exposure. The high recovery time is possibly linked to the porous morphology. This porous structure allows gas molecules to penetrate deeply into the film, potentially slowing down the process of releasing the gas molecules once exposure stops. An additional benefit of the PPy-Ag sensor is that even with a minimal amount of silver (0.1 M), it exhibits reversible changes in conductivity upon exposure to ammonia at ppm levels.

Table 2.2 Gas sensing performance of the PPy-Ag film sensor relative to previously reported PPy-based sensors and their nanocomposite counterparts .

Used Material	**Active - layer**	**Synthesis Method**	**Limit of detection**	**Response at 20 ppm**	**Response time**	**Ref**
Glass	Polypyrrole	Chemical oxidative polymerization	5ppm	8%	15 second	[16]
Silicon	Polypyrrole	Electrodeposited polymerization	10ppm	8%	150 second	[41]
Ceramic	Polypyrrole based Pd composites	Vapor- phase polymerization	50ppm	13%	14 second	[51]
Resin	Polypyrrole based Ag composites	Chemical oxidative polymerization with drop casting	10ppm	38%	20 second	[52]
Pellet	$ZnSnO_3$/ PPy	Chemical oxidative polymerization	50ppm	40% at 50 ppm	20 second	[53]
Glass	Carbon/ PPy	Vapor deposition as well as chemical oxidative polymerization	10ppm	150%	10 second	[54]

In 2020, Jlassi et al. created a new type of material for gas sensors. This material combines PPy (a conductive polymer) with tiny clay tubes (halloysite) and silver nanoparticles. They made this composite using a technique called in-situ photopolymerization, where light triggers the formation of the polypyrrole in the presence of halloysite and silver nitrate, which initiates the reaction [55]. The researchers tested different amounts of PPy/Ag composite material (0.25%, 0.5%, and 1% by weight) mixed with HNT-DMA. These mixtures were then applied as a thin layer onto special finger-like electrodes made of Indium Tin Oxide (ITO) using a spin coating technique. They found that adding silver nanoparticles to the PPy material stiffens the sensor film. This stiffer film translates to better sensitivity for detecting humidity changes. Interestingly, the mixture with 0.5% PPy/Ag by weight showed the best sensitivity compared to the other concentrations. However, there is a challenge to address. At high humidity levels (80% relative humidity or RH), the sensor exhibits a hysteresis loss. This means the sensor's response might not perfectly match when increasing and decreasing humidity levels. Nanocomposite recovery and response time were found to be the 30s and 35s. Comparative analysis of this method is explained in **Table 2.3.**

Table 2.3 Contrast of the gas sensing features of Halloysite/PPy/Ag with previous work related to PPy based nanocomposites [93].

Material	**Method**	**Gas Sensing range**	**Response vs Recovery time**	**Ref.**
Polypyrrole-cellulose nanocomposites TiO_2	Chemical polymerization at RT	30-80% RH	~418 second	[56]
TiO_2 based "NPs/PPy/PMAPTAC"	Photo polymerization Time of 20 min (UV light)	11-90%RH	~45second	[48]
TiO_2/PPy nanocomposites	In-situ polymerization Time of 20min deposition	5-92%RH	~66 second	[57]

2.1.3 Enzymatic polymerization

During the last decade, pie conjugated polymers have attracted scientists because of the electrical conductivity as well as uv-visible characteristics of these compounds [58]. Enzymatic polymerization synthesis is considered as the best extent and accurate polymer synthesis [59]. In this way, the product is obtained under mild conditions without the use of toxic reagents. Glucose oxidase (GoX) is considered to be the most interesting enzyme because of its cheapness, strong natural analysis, and active sugar in the field of research. Some conductive polymers, like polypyrrole (PPy), polyaniline (PANI), and polythiophene (PTh), are useful in creating biosensor devices [60,61]. These devices often combine the conductive plastic with an enzyme called glucose oxidase (GOx).The effectiveness of PANI/GOx and PPy/GOx sensors depends on how long it takes to form the plastic using a technique called dynamic light scattering (DLS).

Enzymatic polymerization offers an alternative route for PPy synthesis. It operates under mild oxidation conditions and utilizes neutral pH solutions. This approach yields PPy with stable electrical conductivity. [62,63]. PPy can be made in various ways using water-based solutions. This versatile material is then used to create biosensors that can detect biological molecules like enzymes, antibodies, and even DNA [64,65]. Biological molecules such as uricase [66] are widely used in the synthesis of polymers [67].

Nabid *et al.* created a water-soluble conductive polymer called PPy. To achieve this, they used an enzyme called horseradish peroxidase and a special molecule (sulfonated polystyrene) that acts like a template [68]. This process occurs under environmentally mild conditions. PPy limits processability, characterization and applications due to lack of solubility. To overcome these challenges, various strategies have been employed to enhance the solubility of PPy, thereby improving its characteristics . A common approach involves the chemical synthesis of pyrrole monomers using ammonium persulfate as an oxidant and dodecyl benzene as a dopant. Conducting and electroactive form of PPy was confirmed by morphological pattern. The polymerization process yields a product that necessitates minimal post-processing steps for isolation and purification. The solubility of polymer makes it ideal for assembling them into organized structures with biological macromolecules such as process enzymes. Won *et al*. [69] indicated that a redox meditator would be used to achieve the polymerization of monomer that acts as poor enzyme substrate. They used HRP as an enzyme and various phenothiazine derivations as redox mediators to

polymerize cardanol.

Bouldin *et al*. [70] prepared a single polypyrrole composite with similar electrical properties at a high pH used for chemical procedure. This method uses a natural enzyme called soybean peroxidase to create a water-based polymer at room temperature. This polymer conducts electricity very well (over 0.1 siemens per centimetre) and doesn't need additional chemicals to function. The pyrrole monomer reaction was modified with other dopants other than PSS such as CSA and PVP. Response temperature control is designed for high-performance PPy under conditions with good yields.

2.1.4 Chemical oxidative polymerization

For large-scale production of conducting polymers, the chemical oxidative polymerization method stands out for its simplicity and effectiveness [71, 72]. In this case, PPy was prepared using chemical oxidative pyrrole monomer [73,74]. Due to the variety of applications of chemical-prepared polypyrrole, structures such as processability, thermal stability, and behavior require improved application continuity. In general, redox reactions between PPy and ammonia are considered to be in response to ammonia sensing from multiple sources. The equation representing the redox reaction between PPy and ammonia can be expressed as:

$$PPy^{+} + NH_3 \longrightarrow PP\mathring{y} + NH_3^{+} \quad \text{(Adsorption)} \ \mathbf{(2.1)}$$

$$PP\mathring{y} + NH_3^{+} \longrightarrow PPy^{+} + NH_3 \quad \text{(Desorption)} \ \mathbf{(2.2)}$$

When PPy is exposed to certain gases, like iodine (I_2) and nitrogen dioxide (NO_2), it loses electrons from its rings. In the case of ammonia, however, the interaction reduces the number of positive charges (holes) in the PPy, making it more sensitive. Therefore; in this type of polymerization, many researchers reported the synthesis of PPy using different oxidants. Iron (III) chloride ($FeCl_3$) has been employed as an oxidant for the synthesis of PPy films, facilitating the study of their ammonia gas sensing capabilities.

Chitte *et al*. [73] synthesized PPy purely and uses dopants like $LiClO_4$, p-TS, and NSA.. The response of these materials is explained by the exposure of ammonia and LPG and the DC electrical conductivity is measured by four probe method. The electrical current versus voltage (I-V) curve showed an increase in conductivity when dopants were added. Using ferric chloride ($FeCl_3$) as an oxidant during synthesis, the conductivity of the material improved from 0.001 to 0.01 S/cm. The electrical conductivity exhibits a gradual decrease

across all samples within the temperature range of 300 to 700 C. The added molecules (dopants) help the material conduct electricity by creating special charged particles inside it . **Figure 2.6** represents a plot for current vs time and samples are read in 3 cycles. The way the material releases the iodine (I) over time (shown in the graph) is clearly different between the first cycle and the second and third cycles. This suggests that some of the iodine wasn't completely removed during the second and third cycles. It is noted that a current decrease is observed when ammonia gas is exposed using p-TS and NSA as dopant and electrical conductivity of PPy decreases. The same samples were further used to detect LPG gas and when LPG gas was added, decrease in electrical conductivity takes place as shown in **Figure 2.7**. The sensor responded to ammonia gas very quickly, within a few seconds. In contrast, it took several minutes to detect LPG gas. This suggests that PPy- based materials are well-suited for ammonia detection, but less effective for LPG. The gas sensing response of the proposed route is illustrated in **Figure 2.7**.

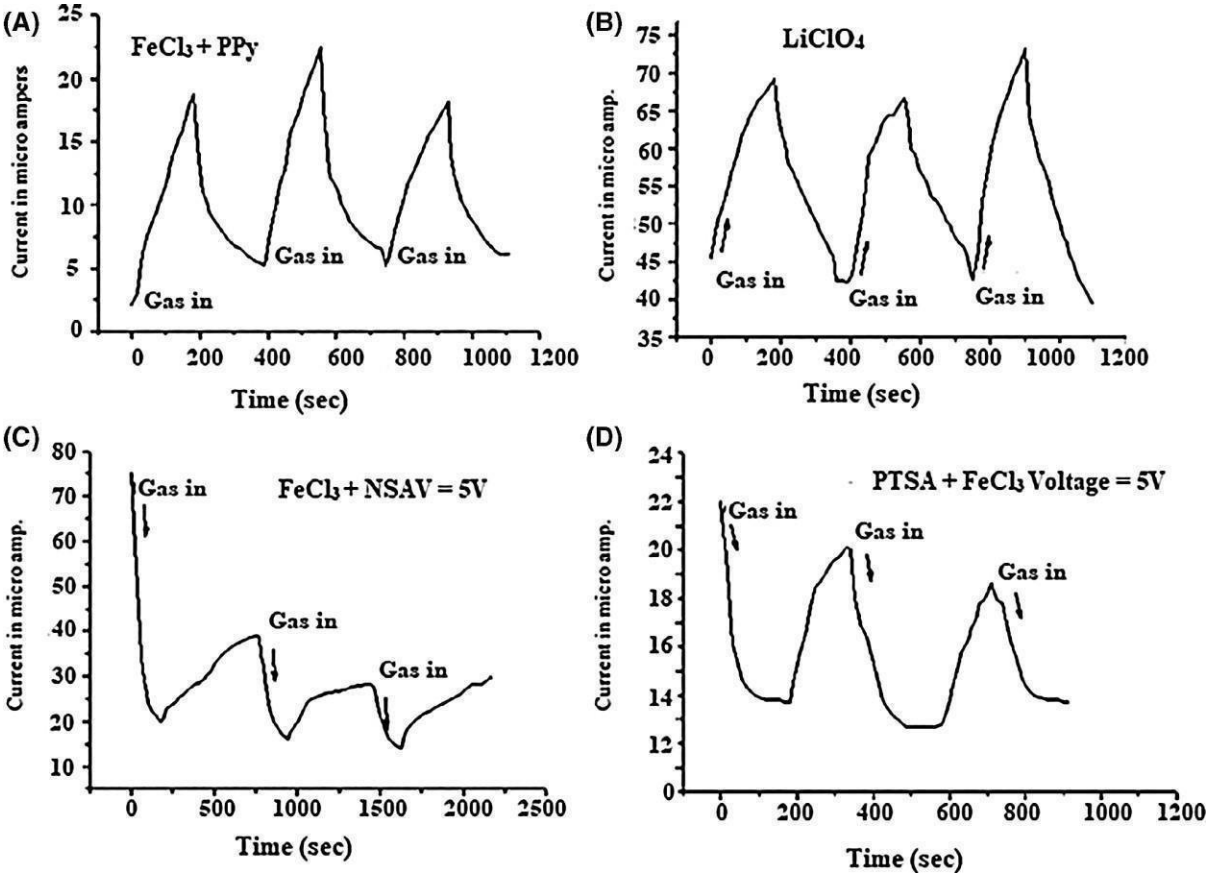

Figure 2.6 Gas sensing sensitivity for NH_3 gas using $FeCl_3$ (a) $FeCl_3$+ $LiClO_4$ (b) $FeCl_3$+ NSA (c) $FeCl_3$+ p-TS (d) [73]. Reproduced with permission from Scientific Research

Studies by Chitte *et al.* [73] and Khadem *et al.* [22] support the observed increase in conductivity with ferric chloride ($FeCl_3$) as an oxidant. They attribute this enhancement to

structural differences between oxidizing agents and the pyrrole monomer during synthesis. Furthermore, **Figure 2.8** shows that the $FeCl_3$ containing sample exhibits a fibrillar morphology, whereas the sample with ammonium persulfate has a spherical morphology **(Figure 2.9).** As reported by Khadem *et al*., fibrillar structures promote better electron transport within the polymer chain, leading to higher conductivity. This aligns with our findings of the $FeCl_3$ sample demonstrating both superior conductivity and thermal stability.

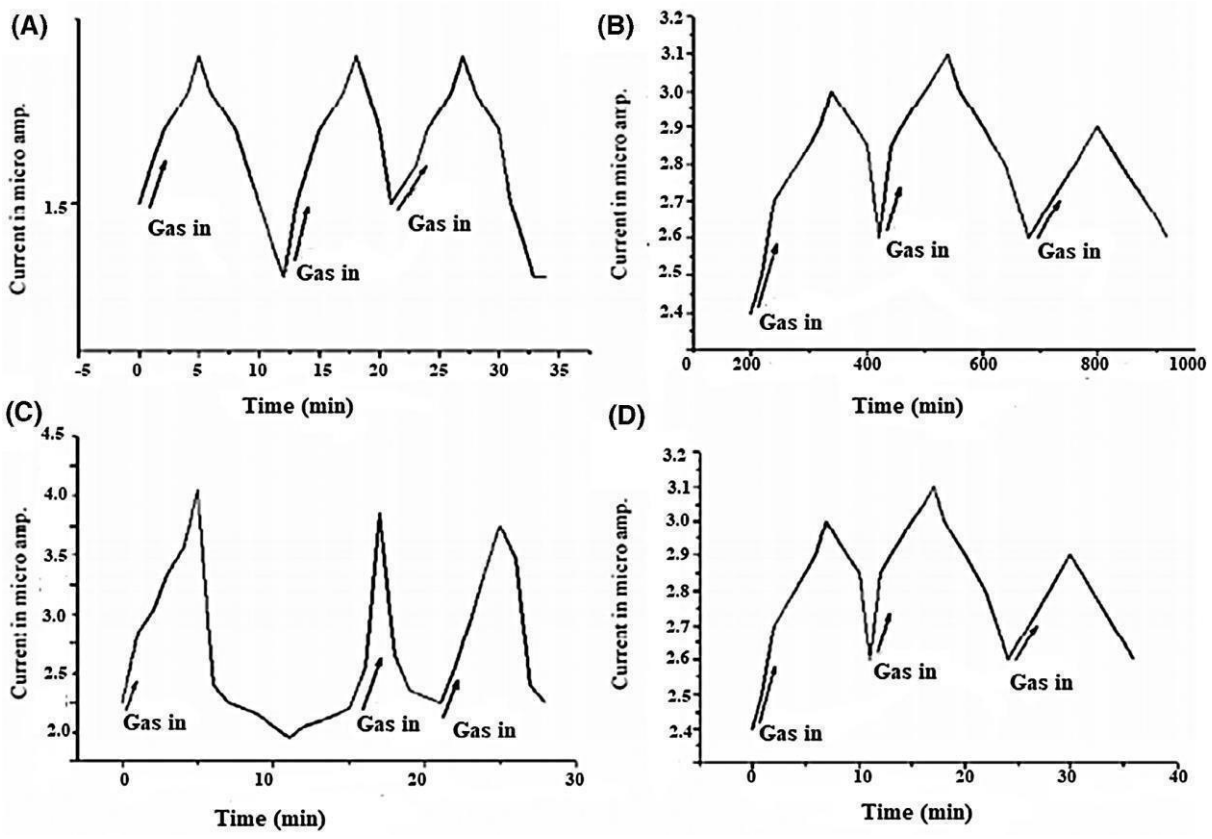

Figure 2.7 Gas sensing sensitivity for LPG - PPy+ $FeCl_3$ (a) PPy+ $LiClO_4$ (b) PPy+ p-TS (c) PPy+ NSA (d) [73]. Reproduced with permission from Scientific Research

Following a similar approach, Waghuley *et al.* [77] employed ferric chloride ($FeCl_3$) as an oxidant for chemically synthesizing PPy. Their process resulted in two PPy samples in the form of a black, odorless powder. These samples were prepared with different weight ratios of PPy to $FeCl_3$: a low ratio of 0.429 and a high ratio of 4.29. To establish electrical connections, silver paint electrodes were printed on opposing sides of the sensor film. PPy-I and PPy-II sensors were used to test CO_2 gas sensing exploration using screen-printed techniques**.** Microscopic images (SEM) revealed differences in the structure of the PPy samples depending on the ratio of PPy to $FeCl_3$ used during synthesis. The sample with a

lower ratio (0.429) showed a uniform, porous texture with a variety of void sizes ranging from about 500 nm to 2 mm. In contrast, the sample with a higher ratio (4.29) had unevenly shaped voids, including larger and flatter areas, with sizes varying from about 20 nm to a much larger 200 mm. This suggests that the ratio of PPy to $FeCl_3$ during chemical polymerization, along with the chosen preparation method (which might be influenced by solvent polarity), plays a role in shaping the final structure of the material. These structural differences can potentially affect the material's performance in sensing applications [78].

Both PPy-I and PPy-II sensors showed increasing resistance as the CO_2 gas concentration went up. However, the PPy-I sensor reached a saturation point (stopped responding effectively) at a concentration of 800ppm, while PPy-II could handle higher concentrations, reaching saturation at 950 ppm.

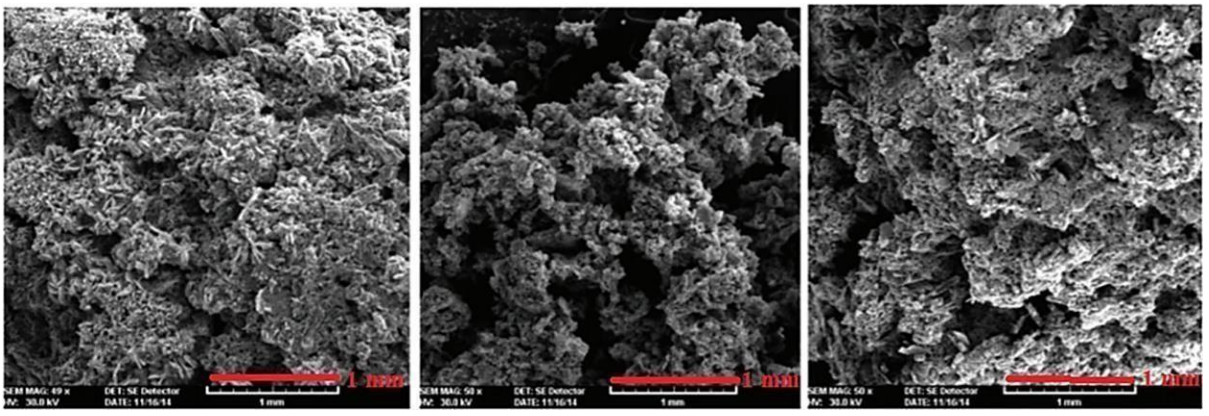

Figure 2.8 Images of PPy samples, $FeCl_3$ as an oxidizing agent (oxidant 0.1M, pyrrole 0.05M and surfactant 0.025 at 25^0C and duration of 4h) [22]. Reproduced with permission from Hindawi

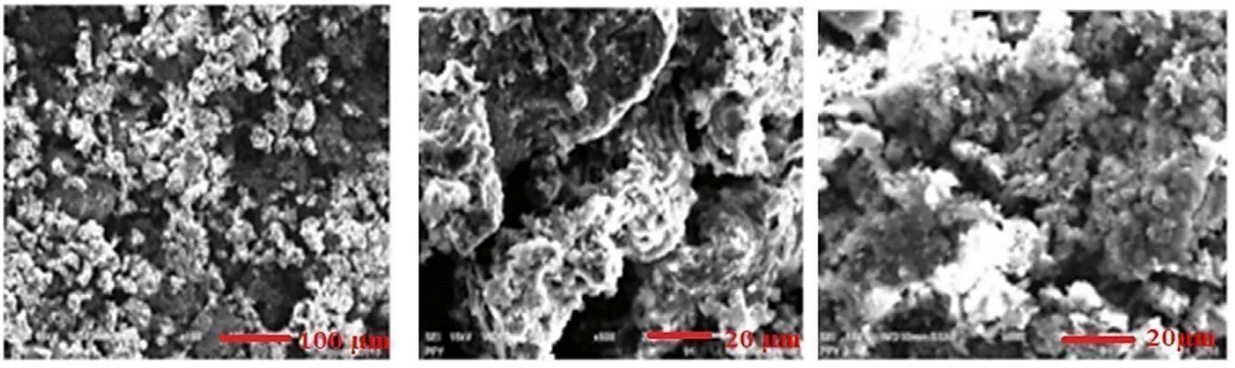

Figure 2.9 Images of PPy samples, APS as an oxidizing agent (oxidant 0.1M, pyrrole 0.05M and surfactant 0.025 at 25^0C and duration of 4h) [22]. Reproduced with permission from Hindawi

Interestingly, within this range (up to saturation), the response of both sensors increased

proportionally to the CO_2 concentration for 15 minutes at room temperature**.** In **Figure 2.10a**, the response rates of both sensors exhibit a linear correlation with the concentration of CO_2 gas over a 15-minute period. In **Figure 2.10b**, the dynamic responses of PPy-I and PPy-II sensors to CO_2 concentrations of 100, 400, and 700 ppm at ambient temperature are depicted. Notably, the response time for PPy-I at 300 ppm is approximately 270 s, while for PPy-II, it is around 210 s. Upon exposure to air, the recovery time for PPy-I and PPy- II is approximately 1760 s and 1560 s, respectively. This indicates that PPy-II sensor also demonstrates shorter response and recovery times under room temperature conditions. Furthermore, both sensors exhibit a notable change in resistance when the temperature is raised from 303 K to 343 K, resulting in a decrease in their response, as illustrated in **Figure 2.11**. At room temperature, the average CO_2 sensor readings for PPy-I measure 139.3×10^6 Ω/ppm, while for PPy-II, it registers at 129.9×10^6 Ω/ppm. Conversely, at 343 K, these values notably decrease to 9.2×10^6 Ω/ppm for PPy-I and 4×10^6 Ω/ppm for PPy-II, as evidenced by SEM images. This result suggests a more significant response to CO_2 in PPy-II, attributed to the smaller kinetic diameter of the CO_2 molecule.

Malook *et al*. [79] investigated a material for detecting ammonia gas at room temperature. They created a composite by combining PPy, a conductive polymer, with two metal oxides (V_2O_5 and MnO_2) using $FeCl_3$ as an oxidant. They tested different blends of these materials and found that a specific mix (PPy with 4% V_2O_5 and 5% MnO_2, labeled S3) performed best in terms of sensitivity and selectivity towards ammonia gas. This material also showed a good response time (around 75 seconds to detect the gas and 76 seconds to recover) and functioned well within a certain range of ammonia gas concentrations (5 ppm to 60 ppm). Overall, the findings suggest that this specific PPy-based composite (S3) is a promising candidate for ammonia detection at room temperature.

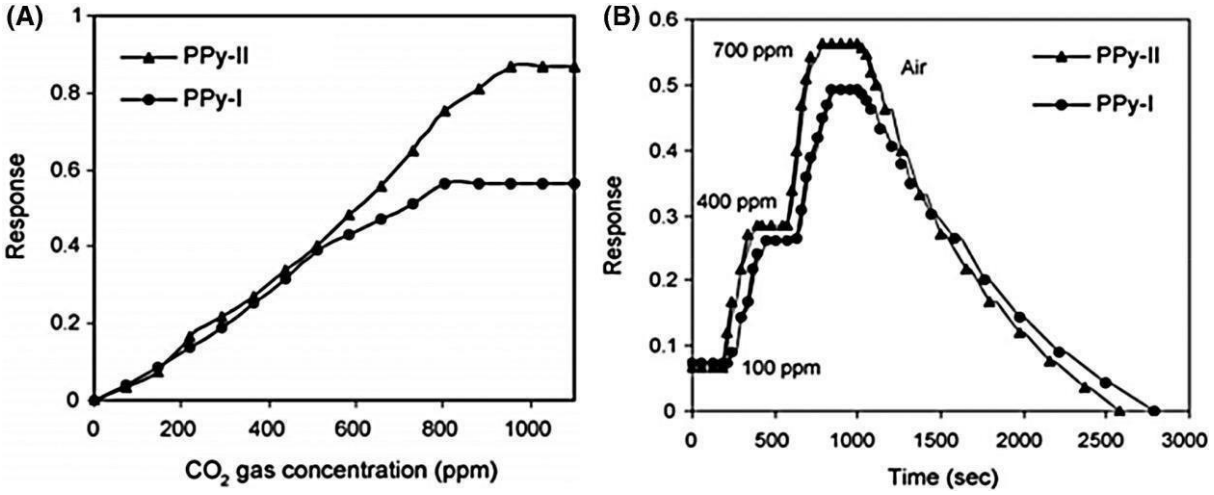

Figure 2.10 (a) Response % of PPy-I and PPy-II sensors of CO_2 gas conc. at RT[77] (b) Dynamic response of PPy-I and PPy-II gas sensors at RT to 100 ppm, 400 ppm and 700 ppm [77]. Reproduced with permission from Elsevier

2.1.5 In-Situ chemical oxidative polymerization

This polymerization technique utilizes polymerization mixtures to synthesize polymer nanocomposites from nanoparticles. This cost-effective method facilitates homogenous mixing, achieving a uniform distribution of particles within the polymer matrix. Additionally, it promotes synergistic interactions between the nanomaterial and the polymer matrix.

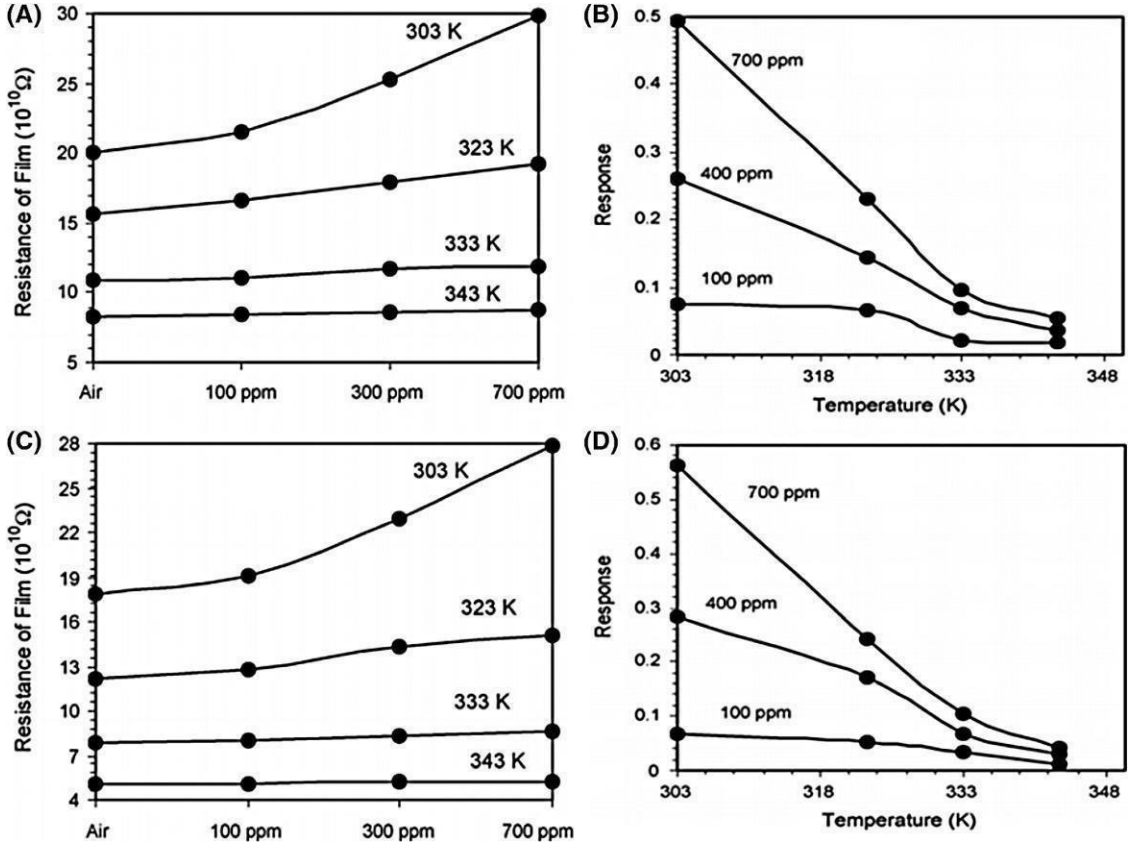

Figure 2.11 (a) Resistance of PPy-I and PPy-II films in air (b) Variation of sensor response % of (a) PPy-I and (b) PPy-II to 100, 300 and 700 ppm of CO_2 at various temp. [77]. Reproduced with permission from Elsevier

Jun *et al.* [80] developed a method to coat tin dioxide (SnO_2) hollow spheres with polypyrrole (PPy) using a chemical reaction. This involved starting with pyrrole (the building block molecule for PPy) dissolved in chloroform. They then added iron (III) chloride ($FeCl_3$) to trigger the reaction and coat the SnO_2 spheres with PPy while the spheres

were present in the mixture. A TEM image of the empty SnO_2 spheres shows rough and porous morphology containing various SnO_2 nanoparticles. **Figure 2.12** shows TEM micrograph of empty PPy and coated SnO_2 spheres which were homogenously entrapped by PPy coatings. Experimental data showed synergic interaction that leads to thermal stabilization of PPy in the frameworks. In this work, PPy/SnO_2 was used for sensor applications and found that hybrid showed good performance on ammonia gas at RT. It also shows that the pure SnO_2 sensor does not show a response to ammonia gas at RT. The sensor utilizing hybrid materials demonstrates a rapid response when exposed to gas and recovers quickly afterwards. This translates to a two-fold increase in sensitivity compared to sensors based on pure PPy. Microscopic images (TEM) show that these sensors made from combined materials (hybrids) have a good pathway for electrons to move within them. Additionally, the porous structure of these hybrids creates a large surface area compared to their volume. This large surface area is why the hybrid sensors are so sensitive [81–84].

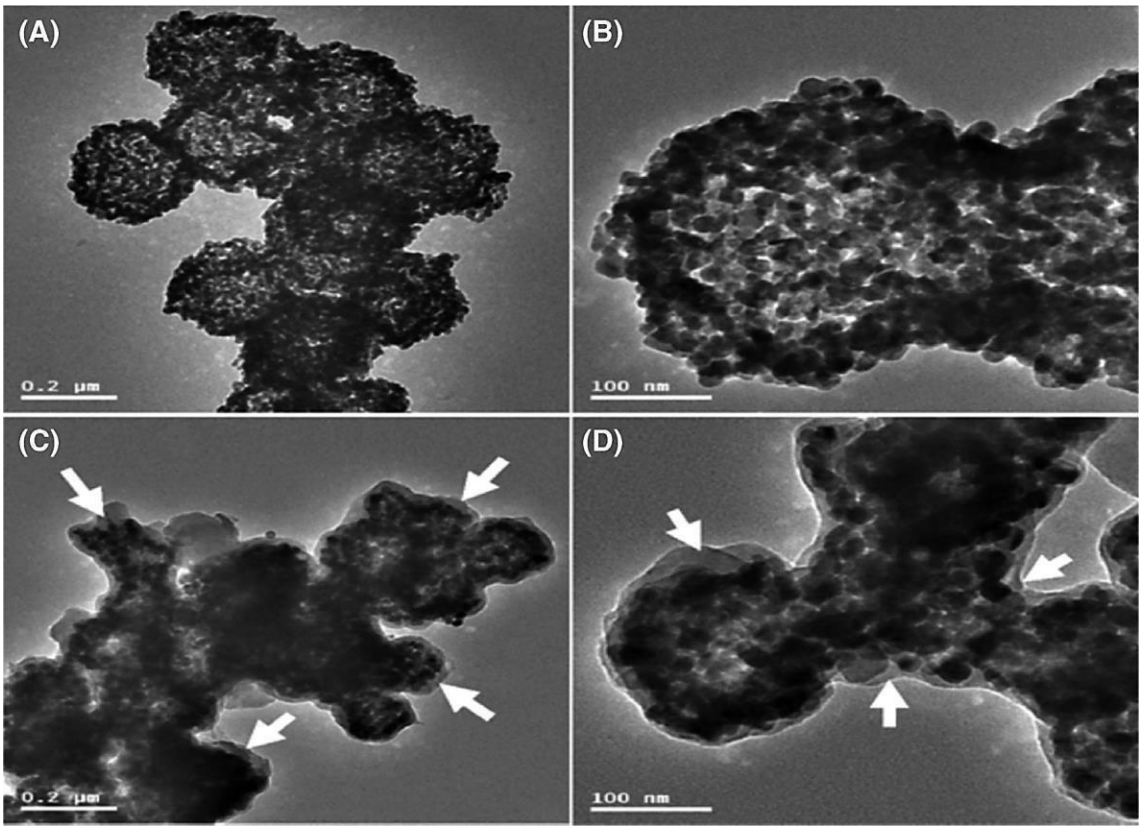

Figure 2.12 TEM micrographs of (a and b) SnO_2 hollow spheres (c and d) PPy coated SnO_2 hollow spheres [80]. Reproduced with permission from American Chemical Society

The combined effect of PPy and SnO_2 hollow spheres creates special zones within the sensor material. These zones help improve the sensor's response by making it more difficult for electrons to move in a certain direction.

Qin *et al*. [85] prepared a three- dimensional rGO by hydrothermal treatment from GO at 190^0C for 14 h and rGO/PPy nanocomposite was prepared by in situ chemical oxidative polymerization method. The three-dimensional rGO/PPy nanocomposite shows a 4-5 times increase in ammonia (300ppb – 5ppm) sensing compared to pure PPy on the alumina surface. SEM images shows granulated morphology of PPy transforming into a porous, nanostructure similar to 3D rGO. The sensor response was (~4-~11) at a concentration of 1.0 ppm - 5.0 ppm.

The sensor exhibits rapid response and recovery times, with a response time of 5 seconds and a recovery time of 20 seconds. The updated sensing parameters are associated with a porous surface. Sun and his co-workers [86] developed a new type of NH_3 sensor. This sensor is made from a combination of PPy nanoparticles and reduced graphene oxide (rGO). The PPy nanoparticles, about 80 nanometers in size, are evenly spread over the rGO sheets using a chemical process. The entire sensor is then placed on a flexible plastic base (PET) to create a thin film. This new sensor design offers several advantages: it's flexible, portable, cost-effective, and works at room temperature. **Figure 2.13a** shows that the PPy nanoparticles are tiny particles, each about 80 nanometers in size. When combined with rGO **(Figure 2.13b)**, the shape and size of these PPy nanoparticles change somewhat. Additionally, the PPy nanoparticles appear to be scattered throughout the rGO, both on its surface and in between its sheets. 5 wt% of rGO-PPy hybrid sensors on NH_3 show good selectivity for VOCs at room temperature and show 2.05 times more response than pure PPy. The improved response of the sensor to ammonia gas (NH_3) can be explained by several factors. First, the PPy and rGO materials interact in a specific way, with their flat surfaces (π-π stacking) and hydrogen bonds forming between them. Second, the rGO sheets provide a large surface area for the gas molecules to interact. Finally, the structure of the sensor allows for fast movement of electrical charges (carriers) within the material.

Mahajan *et al*. [87] created a new method to build nanoparticles of PPy at room temperature. They used a special solution (ferric chloride) to trigger a reaction and combined the PPy with several other materials: reduced graphene oxide (RGO), multi- walled carbon nanotubes (MWCNTs), and zinc oxide (ZnO). These additional materials act- like fillers within the PPy. By examining the material under a microscope **(Figure 2.14),** they observed that the PPy nanoparticles have a round or spherical shape, with an average size between 150 and 200 nanometers. Interestingly, the other materials (fillers) seem to be well-distributed throughout the PPy. The amount of filler material (nanofiller) added significantly impacted the surface area of the PPy composites. As the filler concentration increased from

2% to 20% by weight (wt%), the surface area also increased. Because more filler creates more surface area for gas molecules to attach. Interestingly, at concentrations of 5%, 10%, and 20% wt%, the PPy composite material seems to be organized in layers on the rGO sheets. The gap between PPy spheres has increased with the increase in the concentration of fillers.

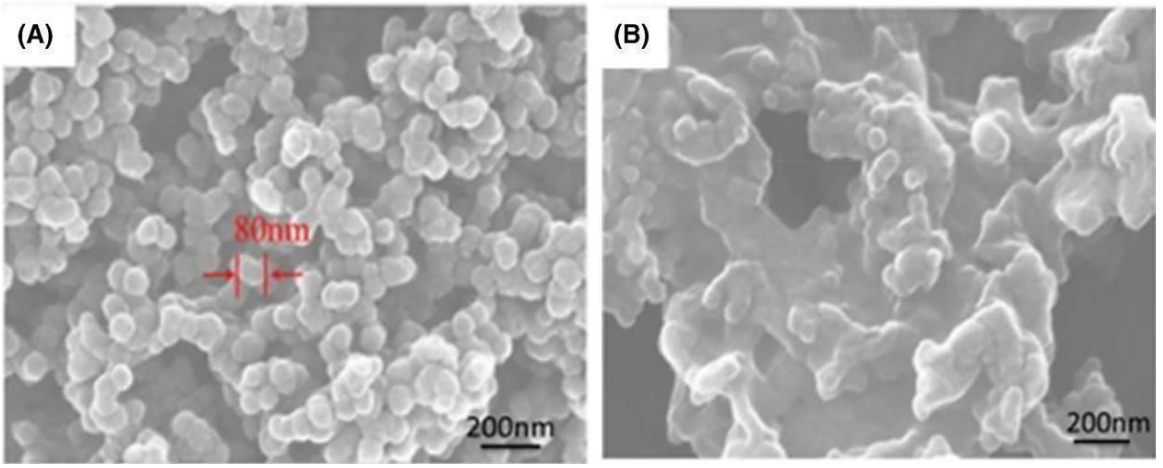

Figure 2.13 SEM images of (a) PPy nanoparticles with diameter 80 nm (b) rGO/PPy hybrid material [86]. Reproduced with permission from Elsevier

Sensitivity was determined by NH_3 gas at room temperature. Ammonia gas being reducing gas and PPy as a p-type semiconductor, electrons obtained through holes from the NH_3 gas in PPy showing a change in resistance. Gas sensitivity experiments were conducted on PPy, 2RCZPPy, 5RCZPPy, 10RCZPPy, and 20RCZPPy at ambient temperature, as depicted in **Figure 2.15**. Removal of NH_3 gas at concentrations of 50, 100, and 200 ppm revealed that 20RCZPPy exhibited a remarkable response of 325%, owing to its superior conductivity is shown in **Figure 2.16.**

Similarly, Kiani *et al*. [88] reported a highly selective NH_3 sensor on PPy/Ag nanocomposites and gas sensor comparing PPy nanosphere/Ag nanocomposites and pristine PPy. Thin films made of PPy fibers and silver nanoparticles were layered onto special electrodes (interdigitated electrodes). These sensors exhibited faster response and recovery times compared to sensors made with PPy spheres and silver nanoparticles. This difference is likely due to a stronger chemical reaction between the fiber/silver composite and ammonia gas compared to its reaction with other vapors. Scientists investigated how well

the sensor conducts electricity (electrical conductivity) at different temperatures, ranging from 220 to 700 ̊C. They observed that the sensor's ability to conduct electricity (conductivity) gradually decreased as the temperature increased. Hence, PPy fiber/Ag nanocomposites show better sensing properties. Ramesan synthesized polypyrrole coupled with copper sulfide (CuS) through in-situ chemical oxidative polymerization, followed by comprehensive characterization using FTIR, SEM, XRD, DSC, and conductivity analyses. The findings indicated that the FTIR spectrum affirmed the incorporation of CuS nanoparticles within the polymer nanocomposites. Structural and morphological assessments revealed improved surface characteristics, displaying porous, granular, and globular morphology with excellent uniformity. The optimal dielectric properties make it suitable for sensor applications.

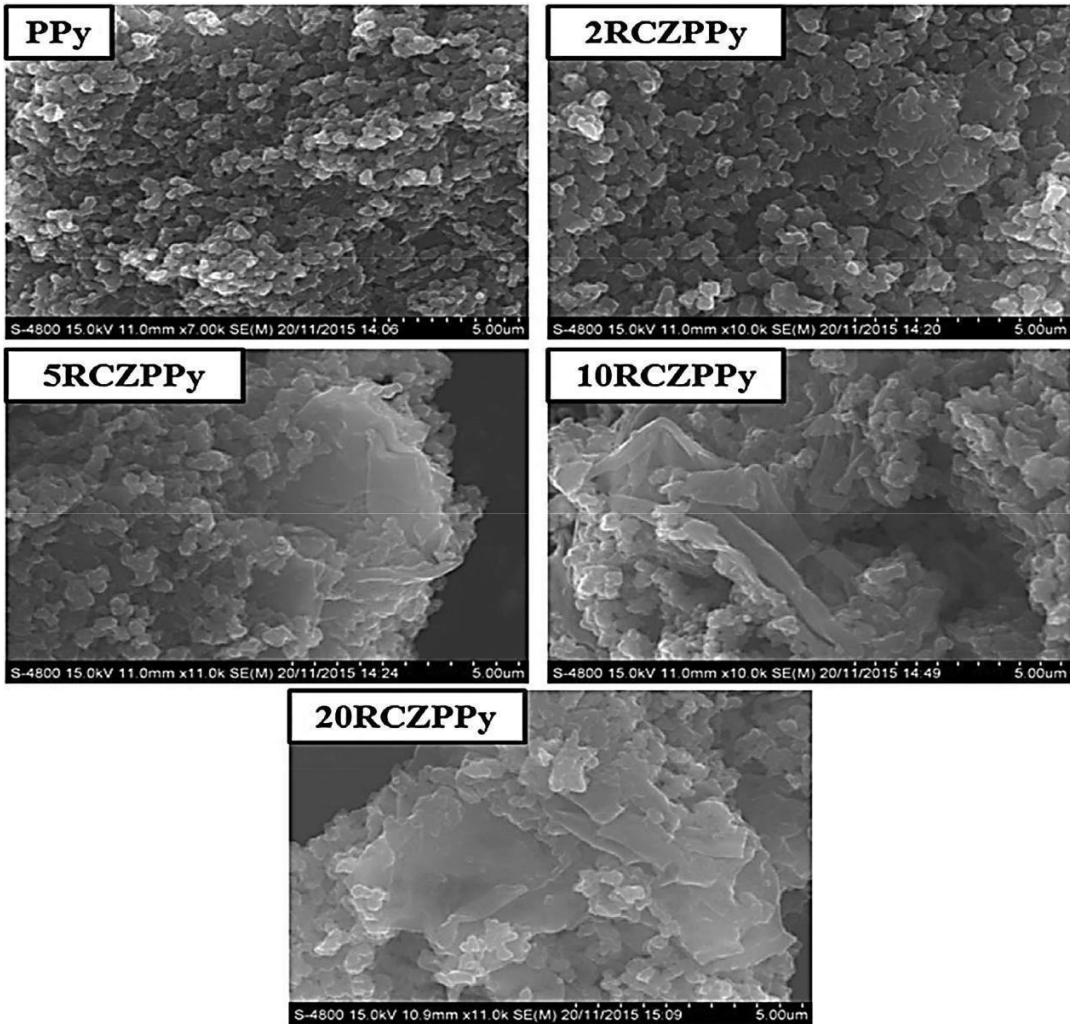

Figure 2.14 FE-SEM images of PPy, 2RCZPPy, 5RCZPPy, 10RCZPPy and 20RCZPPy Nanocomposites [87]. Reproduced with permission from Springer

The direct current (DC) conductivity of the CuS/PPy composite was higher than that of pure PPy. Interestingly, the conductivity also increased as the amount of CuS added (filler content) increased. This suggests that adding more CuS creates more free space within the PPy matrix. This extra space allows ions or molecules to move more easily throughout the material, ultimately improving its conductivity [89]. Yeole *et al.* [90] investigated a new material for detecting ammonia (NH_3) gas at RT. They created nanocomposites by combining PPy with Ag_2S using a special process called in-situ polymerization. Interestingly, they studied how the amount of Ag_2S affected both the electrical properties of the material and its ability to sense NH_3 gas. They then tested these new materials to see how well they detected ammonia gas at room temperature in normal air conditions (ambient conditions). The results were promising: the nanocomposites made with PPy and Ag_2S showed an excellent response to ammonia gas at a concentration of 100 ppm.

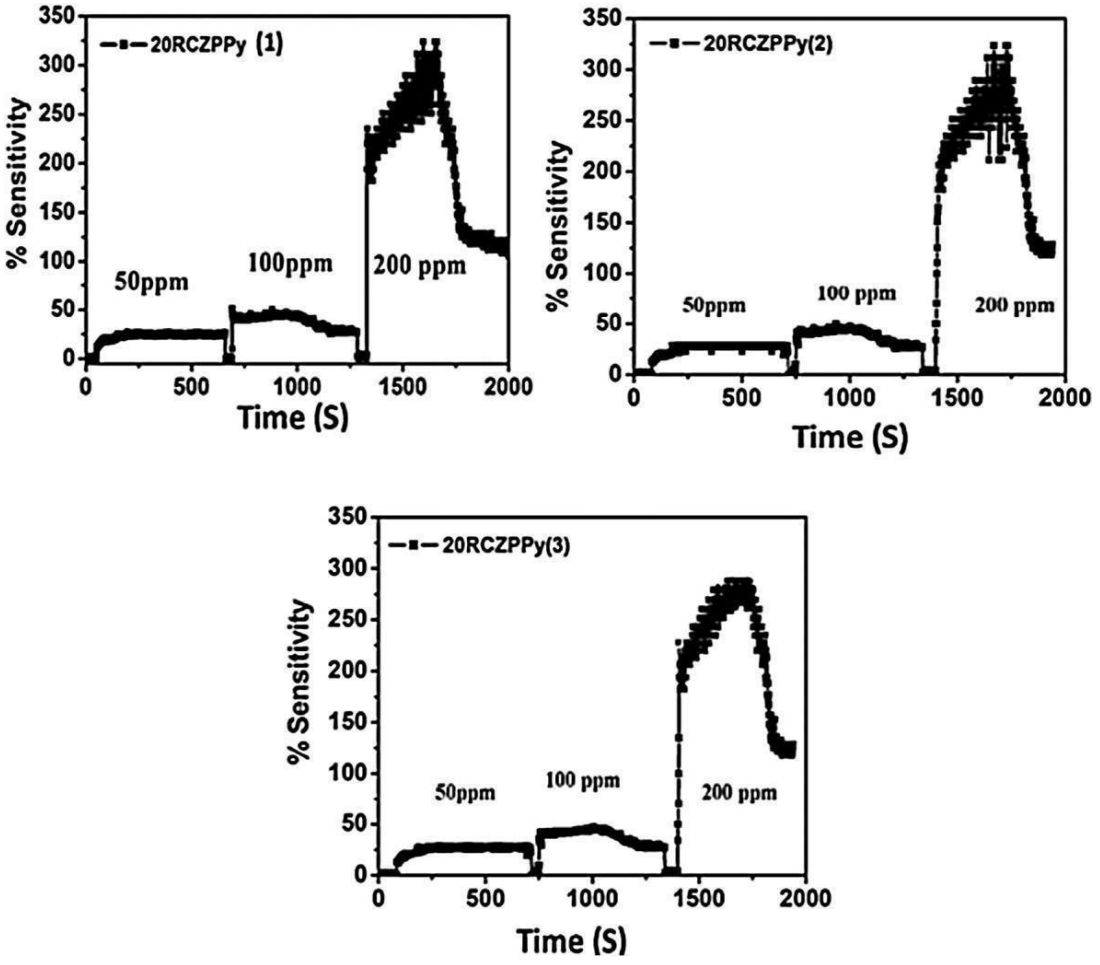

Figure 2.15 Response % of 20RCZPPy nanocomposites at different conc. of 50, 100 and 200 ppm NH_3 gas [87]. Reproduced with permission from Springer

2.1.6 Plasma Polymerization

Several methods are employed to produce polypyrrole including chemical oxidation polymer, electrochemical polymerization, and gelation. Plasma polymerization emerges as an optimal method for crafting small pyrrole films, ensuring high-quality outcomes. Films generated through plasma polymerization exhibit notable characteristics such as thermal and chemical stability, transparency, uniformity, and density. Li *et al*. [91] prepared polypyrrole films on Si substrate by this type of polymerization using RF power in the Ar atmosphere in an empty chamber. They chose the power level as 10, 12, and 14 W and characterized the films by SEM, FTIR, EDS, and XPS. FTIR shows three major shifts in films that lead to unbreakable pyrrole rings and pyrrole containing nitrogen groups and low RF power to improve the electrical conductivity.

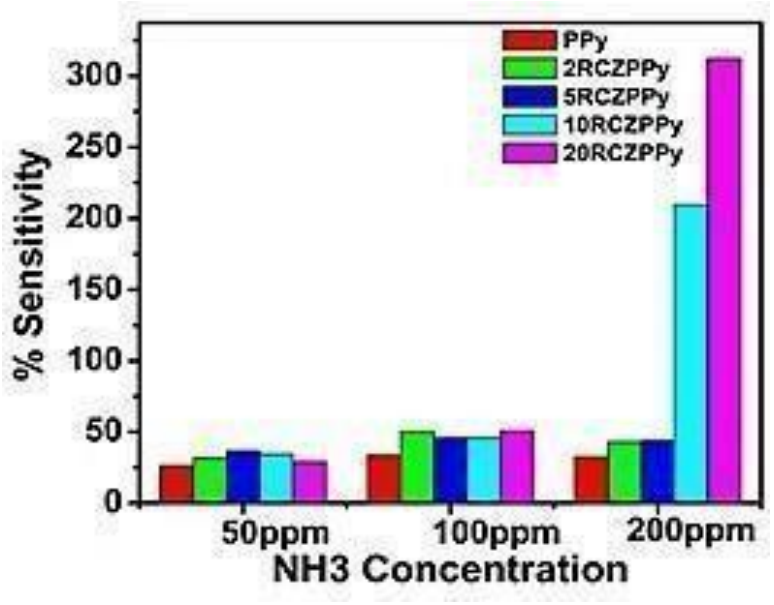

Figure 2.16 Sensitivity of PPy, 2RCZPPy, 5RCZPPy, 10RCZPPy, and 20RCZPPy nanocomposites on NH_3 gas [87]. Reproduced with permission from Springer

Yague *et al*. [92] reported deposition of small PPy films on nanostructured surfaces and showed that the incorporation and growth of PPy increased with the construction of pyrrole terminated self-assembled monolayer on gold surface. In this, the synthesis of different N-pyrrole alkane thiol is explained. The length of the monolayer chain and the plasma polymerization conditions were studied to determine their role in determining in high monolayer structure and film growth. The conditions for plasma polymerization were to promote the formation of solid thin films with rough value and control thickness and further used in sensor array development. Dhillon *et al*.

[93] prepared semi-crystalline films of PPy, thin and pin hole free by RF plasma polymerization using PPy monomer as a precursor in the field of Ar plasma zone. For the formation of plasma, RF was used in constant argon gas pressure. It shows confirmation of crystalline regions and inter plane separation calculation. It is evident that the films obtained by polymerization are very stable and show adhesion to all types of substrate. It can also be seen that the films contain the finest grains of globular contrast and grains are dispersed evenly at a ratio of 1 nm in the matrix shown in **Figure 2.17a** and regions with a diameter 15-20 nm observed with sharp lattice planes of 0.68 nm inter plane separation in **Figure 2.17b** and confirms the formation of semi crystalline phases in the amorphous matrix. In addition to electrochemical and chemical polymerization methods, the spin coating technique is utilized to fabricate PPy based NiO hybrid film sensors on glass substrates. While Geng *et al.* [94] demonstrated that PPy-WO_3 materials are sensitive to H_2S gas, Nalage *et al.* were the first to explore the gas sensing properties of PPy/NiO hybrid nanocomposites in detail. Their study investigated factors like stability, reproducibility, and selectivity alongside sensitivity [95]. In addition, nanocomposite was used to detect NO_2 gas compared to PPy and nano-NiO. PPy-NiO gas sensitivity (10%, 20%, 30%, 40%, and 50%) was carried at room temperature at 100ppm concentration to test different gases and the reaction of PPy based NiO (50%) shows a very high response rate of 47% to 100ppm for NO_2. The selectivity of PPy, nano-NiO, and PPy-NiO (50%) was investigated using test gases including Cl_2, NO_2, H_2S, C_2H_5OH, and NH_3, each at a concentration of 100 ppm. The responses obtained were 13%, 26%, and 47%, respectively, with minimal response observed towards other gases. Hence, PPy-NiO exhibits high sensitivity and stability at room temperature and the response slows down the higher concentration.

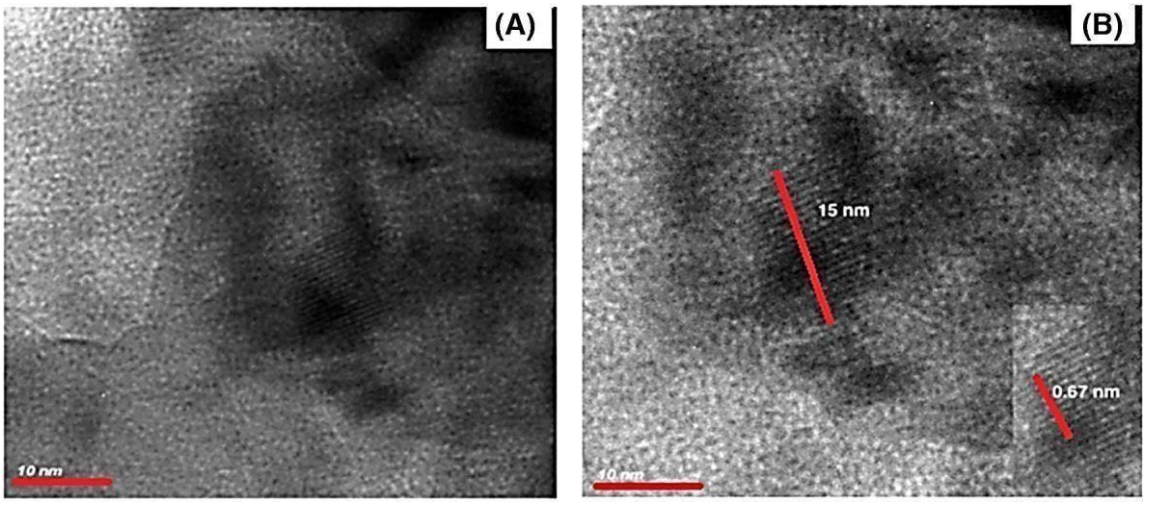

Figure 2.17 (a) HR TEM image of polypyrrole at scale bar of 10 nm. (b) Inter plane spacing by HR TEM [93]. Reproduced with permission from Elsevier

The combination of nickel oxide (NiO) and polypyrrole (PPy) in the sensor creates a special effect. NiO acts like a material with positive charges (p-type semiconductor) and NO_2 gas tends to attract electrons. When NO_2 gas comes in contact with the sensor, it pulls electrons away from the composite material, increasing the number of positive charges (holes) within it. This increase in holes makes it easier for electricity to flow through the material, resulting in a decrease in resistance.

2.1.7 Vapor-phase polymerization

Vapor- phase polymerization is simple and successful solvent process for the formation of high- quality polymer chains on substrates.

An *et al*. [96] found that combining PPy with single-walled carbon nanotubes made a sensor ten times more sensitive to nitrogen dioxide (NO_2) gas compared to a sensor made of PPy alone. They also observed that combining PPy with multi-walled carbon nanotubes resulted in a sensor with some sensitivity to ammonia (NH_3) gas, especially at room temperature. Hong *et al*. developed a new method to create a sensor material for ammonia (NH_3) gas detection [51]. Their method involved a simpler process using heat (thermal refluxing) and vapor phase polymerization to combine PPy with palladium (Pd). Interestingly, the study found that the structure (morphology) of the sensor material was significantly affected by three factors: the amount of Pd used, the ratio of PPy to Pd, and the duration of the reaction. These nanocomposite sensors made with PPy and Pd showed a response rate between 13.9% and 58.9% for ammonia gas concentrations ranging from 60 ppm to 2000 ppm, all at room temperature. This response rate was considerably higher than that of pure PPy sensors. Additionally, the sensor recovered from exposure to ammonia gas quite quickly (recovery time of 14 seconds) and responded within 148 seconds for a high ammonia concentration (1000 ppm). Finally, the research suggests that the performance of these sensors is influenced by two key features: the size of the palladium nanoparticles and the overall structure of the sensor film. Jang *et al*. [97] developed a sensor material for detecting hydrogen gas (H_2) at room temperature. Their design involved combining carbon nanotubes (CNTs), polypyrrole (PPy), and palladium nanoparticles (Pd). First, they modified the CNTs with a special molecule (pyrene carboxylic acid) that helped the PPy stick to them better. Then, they used a vapor process at 800℃ to coat the CNTs with PPy. Finally, they used sound waves (ultrasound irradiation) to attach tiny Pd nanoparticles onto the CNT/PPy composite. This sensor, based on a field-effect transistor (FET) system, could detect H_2 gas

at concentrations as low as 1 ppm (parts per million) at room temperature, with a sensitivity of around 1.6%. For comparison, the study also suggests that single-walled carbon nanotubes combined with PPy (single-enclosed CNT/PPy) might be a better choice for sensing hydrogen sulfide (H_2S) gas at room temperature.

2.1.8 Gas sensing

A sensor acts like a translator for the environment. It can detect various physical changes around it, such as light, heat, movement, humidity, or pressure. The sensor then converts these physical changes into data (electrical signals) that can be understood by other devices or even people. Conducting polymers are a special type of plastic that conducts electricity well. This makes them very useful for building sensors, especially in chemistry and biology. Scientists are interested in these polymers because several things can influence their electrical properties. These influences include chemical reactions (analyses), adding small amounts of other materials (doping), and changes in the polymer's structure (redox regions). When these things happen, the conducting polymer's ability to conduct electricity (resistance) or the amount of current it carries can change. These changes in electrical properties can then be used to detect the presence of specific chemicals or biological molecules. Nanomaterials are finding a valuable role in the development of gas sensors. Their unique properties, including high surface area and good electrical conductivity, make them ideal for this application. The high surface area allows gas molecules to readily come into contact with the sensor material, increasing the sensor's sensitivity. Additionally, the good electrical properties of some nanomaterials allow them to convert the interaction with gas molecules into a measurable electrical signal, facilitating gas detection [98]. Sensors developed for metal oxides work efficiently but their low selectivity and short life span have their shortest arrival and should be improved. The limitations mentioned can be overcome by the construction of room temperature operable gas sensors. MWCNT enhances its sensory performance when used to create a polymer matrix. The addition of MWCNT to PPy greatly affects sensitivity towards NH_3. The PPy-MWCNT nanocomposites sensor shows fine sensitivity to NH_3 at room temperature.

Kondawar *et al*. [99] designed to operate a composite based sensor with a different NH_3 sensor. Tiwari *et al*. [100] improved the PPy-rGO thin film composite sensor for NH_3 and ensured the integration of rGO into PPy improved sensitivity and response time. The PPy-rGO hybrid sensor to NH_3 shows good sensing response and sense ammonia at 3ppm. With the increase in the concentration of ammonia gas, the sensitivity also increases due to which

it starts saturating at high concentration and sensitivity of PPy-rGO are more than PPy thin film sensor. Lin *et al*. [101] prepared a novel graphene/PPy sensor with different percentages of graphene for humidity sensor measured using LCR analyzer. The results show a sample with 10% graphene /PPy with excellent sensitivity at RH (Relative humidity) in the range of 12-90%. The prepared sensor showed high sensitivity and the hysterious value was very small which is suitable for high-performance humidity sensors.. Shukla *et al*. [102] developed a humidity sensor using a composite material made of PPy and ZnO. They combined these materials using a technique called in-situ polymerization, which resulted in a well-ordered (crystalline) composite with good electrical conductivity. The researchers tested the sensor's ability to detect humidity by measuring its electrical resistance at different humidity levels. The sensor showed fast response and recovery times: it took only 12 seconds to respond to a change in humidity and 8 seconds to recover to its original state. To explain how the sensor works, the researchers proposed a model that considers the combined effect of water molecules ionizing (gaining a charge) and dissociative adsorbing (breaking apart and attaching) on the sensor surface. This combined effect likely influences the electrical conductivity of the composite material. Gaikwad *et al.* [103] investigated the use of platinum (Pt) nanoparticles and polypyrrole (PPy) for creating a sensor for liquefied petroleum gas (LPG). Interestingly, they made the PPy in the presence of hexachloroplatinate, which acted as a starting point (precursor) for the Pt nanoparticles. Precursor of the Pt nanoparticles plays a role at temperatures 100℃, 150℃, 200℃ respectively. The composite at 150℃ shows the highest response enhances synergistic effect between Pt nanoparticle and PPy. The effective temperature of the gas sensing experiment was 170℃. Hassan *et al.* [104] explored the sensitivity of PPy-coated small copper films to CO_2 and O_2 at temperatures.

They observed that the sensitivity of PPy-Cu nanocomposites reached 160% and 300% respectively at a concentration of 100 ppm. Wang *et al.* [105] conducted a comparative analysis of PPy nanosphere/Ag nanocomposite and PPy fiber/Ag nanocomposite, fabricated through template-free and template-assisted methods, respectively. The results revealed that the PPy fiber/Ag nanocomposite demonstrated superior NH_3 gas sensing capabilities, exhibiting enhanced sensitivity, response time, and recovery time. Notably, even in the presence of 250 ppm NH_3, the PPy fiber/Ag nanocomposite remained unsaturated, whereas the PPy nanosphere/Ag nanocomposite reached saturation at 100 ppm NH_3 gas concentration. **Table 2.4** provides an overview of polypyrrole, including response time, recovery time, selectivity, and operational temperature.

Table 2.4 A comprehensive literature review on the sensing capabilities of gas sensors utilizing PPy-based hybrid nanocomposites.

Material	Gas Sensing used	Conc. (ppm)	Sensitivity	Response time	Recovery time	Selectivity	Operating Temp
Py-rGO/PPy	Ammonia	50 ppm	~22%	-	-	-	RT[106]
Chemically oxidized PPy-rGO	Ammonia	10-500 ppm	1.1%-34.7%	400s	-	-	RT[100]
PPy-Au nanoparticle	Ammonia	100-300 ppm	1.35,1.45 @100,300ppm	-	-	More sensitive to NH_3	RT[107]
PPy-Pd nanoparticle	Hydrogen	10-10000 ppm	15%-70%	-	-	More sensitive than CO,NO_2	RT[108]
PPy-Pt nanoparticle	LPG	400 ppm	~9	-	-	Selective to LPG than other	RT-207^{0}C[104]
PPy-Cu nanowire	oxygen	100 ppm	160%, 300% [~35^{0}C]	-	-	-	RT-150^{0}C[105]
ZnO-PPy	LPG	1000-1800 ppm	21-34.5%	240s @1400 ppm	2400 s	-	RT[109]
PPy-CdS	Ammonia	100-500 ppm	~160%	-	-	More selective to NH_3	RT[110]
PVA-PPy	Ammonia	5ppm- 13ppm	61% - 73%	25 min	-	-	RT[111]
PPy-CeO_2	LPG	Up to 20,000 ppm	<30% - 85%	-	-	Selective to LPG than NH_3	RT[112]
PPy-SnO_2 /ZnO	Ammonia	30-80 ppm	~0.7,~0.82@30ppm, 70 ppm	67.2s @70 ppm	106 s	-	RT[113]
SnO_2-ZnO/PPy	Ammonia	10-85 ppm	47-48% @ 50 ppm	-	-	More selective to NH_3	RT[114]
PPy-WO_3	Hydrogen Sulfide	100-1000 ppb	~9% - ~81%	~ 360 s	-	More selective to H_2S than others	RT[115]
Au nanoparticle-PPy	Ammonia	10- 200 ppm	~ 1.07 @ 80 ppm	-	-	-	RT[107]
rGO-PPy	Ammonia	33.2 ppm	7%	-	-	-	RT[116]

PPy-Graphene	Ammonia	1-5 ppm	~2.5% - ~9%	120 s	300 s	More selective	RT[117]
PPy/Ag-doped NiO	Nitrogen dioxide	30%	~67%	~36s	~37s	-	RT[118]
PPy-rGO	Ammonia	1-10 ppm	50% @10 ppm	-	-	More selective	RT[86]
PPy-MWCNT	Ammonia	33.2 ppm	65%	<10 min	-	-	RT[97]
PPy thin film-TiO_2	Ammonia	24-141 ppm	~2.7 ~ 7.95%	~ 17 s @ 23 ppm	~ 60 s	Highly sensitive towards humidity	RT[37]
1D ZnO nanorod- PPy	Ammonia	300-1000 ppm	~36.1%@1000 ppm	3-5 ppm	600s	More selective to NH_3	RT[119]
Ag_2S-PPy (1%)	Ammonia	100-150 ppm	~ 7.7%	20 s	>600 s	-	RT[120]

CHAPTER THREE

Methodology

This chapter provides comprehensive details regarding the materials procured, synthesis methods employed for PPy (utilizing oxidants $FeCl_3$ and APS), and the process of preparing nanocomposites by incorporating various metal sulphides such as WS_2, MoS_2, and SnS_2 fillers into the PPy matrix. Moreover, it extensively discusses the characterization techniques employed, including XRD, FT-IR, SEM, TEM and I-V measurement to analyze the synthesized materials. Additionally, the chapter thoroughly explains the gas sensing measurements conducted, offering a detailed insight into the experimental process.

The chemical oxidative polymerization method was employed for synthesizing PPy, utilizing various oxidants such as $FeCl_3$ and APS while maintaining consistent parameters such as temperature and time. PPy synthesized with $FeCl_3$ was chosen as the matrix for subsequent fabrication of nanocomposites, incorporating different metal sulfides like WS_2, MoS_2 and SnS_2 as filler materials through in-situ chemical oxidative polymerization. These PPy-based metal sulfides were then subjected to various characterizations and utilized for gas sensing applications.

3.1 Materials

Metal sulfides like WS_2, MoS_2 and SnS_2 were used as a fillers in globular like morphology PPy matrix. Prior to utilization, the as-received WS_2, MoS_2, and SnS_2 underwent ultrasonication to ensure optimal dispersion within the PPy matrix. The conductive fillers were additional employed to improve electrical conductivity of PPy composites with globular morphology.

The subsequent chemicals were utilized in the preparation of all samples; Pyrrole (C_4H_5N; 98% purity, Spectrochem) as a monomer. Ferric chloride ($FeCl_3$; spectrochem) and Ammonium peroxydisulfate [APS; 97% purity, Loba Chemie)] used as an oxidant. Distilled water used as the solvent for the preparation of PPy. Fillers Tungsten disulfide (WS_2; 98% purity, Sigma Aldrich), Molybdenum disulfide (MoS_2, 98% purity, Sigma Aldrich), Thioacetamide (TAA, CH_3CSNH_2, Loba Chemie), Tin chloride pentahydrate ($SnCl_4 \cdot 5H_2O$, Loba Chemie), Tin disulfide (SnS_2) were used. For the synthesis of MoS_2, HCl was used as dopant' and for SnS_2, ethylene glycol (EG,) was used as solvent.

3.2 Synthesis of Polypyrrole

The synthesis of PPy involved the chemical oxidative polymerization method, employing $FeCl_3$ and APS as the oxidizing agents.. For the synthesis of PPy, parameters like temperature and time were kept fixed. Sapurina studied oxidative polymerization by different oxidants like APS, $FeCl_3$, and $AgNO_3$ for which the values of oxidation potential are 2.01 V, 0.77 V, and 0.8 V, respectively. The use of oxidants shows different

morphological features like APS, which shows globular structure, whereas $FeCl_3$ and $AgNO_3$ show fibers and tubes like structure, respectively.

3.2.1 Using oxidant $FeCl_3$

PPy was synthesized via chemical polymerization of the pyrrole monomer in the presence of a solvent. The monomer to oxidant ratio used for the synthesis of PPy with $FeCl_3$ oxidant was 1:2**.** In order to attain uniformity, 0.5 M (3.47 ml) of pyrrole (Py) was dispersed in 100 ml of distilled water within a beaker, and the mixture was stirred for 30 minutes. A solution of 1 M (16.22 g) $FeCl_3$ was added to the above aqueous pyrrole solution. The pyrrole solution turns green when 10 to 15 drops of aqueous $FeCl_3$ (one drop every 10 sec) are added, showing the formation of PPy in a colloidal solution at 300-1200 rpm. As more $FeCl_3$ is added, the color changes from light green to dark green, then to black. This reaction was carried out for about four hours. The colloidal solution underwent purification through multiple washes with distilled water and ethanol to eliminate impurities. Subsequently, the resulting powder was collected and dried at 40-60°C until completely dry. The synthesis of PPy has been carried out at temperature 0-5 by keeping it in the ice bath. The dried PPy powder was grinded and kept for characterization techniques [73].

3.2.2 Using oxidant APS

The synthesis of PPy with APS was also done by chemical oxidative polymerization method. First, the pyrrole monomer of concentration 0.5 M (3.47 ml) was dissipated in 100 ml of distilled water in a beaker and agitated for 30 minutes to achieve homogeneity. A solution of 1 M (22.18 g) APS ($NH_4(SO_4)_2$) was added to the above aqueous pyrrole solution. With the addition of 10 to 15 drops of aqueous APS (one drop every 10 sec) to the pyrrole solution, the solution turns green. On further addition of APS, color becomes dark green and then black. This reaction was carried out for about four hours at 300-1200 rpm. The colloidal solution was purified and repeatedly washed with distilled washed and ethanol. The sufficient powder was collected as well as dried at 40-60 $^{\circ}$C. Synthesis of PPy has been carried out at temperature 0-5 $^{\circ}$C by keeping it in the ice bath. The dried PPy powder was grinded and kept for characterization techniques [121]. **Figure 3.1** depicts the synthesis process using oxidant APS and $FeCl_3$**.**

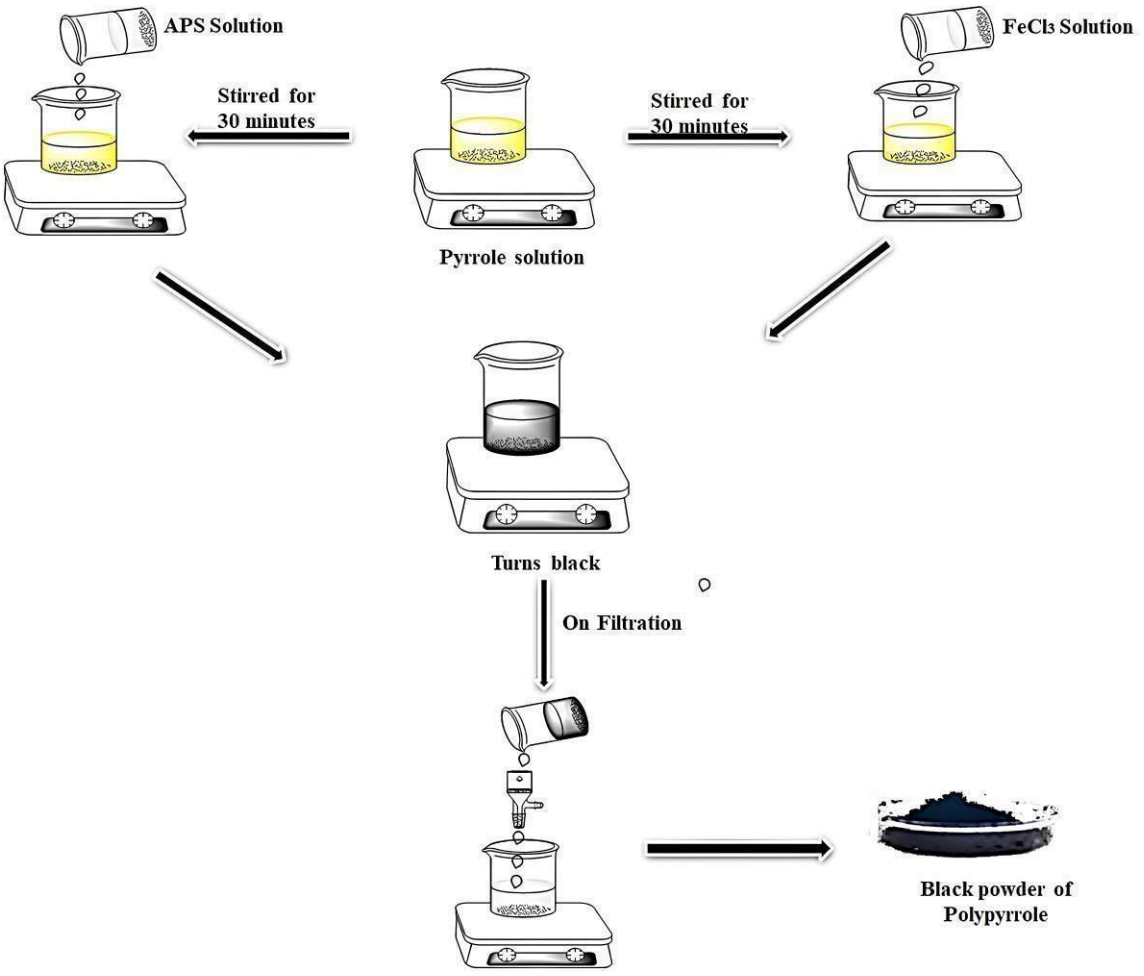

Figure 3.1 Representation for the synthesis of PPy using oxidant APS and $FeCl_3$

Out of all the synthesized PPy variants, PPy utilizing $FeCl_3$ as the oxidant was chosen as matrix for subsequent preparation of hybrid nanocomposites. These composites incorporated transition metal dichalcogenides WS_2, MoS_2, and SnS_2 as filler materials. These PPy based hybrid nanocomposites are further used for gas sensing application.

3.3 Nanocomposites Preparation

Usually, nanocomposites are fabricated through a variety of methods including "electrochemical polymerization", "chemical oxidative polymerization", "plasma polymerization", "photo-induced polymerization", "enzymatic polymerization", "vapor-phase polymerization", and "in-situ chemical oxidative polymerization" techniques. "In-situ polymerization" method has more advantages over other routes as its composite formation is good, cost-effective and less-time consuming which have been further employed for detecting a number of gases.

3.3.1 Polpypyrrole/Tungsten disulfide

The synthesis of PPy/WS_2 was carried out through an in-situ oxidative polymerization approach. Initially, tungsten disulfide powder, varying in weight percentages (1 wt%, 5 wt%, 10 wt%, 20 wt%, and 30 wt%), underwent ultrasonication for 1 hour to ensure proper dispersion. This dispersed powder was then added to a pyrrole solution (0.03 M) and mixed using a magnetic stirrer. Ferric chloride (0.06 M) was subsequently added dropwise to the resulting solutions while stirring continuously, yielding PPy/WS_2 nanocomposites [122] as shown in **Figure 3.2**. For different wt% of WS_2, samples have been named as PPy/ WS_2- 1 wt%, PPy/ WS_2- 5 wt%, PPy/ WS_2- 10 wt%, PPy/ WS_2- 20 wt% and PPy/ WS_2- 30 wt% respectively.

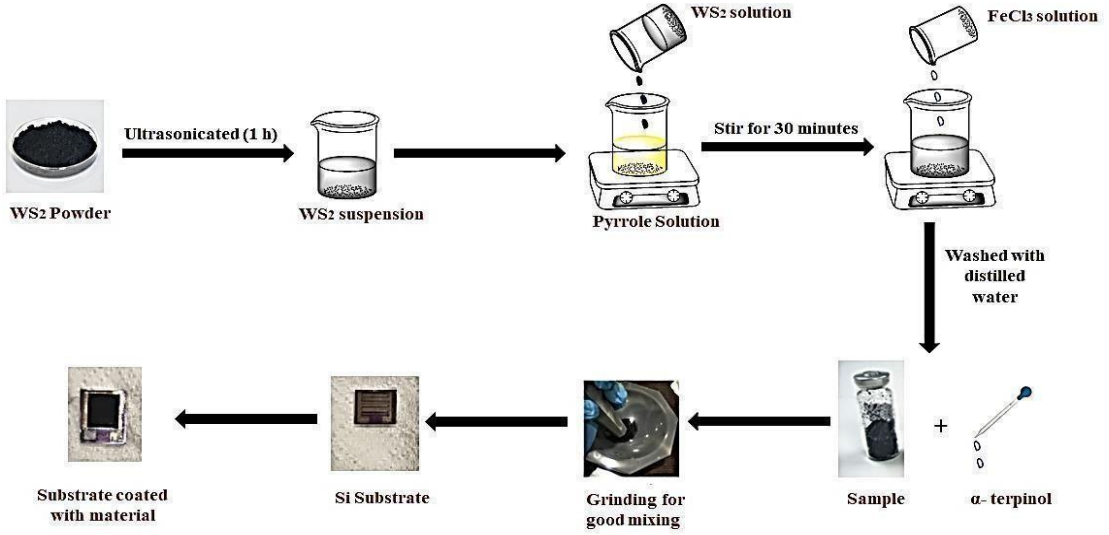

Figure 3.2 Illustration depicting the synthesis process of PPy/WS_2 nanocomposites along with the gas sensor fabrication.

3.3.2 Polpypyrrole/Molybdenum disulfide

PPy/MoS_2 nanocomposites were synthesized using in-situ chemical oxidative polymerization method using Py and MoS_2 as a monomer and filler, respectively. The oxidizing agent iron (III) chloride hexahydrate ($FeCl_3$) was used as an aqueous medium at the temperature range of 0-5° C. To initiate the experiment, pyrrole was first added to the MoS_2 suspension in water. This mixture was then sonicated for 1 hour to promote dispersion of the MoS_2 powder and facilitate intercalation of the pyrrole. Next, a solution of $FeCl_3$ was introduced, triggering the polymerization of pyrrole. After adjusting the pH

in a strongly acidic medium with hydrochloric acid as a dopant, the mixture was continuously stirred for 5 hours. The purpose of controlling pH and dopant at 700-800 rpm is for effective polymerization of monomer and accelerating the electronic cloud in the polymeric backbone. After completion of the reaction, the resulting nanocomposite powder was collected, washed with 0.2 M HCl, ethanol, and dried at RT as shown in **Figure 3.3**. The prepared samples were designated as PPy/MoS_2- 1 wt%, PPy/MoS_2- 5 wt%, PPy/MoS_2- 10 wt%, PPy/MoS_2- 20 wt%, and PPy/MoS_2- 30 wt% correspond to different weight percentages (wt%) of MoS_2.

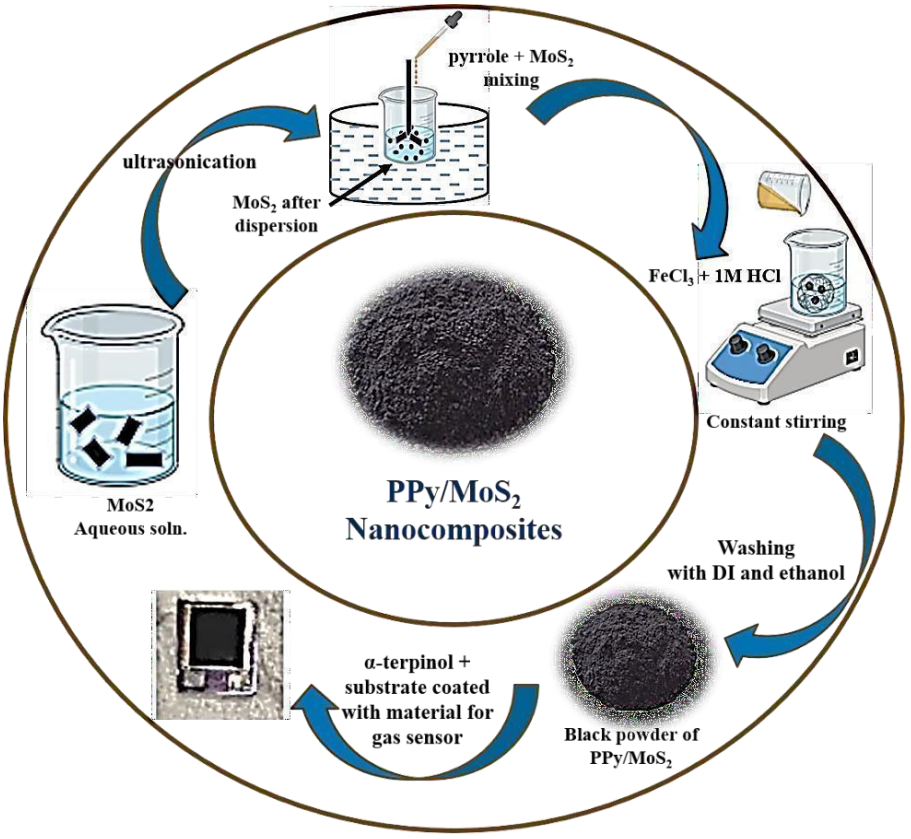

Figure 3.3 Schematic illustration of PPy/MoS_2 nanocomposites with gas sensor fabrication.

3.3.3 Polpypyrrole/Tin disulfide

Our work presents a straightforward and scalable approach for the synthesis of SnS_2 in large quantities. This method utilizes a refluxing route. To begin, 8 mmol of thioacetamide (TAA, CH_3CSNH_2) was dissolved in 30 mL of ethylene glycol (EG) at a moderate temperature of

45 °C. Simultaneously, a separate solution of $SnCl_4 \cdot 5H_2O$ (2 mmol) in EG (30 mL) was prepared. The prepared tin(IV) chloride pentahydrate ($SnCl_4 \cdot 5H_2O$) solution was transferred to a three-neck flask. This flask was equipped with a condenser for reflux, a thermometer for temperature monitoring, and a constant pressure funnel containing the previously prepared thioacetamide (TAA) solution in ethylene glycol (EG). The TAA solution was then slowly added to the $SnCl_4 \cdot 5H_2O$ solution in the flask. With continuous stirring, the reaction mixture was heated in an oil bath at a controlled rate of 10°C per minute. Once the temperature reached 140°C, the pre-added TAA solution in ethylene glycol (EG) was swiftly injected into the flask using the constant pressure funnel. To ensure complete reaction, the mixture was maintained at 140 °C for an additional hour. Finally, the flask was removed from the oil bath and allowed to cool down to room temperature naturally. The resulting product was then centrifuged at 4000 rpm for 30 minutes and subsequently washed three times with absolute ethanol using ultrasonication [123].

To achieve uniform dispersion, SnS_2 powder, at varying weight percentages (1 wt%, 5 wt%, 10 wt%, 20 wt%, and 30 wt%), was first subjected to ultrasonication for 1 hour using the in-situ chemical oxidative polymerization method. Subsequently, the dispersed powder was introduced into a pyrrole solution (0.03 M) and mixed using a magnetic stirrer. Dropwise addition of ferric chloride (0.06 M) to the resulting solutions with continuous stirring yielded PPy/SnS_2 nanocomposites, culminating in the formation of black products. The obtained product underwent washing with distilled water and acetone. The sample was dried in an oven at 100°C to remove water until a constant weight was reached.

3.4 Characterizations of PPy powder and PPy nanocomposites

Various characterization techniques were used to analyze filler component, matrix, and hybrid composites/nanocomposites. The subsequent paragraphs will detail the techniques employed, which are as follows.

3.4.1 XRD (X-ray Diffractometry)

Using XRD information related to crystallite size of synthesized materials (Pure PPy, hybrid PPy/WS_2, PPy/MoS_2, PPy/SnS_2 nanocomposites) were examined. Cu Kα (λ= 1.5406 Å) radiation produced on “30 kV and 50 Ma” at a scanning rate of “2˚ per min” was used to capture the diffraction patterns of finely powdered prepared samples on a “Bruker D-8,

X-ray diffractometer". For detailed phase identification, XRD data was collected in the 2θ range of 10 to 80 degrees with a high-resolution step size of 0.02 degrees. Amorphous and Crystalline components could be distinguished from the overall area of XRD pattern. The degree of crystallinity (X_c) was calculated using formula as shown in equation 1.

$$X_C\ (\%) = [A_c / (A_c + A_a)] \times 100 \qquad \textbf{(3.1)}$$

A_c = area of crystalline phase, and A_a = area of amorphous phase.

3.4.2 FTIR (Fourier Transform Infrared Spectroscopy)

FT-IR technique (Perkin-Elmer) was employed ranging from 4000 - 400 cm^{-1} to analyze "bond stretching" and "bending" of all samples which includes Pure PPy, hybrid PPy/WS_2, PPy/MoS_2, PPy/SnS_2 nanocomposites. Sample preparation involved combining a small amount of the polymeric sample with KBr powder, followed by the fabrication of a pellet. The FTIR analysis were used for the confirmation of PPy based composites and the presence of functional groups.

3.4.3 SEM (Scanning Electron Microscopy)

FE-SEM using a Jeol model instrument was employed to investigate the surface morphology of the samples. Cross-sectional images of pure PPy, and the hybrid PPy/WS_2, PPy/MoS_2, and PPy/SnS_2 nanocomposites were obtained at magnifications of 5,000x, 25,000x, and 50,000x. Due to the inherent conductivity of PPy and the resulting composites, samples could be directly placed in the instrument holder as pellets without any additional treatments to enhance conductivity.

3.4.4 TEM (Transmission Electron Microscopy)

This technique allows us to probe the internal structure of the matrix, the specific function of the filler material, and the resulting properties of the nanocomposite itself. HR-TEM was utilized to gain a deeper understanding of the morphology, or fine-scale structure, of the hybrid PPy/WS_2, PPy/MoS_2, and PPy/SnS_2 nanocomposites. The distinctive attributes of PPy-based composites were examined using a JEOL model for TEM imaging in high resolution mode, operating within a voltage range of 80 to 200 kV.

3.4.5 I-V (Current-Voltage) Measurements

To ensure consistent electrical measurements, two different pellet thicknesses were employed. Pure PPy pellets were prepared with a thickness of 2 mm, while PPy/WS_2 and

PPy/MoS_2 nanocomposite pellets were made 1 mm thick. Importantly, both types of pellets maintained a consistent diameter of 12 mm. The DC electrical resistance of PPy pellet as well as PPy/WS_2 and PPy/MoS_2 nanocomposites pellets were measured using electrometer (2410, Keithley) in the voltage range -1V to 1V. Prior to electrical measurements, the cross-sectional faces of the pellets were coated with silver paste. Samples resistivity was measured using two probe technique. Due to its high accuracy and minimal sample preparation requirements, the two-probe approach is the most widely used method for measuring semiconductor materials resistivity. It consists of "voltmeter", "two spring- loaded contact probes", "an ampere meter" and "DC current source". Using a hydraulic press and 2000 Pa of pressure, a sample was created for the measurement process. The sample was then dried, cleaned and tested. It was made sure to verify that the voltmeter, ampere meter, and DC current source were all turned on. The sample was positioned on the disk with the measurement area lined up beneath the probe tip. After a brief amount of time during which the voltage stabilized, the measurements were taken. New samples were introduced for testing after the old samples were discarded following sample testing. To determine the DC electrical conductivity of PPy, PPy/WS_2, and PPy/MoS_2 nanocomposites, the following equations were employed for the calculations.

3.4.6 Gas Sensing Measurements

Utilizing the electron-beam deposition method, we applied aluminum interdigitated electrodes (IDEs) onto a silicon (Si) substrate. The Interdigitated Electrodes (IDEs) had a finger thickness and spacing of 400 µm and 200 µm, respectively, with the substrate measuring 1 × 1 cm. Various compositions of PPy as well as hybrid PPy/WS_2, PPy/MoS_2 and PPy/SnS_2 nanocomposites were prepared by incorporating 1–2 drops of α-terpinol into a mortar and pestle. These compositions were then coated onto the prepared IDEs. To improve material adhesion to the electrodes, the coated IDEs were left to air dry at RT. Gas sensing experiments were conducted within a 1547 mL acrylic chamber that was outfitted with gas inlet and outlet ports. The chamber was equipped with a sample stage featuring a resistive heater, which was computer-controlled via a synchronized power supply. To control the concentration of the target gas in the chamber, a syringe system was linked to the chamber, and a vacuum pump attached to the outlet recovered the prepared sensors. By applying voltage and measuring current, the resistance of the sensors was examined. The entire system was computer-controlled and integrated with a Lab VIEW-based program. To conduct ammonia sensing tests, a calibration cylinder containing 1000 ppm NH_3 mixed

with dry air (20% O_2 and 80% N_2) as the baseline was utilized as the target analyte. The sensor response (%) was determined using the formula below:

$$R = \frac{R_g - R_a}{R_a} \times 100 \qquad \textbf{(3.2)}$$

In this context, R depicts “sensor response”, Ra is the “resistance in the air”, and Rg is the “resistance in the presence of the target gas”. The gas pulse was administered for a duration of 10 minutes to observe the response, followed by a 10-minute period for the sensors to recover.

CHAPTER FOUR

Results and Discussion

This chapter extensively covers the structural, electrical and morphological analysis of PPy synthesized with different oxidants, $FeCl_3$ and APS, as well as PPy-based nanocomposites incorporating metal sulfides (WS_2, MoS_2, and SnS_2). Various techniques such as" XRD, FT-IR, SEM, TEM, and electrical conductivity measurements" are thoroughly discussed for the analysis and validation of the prepared nanocomposites. Furthermore, the chapter delves into the gas sensing measurements of the PPy-based WS_2, MoS_2, and SnS_2 nanocomposites.

4.1 PPy with different oxidizing agent $FeCl_3$ and APS

The PPy samples were subjected to characterization using XRD, FTIR, and SEM techniques. The electrical resistance of all samples was determined using an electrometer.

4.1.1 Structural Study and Crystallinity Determination

The formation of PPy samples with various oxidants and percent crystallinity was confirmed by XRD characterization (**Figure 4.1**). According to previous literature, a broad peak was seen in each instance at about $2\Theta = 25^{\circ}$ for PPy with oxidant APS and $2\Theta = 27^{\circ}$ for PPy with oxidant $FeCl_3$ with hkl value = (140) [77].

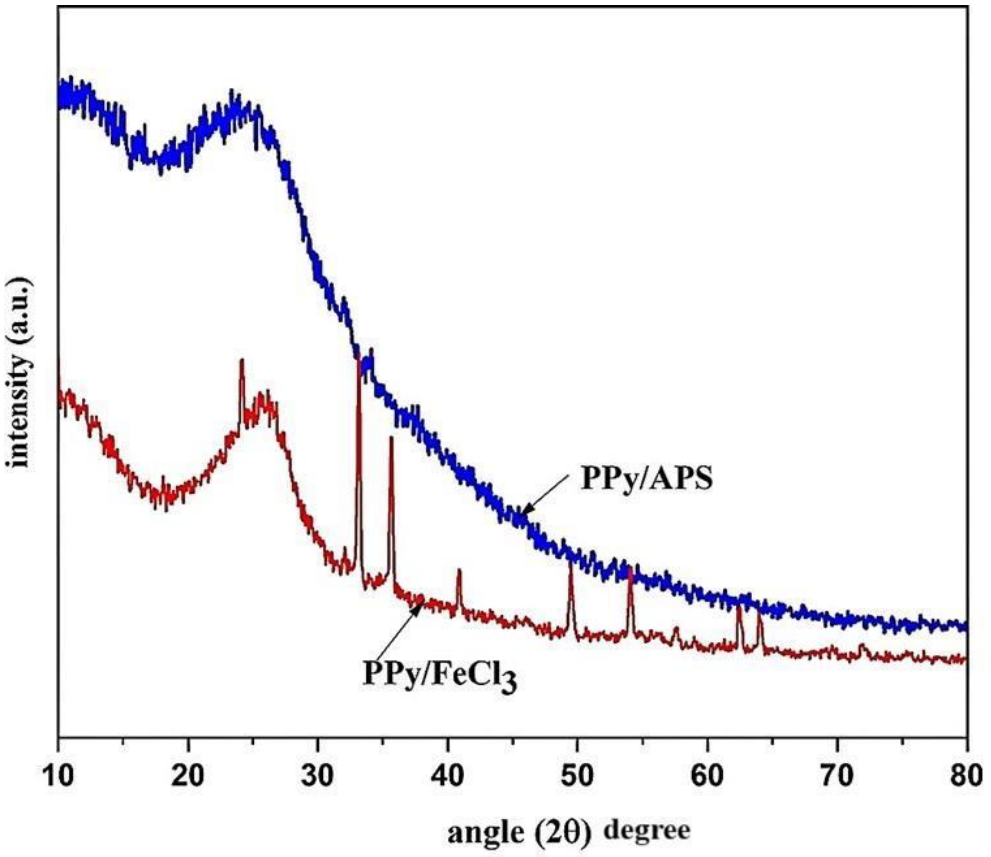

Figure 4.1 XRD graph of PPy/APS and PPy/$FeCl_3$

The wide peaks which are representative of amorphous PPy result from PPy polymeric chains being scattered at interplanar spacing. In the instance of PPy/$FeCl_3$, some distinct

peaks of higher and lower intensity are visible which may be due to the presence of iron. The XRD results clearly showed that PPy with oxidant $FeCl_3$ had a high degree of crystallinity [124,125]. The XRD pattern of PPy/$FeCl_3$ revealed distinct peaks at 25°, 32°, and 39°. These peaks closely match the expected diffraction angles (d-values) for iron (III) chloride ($FeCl_3$) corresponding to crystal planes (102), (104), and (110), respectively. This observation is consistent with the reference data from JCPDS card No. 13-534, indicating the presence of $FeCl_3$ within the PPy composite. The Scherrer equation is applied to calculate the average crystallite size in the material. This calculation is based on the broadening observed in the sharp peak at 25° and 27° in XRD pattern.

$$D = \frac{k\lambda}{\beta \cos\theta} \qquad (\mathbf{4.1})$$

The crystallite size, shape factor, diffraction angle and FWHM (full width at half maximum) are represented by symbol D, K, Θ and β respectively. When above equation is applied to the sharp peaks, the typical crystallite size for PPy/APS and PPy/$FeCl_3$ is about 24 nm and 27 nm, respectively.

4.1.2 Structural Study

FT-IR spectra have been carried out to validate synthesized PPy with both oxidizing agents. **Figure 4.2** shows the FTIR spectrum of PPy particles. Strong bands in the 1600-900 cm^{-1} region, which are characteristic of PPy indicate the formation of conductive type of polymer.

The characteristics PPy ring vibrations and C=C bond can be attributed to the bands at 1536 and 1699 cm^{-1} [126]. The band at 1026 cm^{-1} are for the in-plane deformation of C-H bond of pyrrole ring while the small peak below 1000 cm^{-1} are due to =C-H out of plane vibrations [127]. The peaks observed at 1147 cm^{-1} and 1176 cm^{-1} in the FT-IR spectrum are potentially indicative of in-plane vibrations originating from C-H bonds. These bands are also commonly referred to as bipolaron bands [128]. The broad peak observed around 3420 cm^{-1} in the FT-IR spectrum is likely attributed to O-H stretching vibrations. This signal is commonly associated with the presence of residual solvent molecules within the sample. The band at 690 cm-1, on the other hand, can be assigned to C-H vibration modes

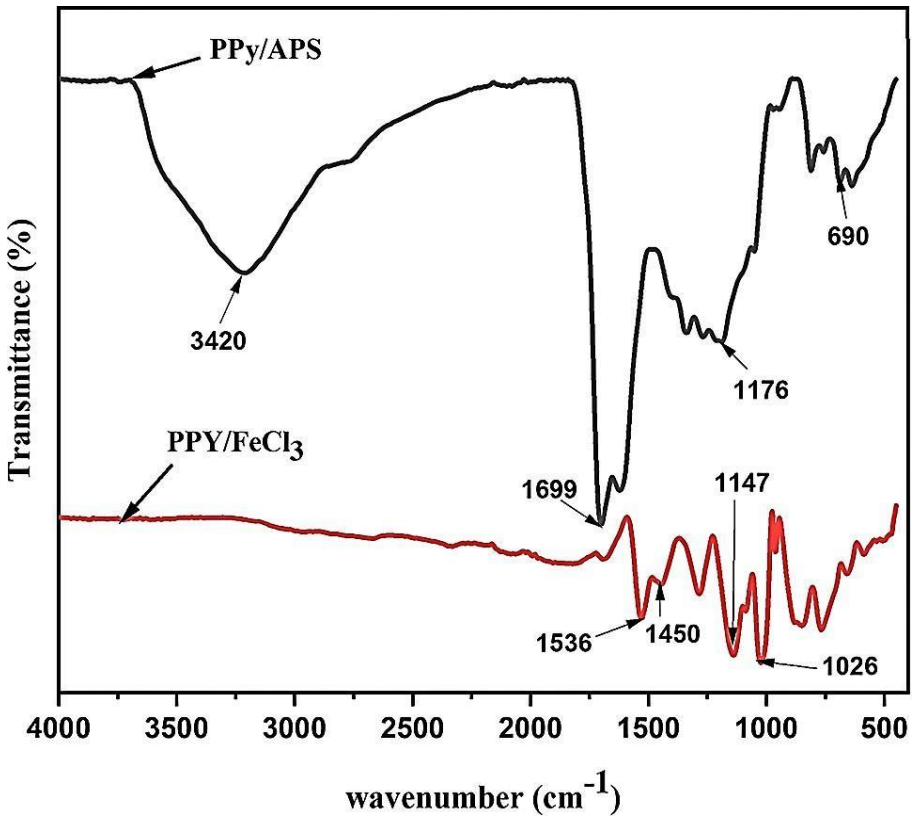

Figure 4.2 FTIR spectra of PPy/APS and PPy/$FeCl_3$

in the material [77,129].

From the figure, it can be observed that there is shifting in frequency from 1536 to 1699 cm^{-1}. It can be described by the equation for the bond of the natural vibrational frequency.

The reduced mass μ of the system is depicted as:

$$u = \frac{m_1 m_2}{m_1 + m_2} \qquad \textbf{(4.3)}$$

The mass of the molecule is reduced if peak shifts towards higher wave number side, as shown by Equations 4 and 5. Because relationship between frequency of vibration and mass of vibrating molecule are inversely related to one another. Therefore, lighter the molecule, more the vibration frequency and greater the wave number. According to above equation, the shifting of C=C bond shows the value of 1682 cm^{-1} as calculated value and 1650 cm^{-1} as experimental value.

4.1.3 Morphological analysis

The morphological characteristics of chemically synthesized have shown that the growth

occurs primarily in the globules like shape [73,130]. **Figure 4.3** displays typical SEM image. In the micrograph, globular structure is visible. Polymerization with APS resulted in the formation of PPy globules with an average diameter of 1.47 µm. Notably, the size distribution of these spherulites exhibited variations, ranging from 0.72 µm to 4.76 µm.

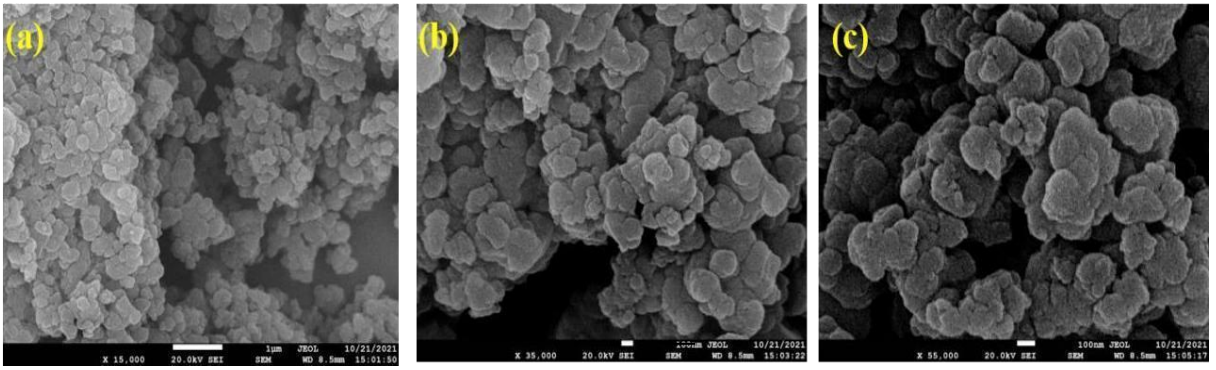

Figure 4.3 SEM micrographs of PPy/APS (a) 15000x, (b) 35000x and (c) 55000x

Analysis of the PPy globules formed during polymerization with $FeCl_3$ revealed an average size of 3.35 µm. The size distribution of these spherulites exhibited significant variation, ranging from as small as 0.66 µm - 12 µm as shown in **Figure 4.4.** The individual granules that were seen were spherical in shape and tightly packed. Such spherulites appear to form continuous structure by growing over the other. As is well known, the concentration of oxidant determines the size of PPy particles; the greater the concentration, the smaller the particles. The average particle size of PPy with oxidant APS decreases owing to the large number of nuclei produced by an increase in oxidant concentration [131].

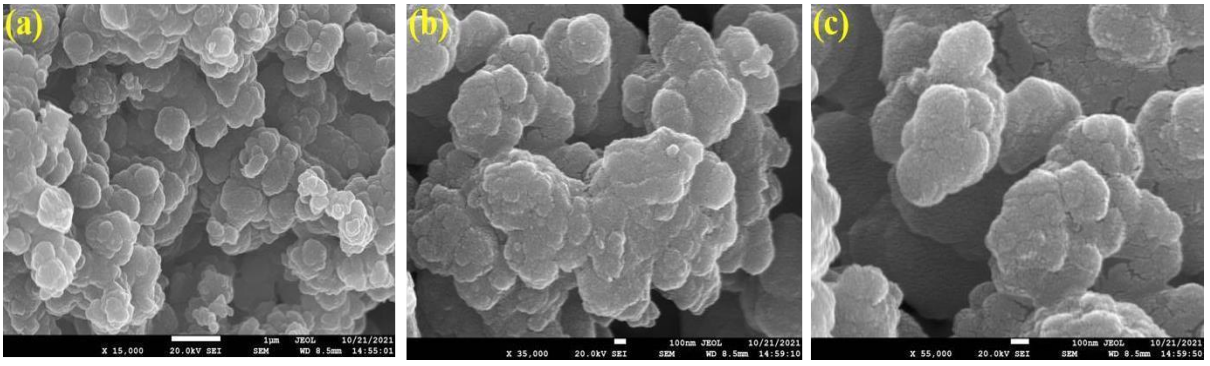

Figure 4.4 SEM micrographs of PPy/$FeCl_3$ (a) 15000x, (b) 35000x and (c) 55000x

Image J software was utilized to analyze the particle size distribution of PPy synthesized using APS and $FeCl_3$ oxidants and related histogram is shown in **Figure 4.5.** The analysis revealed an average particle size of 448 nm for PPy/APS and 240 nm for PPy/$FeCl_3$,

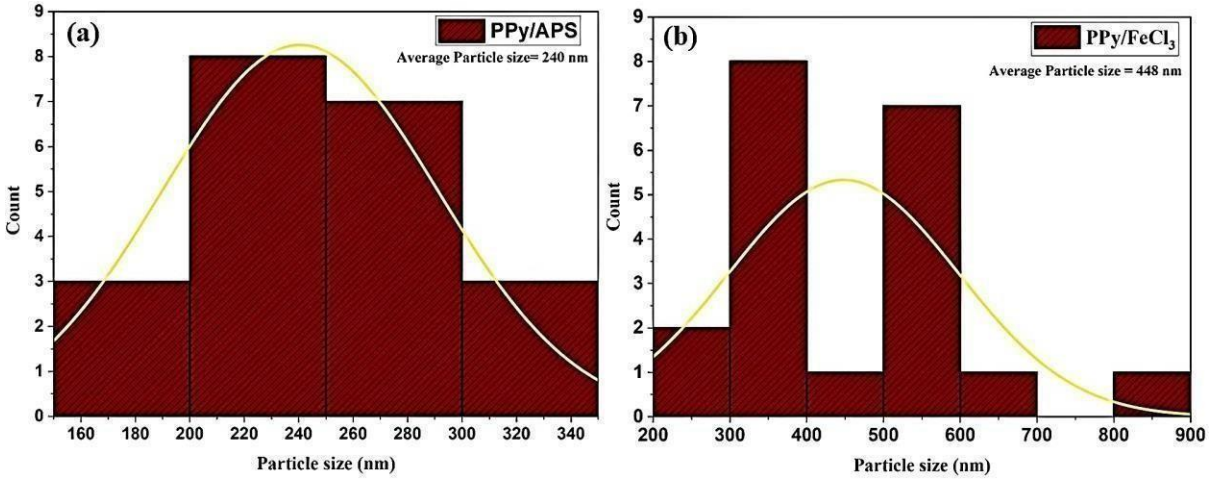

Figure 4.5 Average particle size (a) PPy/APS (b) PPy/$FeCl_3$

highlighting the influence of the chosen oxidant on the final particle size.

4.1.4 Electrical Conductivity

The current-voltage measurement for PPy synthesized using $FeCl_3$ and APS as oxidants is depicted in **Figure 4.6**. The graph illustrates the cubical parabolic nature of the voltage between -1V and 1V measured at room temperature. Upto 0.61 V, both show almost ohmic behavior or linear current growth. Beyond 0.61 V, the current was increasing a little bit steadily displaying non-ohmic nature. Both show ohmic behavior between -2V and 2V up to 0.81 V, after which there is a slight increase in current, indicating non-ohmic behavior.

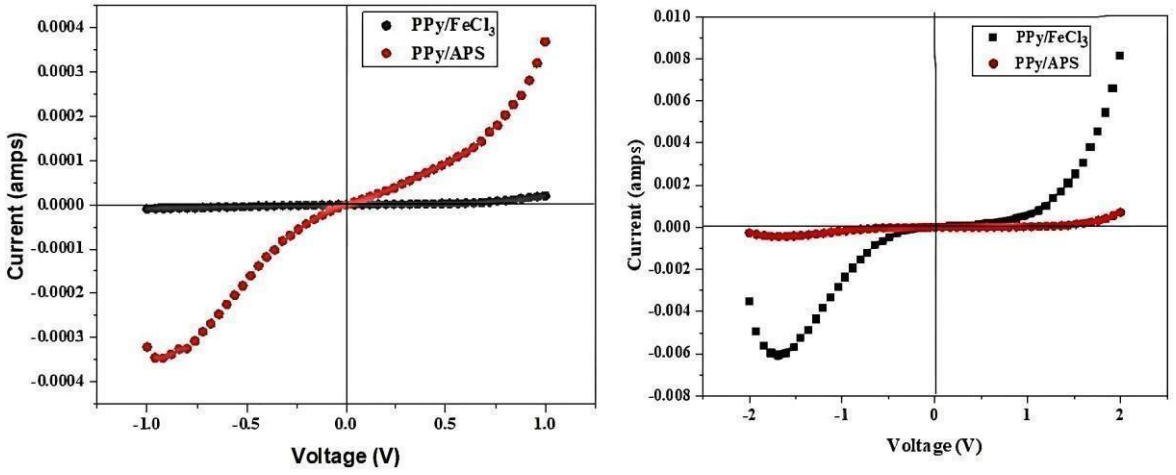

Figure 4.6 Current-voltage characteristics of PPy with oxidant $FeCl_3$ and APS

Conductivity values for PPy with oxidant $FeCl_3$ are slightly higher than that of PPy with oxidant APS as seen from the graph. The value of conductivity of PPy with oxidant APS is 0.16×10^{-4} Scm^{-1} and PPy with oxidant $FeCl_3$ is 2.22×10^{-4} Scm^{-1}. The reason for the high conductivity of PPy/ $FeCl_3$ as compared to PPy/APS is due to the presence of iron ions. This shows that amino groups in the pyrrole rings contribute π–electron to the aromatic network in the PPy chain, reducing their electron density in the process. The conjugated

system creates a donor-acceptor complex when $FeCl_3$ is added to the polymer. As a result, quasi-particles are produced that function as charge carriers and are probably polarons. The polarons show low conductivity and low mobility at low dopant concentrations. A greater amount of Cl^- is bound to the pyrrole ring in the backbone of the polymer chain as the polymerization process continues with more doping. At this moment, numerous polarons are generated and crowded together to gather sufficient energy to create bipolarons [132–134].

In the instance of PPy, the lack of electron results in the formation of holes, or p-type conduction in the chain, which allows for the modification of the energy level by the addition of dopants. The radical cation is then linked via rearrangement, and a bond sequence resembling a quinoid is created. The band gap is symmetrically occupied by empty bipolaron states, and as polymers are continuously doped, more localized bipolaron states are produced. These states eventually overlap to make continuous bipolaron bands. While the polymer band gap widens due to doping, bipolar bands tend to combine with CB and VB and give metal-like conductivity, as shown in **Figure 4.7**. This increases charge carriers' mobility, which leads to a rise in conductivity [87]. **Table 4.1** shows a comparison of PPy conductivity with previous literature.

Table 4.1 Comparison of proposed electrical conductivity of PPy with previous literature.

PPy with different oxidants	**M/O ratio**	**Electrical Conductivity**	**Proposed Electrical Conductivity**	**Reference**
$FeCl_3$	1:2	2.49×10^{-5} S/cm	-	[135]
$FeCl_3$	1:1	1.55 S/cm	-	[136]
APS	1:2	0.6×10^{-3} S/cm	-	[137]
APS	1:1	0.0135 S/cm	-	[138]
$FeCl_3$	1:2	-	2.22×10^{-4} S/cm	-
APS	1:2	-	0.16×10^{-4}S/cm	-

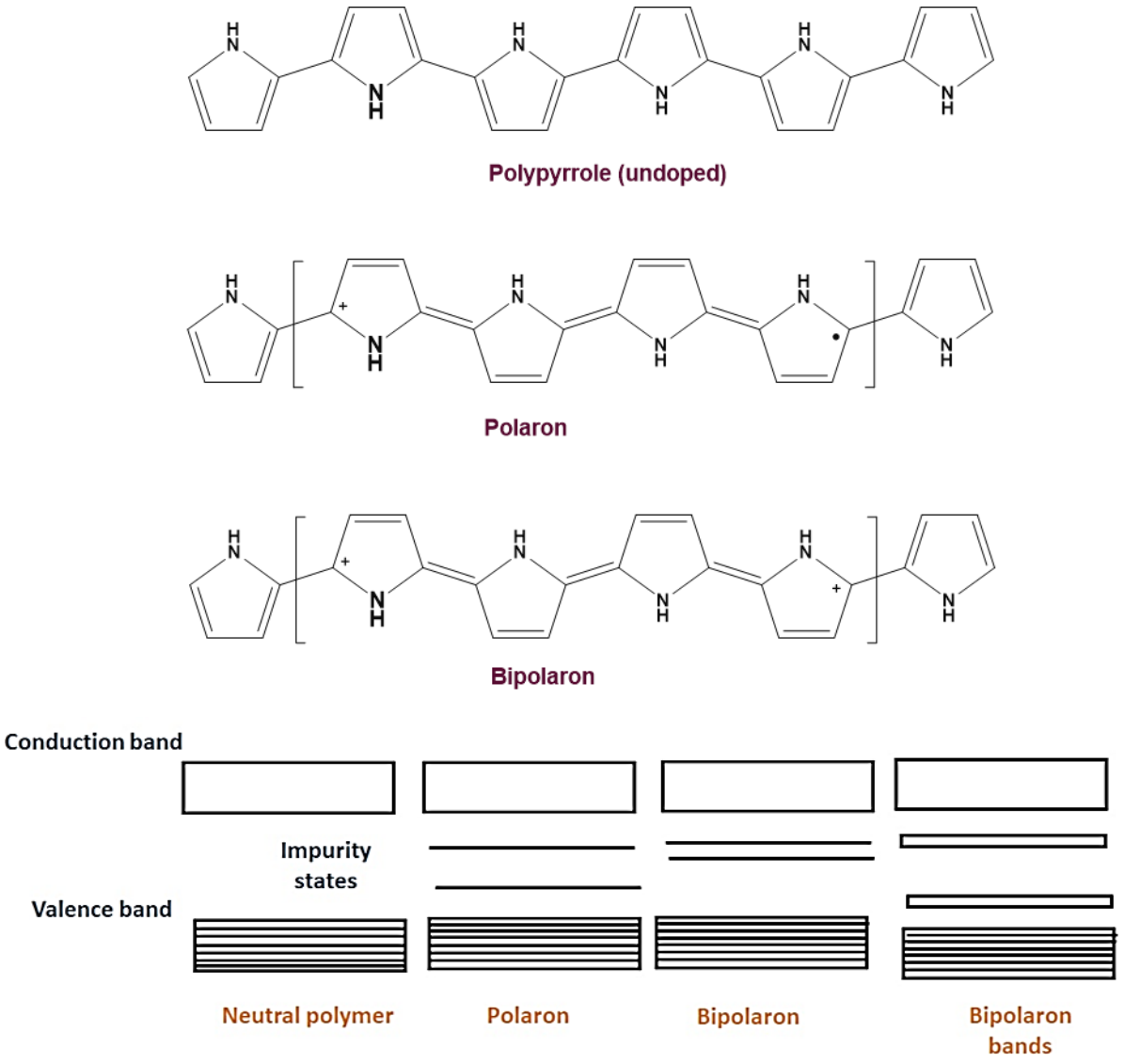

Figure 4.7 Mechanism of polaron and bipolaron in PPy and their energy states.

As indicated in the XRD results, the crystallinity of PPy with oxidant $FeCl_3$ is high as compared to PPy with oxidant APS. Subsequently, the conductivities of nanocomposites increases due to enhanced crystallinity of polymer.

4.2 PPy/WS_2 Nanocomposites

PPy/WS_2 Nanocomposites were prepared with different WS_2 content as given in **Table 4.2.** Before preparing nanocomposites pure PPy were kept fixed. The prepared nanocomposites were characterized using XRD, FTIR, SEM and TGA techniques. The DC electrical conductivity was also measured using electrometer.

Table 4.2 Weight percentages of WS_2 filler in PPy matrix

Sr No.	Weight %
1	1
2	5
3	10
4	20
5	30

4.2.1 Structural Study and Crystallinity Determination

The formation of PPy and PPy/WS_2 (1 wt%, 5 wt%, 10 wt%, 20 wt% and 30 wt%) and percentage crystallinity were confirmed by the analysis of XRD patterns shown in **Figure 4.8**. The broad peak observed at $2\theta = 25^{\circ}$ clearly shows that PPy has an amorphous behaviour due to the more coiled polymeric chains. The broad peak, which is indicative of amorphous PPy is the product of X-rays being scattered by the PPy chain [77]. Bare WS_2 with designated (hkl) values evidence its important peaks at Bragg angles $2\theta = 14.4^{\circ}$, 28.9°, 32.7°, 33.5°, 39.5°, 44°, 49.7°, 58.4° and 60.5° with hkl values (002), (004), (100), (101), (103), (006), (105), (110) and (112) planes respectively. Obtained data have been confirmed using JCPDS file No. 08-237. Figure 2 depicts the XRD of PPy/WS_2 (1 wt%, 5 wt%, 10 wt%, 20 wt% and 30 wt%) where the broad peak of PPy is suppressed and hardly noticeable due to the existence and predominance of crystalline WS_2 in the composite, indicating the PPy-deposited WS_2 and its crystalline nature.

Using Scherrer's method, the crystallite sizes of the PPy were calculated from X-ray line broadening. The equation results in various crystallite sizes for each sample when applied to the distinctive peak (002 plane) of WS_2 shown in **Table 4.3**.

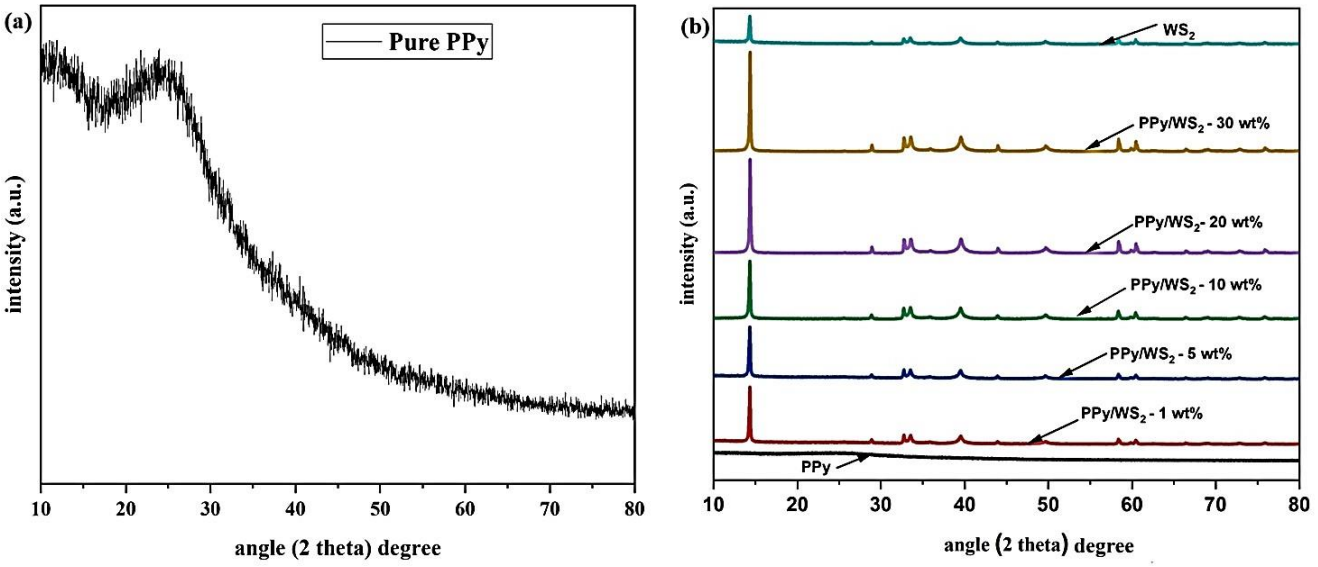

Figure 4.8 (a) XRD spectra of pure PPy (b) XRD spectra of pure PPy, PPy/WS_2- 1 wt%, PPy/WS_2- 5 wt%, PPy/WS_2- 10 wt%, PPy/WS_2- 20 wt%, PPy/WS_2- 30 wt%, pure WS_2.

Table 4.3 XRD data of pure PPy and PPy/WS_2 nanocomposites

Sample name	2θ (◦)	d-spacing (A◦)	FWHM (A◦)	β (Radian)	Cos θ (◦)	T (nm)
Pure WS_2	14.40	6.14	0.234	0.0087	0.9999	35.34 nm
PPy/WS_2- 1 wt%	14.40	6.14	0.195	0.0087	0.9999	40.63 nm
PPy/WS_2- 5 wt%	14.50	6.10	0.227	0.0089	0.9999	41.14 nm
PPy/WS_2-10 wt%	14.55	6.08	0.182	0.0090	0.9999	43.19 nm
PPy/WS_2-20 wt%	14.50	6.10	0.190	0.0056	0.9999	49.00 nm
PPy/WS_2-30 wt%	14.28	6.19	0.207	0.0059	0.9999	50.01 nm

The XRD pattern of WS_2 NPs makes it abundantly obvious that they are single phase in nature. There was no secondary phase detected and the high intensity of the peaks revealed the crystalline nature of as WS_2 nPs. The diffraction peaks of WS_2 NPs appear in the PPy/WS_2 from the **Figure 4.9**, the intensity of these peaks becomes stronger with increase in the nanoparticle loadings, while peak of PPy at 2θ = 25˚ shows a reduced intensity.

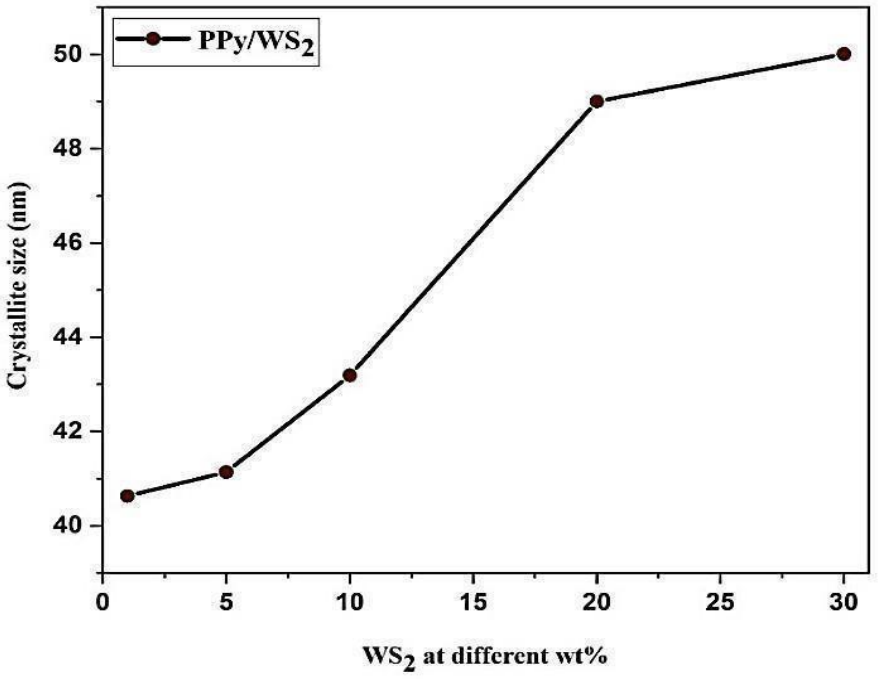

Figure 4.9 Variation of crystallite size at different weight % of nanocomposites.

The XRD pattern also confirm the presence of tungsten disulfide in the PPy/WS_2 (1 wt%, 5 wt%, 10 wt%, 20 wt% and 30 wt%) nanocomposites the crystallite size as calculated, where the average crystallite size are 40.63 nm (1 wt%), 41.14 nm (5 wt%), 43.18 nm (10 wt%), 49 nm (20 wt%) and 50.02 nm (30 wt%) and 33.56 nm (pure WS_2). As shown in Figure 5.2, the appearance of peaks with a slight shift in the diffraction angles for planes suggest that the nanocomposites is semicrystalline with tiny crystallites embedded in amorphous PPy.

4.2.2 Structural study

The FT-IR spectra of pure PPy, PPy/WS_2 (1 wt%, 5 wt%, 10 wt%, 20 wt% and 30 wt%) nanocomposites and pure WS_2 are shown in **Figure 4.10**. The main transmittance peaks of PPy are appeared at 3225 cm^{-1} and 1709 cm^{-1} could be corresponded to the O-H stretching vibration and C=C stretching vibration in the PPy ring, respectively. The band at 1341 cm^{-1} is assigned to N-H bending vibration bond. The bands at 1147 cm^{-1} and 1176 cm^{-1} may match to =C-H in-plane vibration but the band located at 1026 cm^{-1} is for the in-plane deformation of C-H bond of pyrrole ring while the minor peak below 1000 cm^{-1} are attributable to =C-H out of plane vibrations indicating the polymerization of polypyrrole respectively [121,139–141]. When FT-IR spectra of PPy nanocomposites of varying weight percentages of WS2 were compared with pure PPy, it was observed that major characteristics peak of PPy were present with a slight shift in some of the absorption frequencies.

Different types of dopants in the PPy backbone may disturb the conjugate structure of PPy due to which it limits the extent of charge delocalization of polymer chains, leading to downward shift. However, as for PPy/WS_2, except the peaks of PPy, the band at 614 cm^{-1} and 812 cm^{-1} are attributed to W-S stretching and S-S stretching, suggesting that the WS_2 was embedded in PPy matrix [142]. The results indicates that there are some interactions between PPy and WS_2 [143].

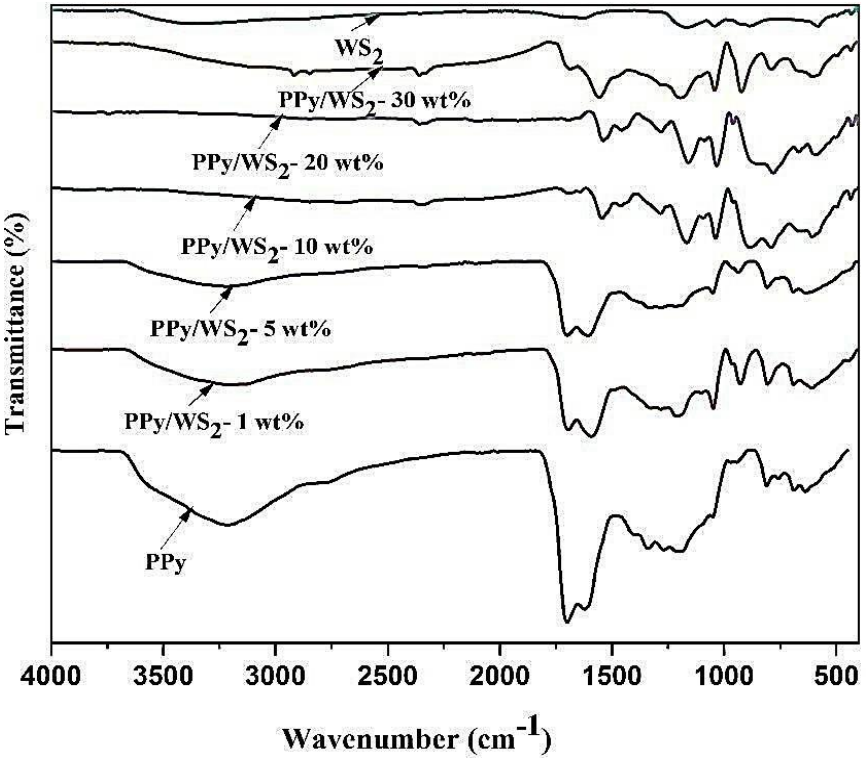

Figure 4.10 FT-IR spectra of pure PPy, PPy/WS_2- 1 wt%, PPy/WS_2- 5 wt%, PPy/WS_2- 10 wt % , PPy/WS_2- 20 wt %, PPy/WS_2- 30 wt % and pure WS_2.

In the spectrum of PPy/WS_2, all the characteristics peaks of PPy were observed which were weakend and shifted at smaller wavelengths. The characteristics peak observed at 3225 cm^{-1}, 1709 cm^{-1}, 1341 cm^{-1} in the spectrum of PPy were detected at 3216 cm^{-1}, 1700 cm^{-1}, 1327 cm^{-1} for PPy/WS_2 (1 wt%); 3130 cm^{-1}, 1700 cm^{-1}, 1327 cm^{-1} for PPy/WS_2 (5 wt%); 3100 cm^{-1}, 1653 cm^{-1}, 1298 cm^{-1} for PPy/WS_2 (10 wt%); 3000 cm^{-1} , 1648 cm^{-1}, 1275 cm^{-1} for PPy/WS_2 (20 wt%) and 3000 cm^{-1}, 1630 cm^{-1}, 1265 cm^{-1} for PPy/WS_2 (30 wt%) respectively, in the spectrum of PPy/WS_2. **Table 4.4** displays the transmittance peaks and associated stretching vibration of pure PPy and PPy/WS_2 nanocomposites. As the wt% increases in case of PPy/WS_2, this may cause WS_2 particles to be dispersed in nanocomposites with broader size distribution.

The characteristic peaks of PPy/WS_2 slightly shifted to higher wavelength when compared to pure PPy, suggesting interaction at the interface. Additionally, PPy/WS_2 characteristic peaks are well preserved in the nanocomposites, proving that PPy has been effectively combined with WS_2 without altering its chemical structure. Peaks of PPy/WS_2 shifts towards lower wavenumber when compared to equivalent peaks of pure PPy. This shifting of absorption bands may be caused by synergistic/electronic interaction acting at molecular levels between PPy chains and WS_2 [144].

Table 4.4 FTIR data of pure PPy and PPy/WS_2 nanocomposites

Sample name	**O-H stretching vibration (cm^{-1})**	**C=C stretching vibration (cm^{-1})**	**N-H bending vibration (cm^{-1})**	**=C-H in plane bending vibration (cm^{-1})**	**=C-H out of plane bending vibration (cm^{-1})**	**W-S stretching vibration (cm^{-1})**	**S-S stretching vibration (cm^{-1})**
Pure PPy	3225.06	1709.95	1341.34	1176.42	812.93	-	-
PPy/WS_2 - 1 wt%	3216.47	1700.03	1327.49	1175.19	807.93	574.22	781.35
PPy/WS_2 - 5 wt%	3130.99	1700.04	1327.42	1170.81	803.78	544 .45	766.45
PPy/WS_2 - 10 wt%	3100.25	1653.11	1298.41	1162.51	780.87	490.43	747.56
PPy/WS_2 - 20 wt%	3000.03	1648.00	1275.78	1162.51	779.56	460.32	736.34
PPy/WS_2 - 30 wt%	3100.18	1630.96	1265.74	1160.42	775.45	441.45	728.21
Pure WS_2	-	-	-	-	-	614	812

4.2.3 Morphological analysis of PPy/WS_2 Nanocomposites

The surface morphology of the prepared PPy and its nanocomposite with WS_2 filler has been analyzed with field emission-scanning electron morphology. **Figure 4.11 (a)** depicts the FE-SEM image of pure WS_2 revealing 2D layered structure of WS_2 in the form of sheets. These bundle of sheets are having an area of few micrometers. **Figure 4.11 (b) and Figure 4.11 (c)** refers to PPy/WS_2- 5 wt% nanocomposite respectively showing WS_2 sheets are uniformly distributed in the PPy matrix. In case of PPy/WS_2- 30 wt% nanocomposite **(Figure 4.12)**, the morphology confirms the highly agglomerated structures of the composite, wherein WS_2 appears to be just embedded in the matrix of PPy.

The amalgamation of WS_2 into PPy matrix has resulted in substantial morphological changes in the composite as a hole, such that these changes enhance the ordered chain arrangement of PPy and increase crystalline domain in the amorphous material [143].

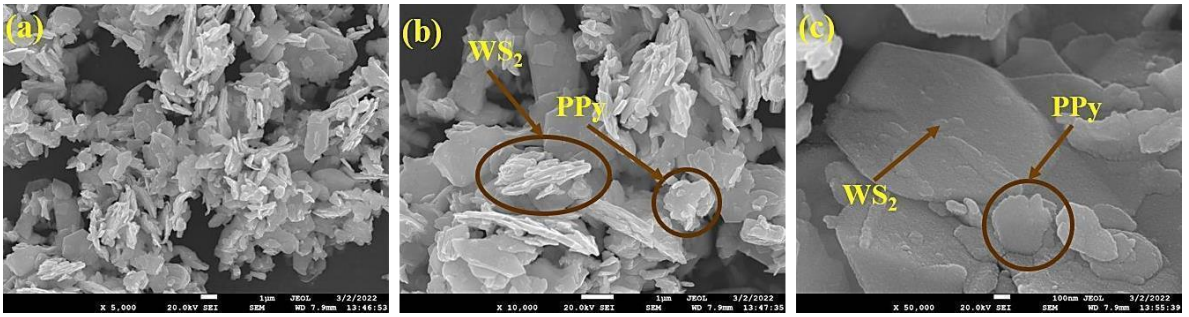

Figure 4.11 FE-SEM images of (a) Pure WS_2 (b) PPy/WS_2- 5 wt% (10,000X) (c) PPy/WS_2- 30 wt% (50,000X).

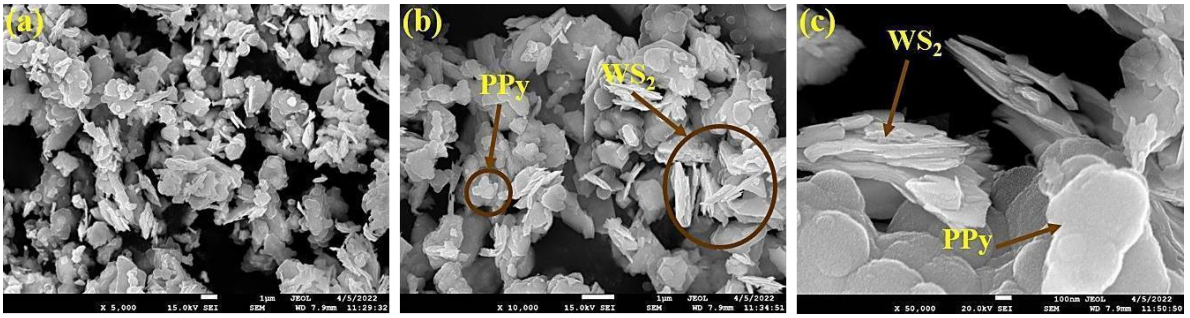

Figure 4.12 FE-SEM images of (a) PPy/WS_2- 30 wt% (5000X) (b) PPy/WS_2- 30 wt% (10,000X) (c) PPy/WS_2- 30 wt% (50,000X).

The confirmation of the 2D structure of WS_2 in the matrix of PPy has been done with TEM study **(Figure 4.13)**. Figure 4.14 (a) shows the 2D sheets like structure of WS_2. However, the existence of PPy and WS_2 is clearly seen from Figure 4.14 (b). The obtained micrograph from TEM has good agreement with the FE-SEM results too.

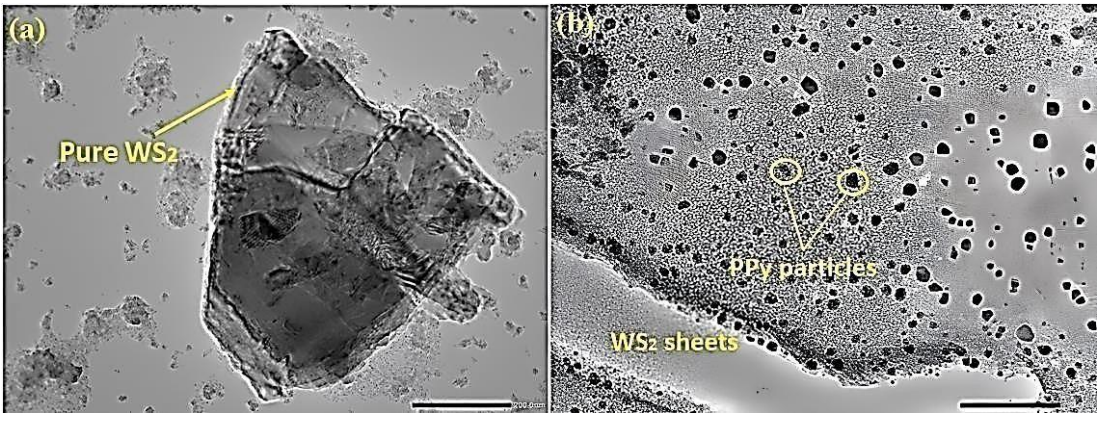

Figure 4.13 TEM images of a) Pure WS_2 b) PPy/WS_2 nanocomposite.

4.2.4 Electrical Conductivity

The DC electrical conductivity of PPy and its nanocomposites with varied weight % of WS_2 content has been measured by two probe method. PPy and its nanocomposites shows room temperature conductivities of 2.22 x 10^{-4} S/cm for PPy, 2.72 x 10^{-4} S/cm for PPy/WS_2- 10 wt% and 0.32 x 10^{-4} S/cm for PPy/WS_2- 20 wt%. The measurement shows that the electrical conducting value of nanocomposites are significantly higher than PPy. The current-voltage characteristic plots for each nanocomposites shows ohmic behavior up to 1 V, however beyond it, it shows non-ohmic behaviour. All plots show very good linearity over a wide range of applied current. The variation in DC electrical conductivity with 10 wt% and 20 wt% of WS_2 content in PPy nanocomposites is given in **Figure 4.14** and shows higher DC electrical conductivity for PPy/WS_2- 10 wt%.

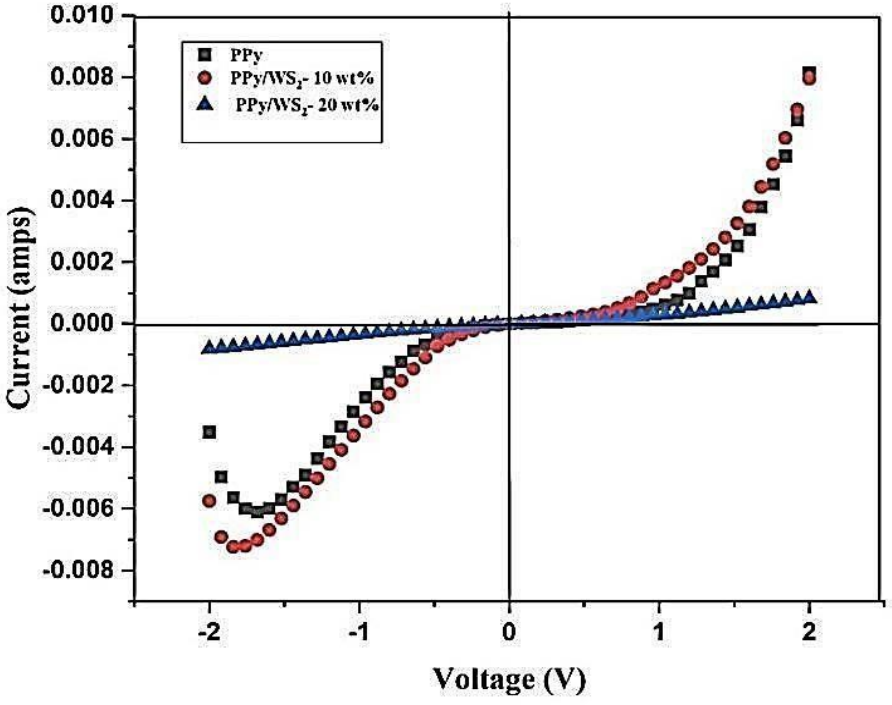

Figure 4.14 Current-Voltage characteristics plot of PPy/WS_2 nanocomposites.

The sharp increase in DC electrical conductivity may be due to particle network / packing dependent electron transport behavior [145]. This means that the particle loading of this level facilitate the hopping of charge carrier through polymer chain and provide better physiochemical linkages between PPy and WS_2 particles**.** The composite with 20 wt% of WS_2 filler shows electrical conductivity less than that of 10 wt% of WS_2. From the graph, the PPy nanocomposites with 20 wt% WS_2 have low electrical conductivity which may ascribed to the low electrical conductivity of filler and reduced fraction of PPy matrix.

Another reason may be also be the increase in the disorderliness in the nanocomposite and reduction in favourable localized sites due to conformational changes in the PPy matrix [143,146].

4.2.5 Ammonia sensing properties

In order to demonstrate the effect of different loading ratio of WS_2 on the gas sensing performance of PPy/WS_2 nanocomposites, a serious of sensors with different WS_2 loading ratio were investigated to make a comparison. The prepared PPy-based sensor was used to perform sensing measurements for ammonia concentrations ranging from 50 to 200 ppm at room temperature, and the findings are displayed in **Figure 4.15**. The PPy-based sensor showed a high response value for increasing ammonia concentrations and provided a suitable value of response for low concentration (50 ppm) of NH_3.

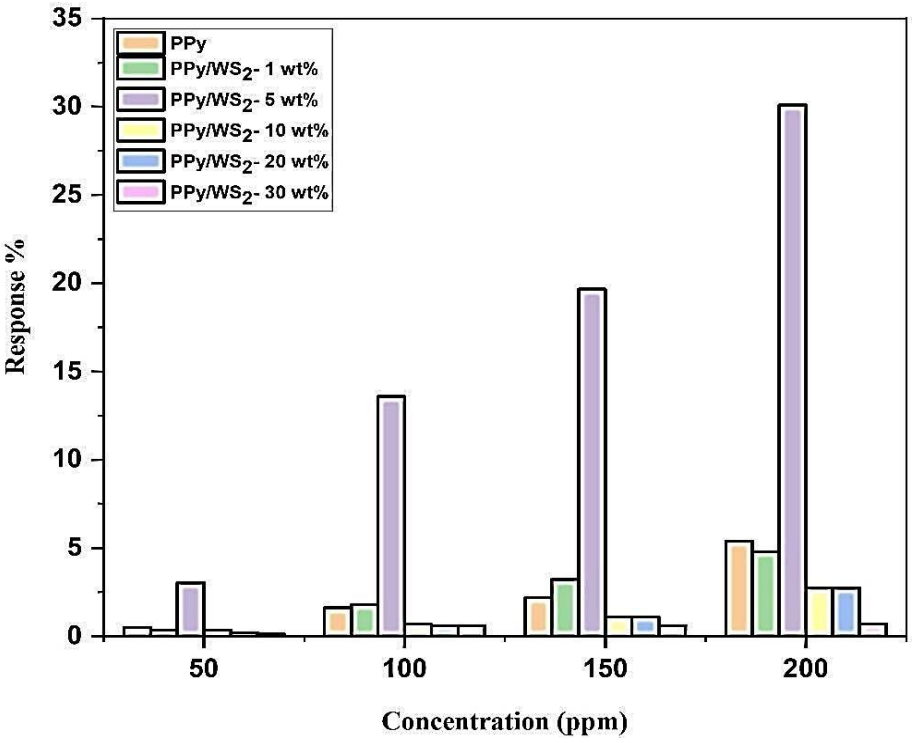

Figure 4.15 Gas sensing measurements of pure PPy and PPy/WS_2 (1 wt%, 5 wt%, 10 wt%, 20 wt% and 30 wt%) nanocomposites for 50-200 ppm NH_3 at room temperature.

Due to the fact that polypyrrole is a p-type material, the interaction with reducing gas NH_3 causes the hole-electron recombination phenomenon, which results in a decrease in the hole concentration and an increase in the resistance of PPy [147]. A significant rise in response could be due to the large number of adsorbed target gas molecules at 200 ppm concentration. Because of its good electrical and chemical properties.

Tungsten disulfide (WS_2) is considered to be known as highly efficient sensing materials. So, adding WS_2 into the PPy matrix will certainly improve the gas sensing properties. In consideration of this aspect, the gas sensing measurements of PPy/WS_2 nanocomposites containing different weight percentages of WS_2 ranging from 1 wt%, 5 wt%, 10 wt%, 20 wt% and 30 wt% were taken for various concentrations of NH_3 at room temperature. A comparison of pure PPy and PPy/WS_2 (1 wt%, 5 wt%, 10 wt%, 20 wt% and 30 wt%) for 50-200 ppm concentration of ammonia at 28 ˚C is shown in Figure 8. The dynamic resistance curve of PPy/WS_2- 5 wt% nanocomposite, as shown in **Figure 4.16 (a)**, demonstrates resistance change of flexible sensors on exposure of various concentrations of NH_3 ranging from 50 to 200 ppm. This also indicates that off-state terminal resistance (R_a) for PPy/WS_2- 5 wt% leads to reduction in the band gap due to WS_2 doping. Due to the utilization of atmospheric air at the time of recovery, the stability of air resistance (R_a) is unstable. **Figure 4.16 (b)** reveals the superior sensing performance of PPy/WS_2- 5 wt% nanocomposite based sensor. The result also demonstrates a linear relation between the response values and ammonia concentration. At high concentrations, a high increase in response is due to the exposure of a large quantity of target molecules that were adsorbed on the surface of sensing element. As can be seen, the nanocomposite prepared by in-situ approach exhibits superior sensing results, which could be due to a large number of interwine between two materials and a higher number of adsorption sites available for target gas molecules on the surface of prepared nanocomposites.

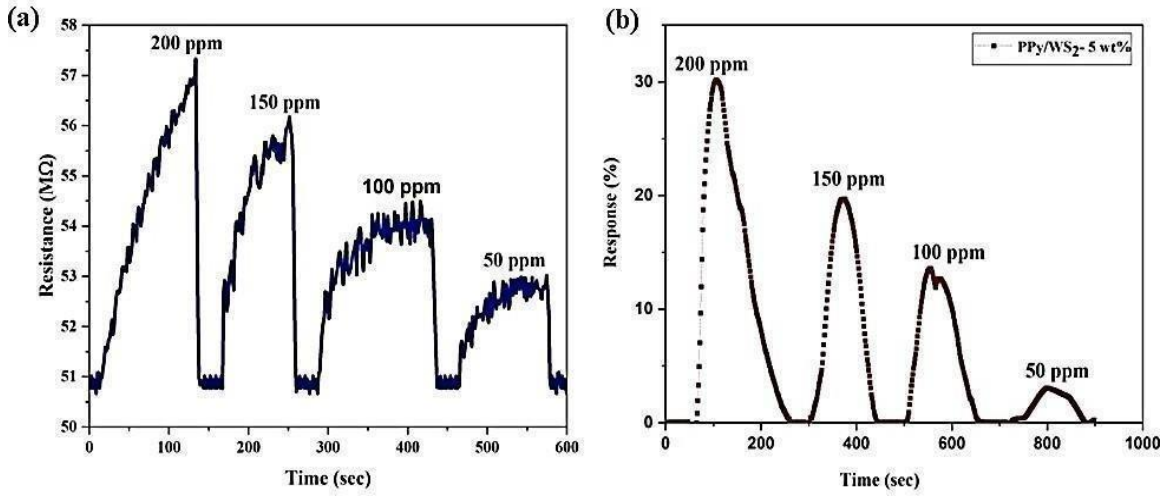

Figure 4.16 (a) Dynamic resistance curve for PPy/WS_2- 5 wt% sensors for various concentrations of NH_3. (b) Response characteristics of PPy/WS_2- 5 wt% nanocomposite synthesized by in-situ approach for 50-200 ppm ammonia at 28˚C.

In addition, as shown in **Figure 4.17**, a volcano curve can be seen for response values of all prepared PPy/WS_2 (1 wt%, 5 wt%, 10 wt%, 20 wt% and 30 wt%).

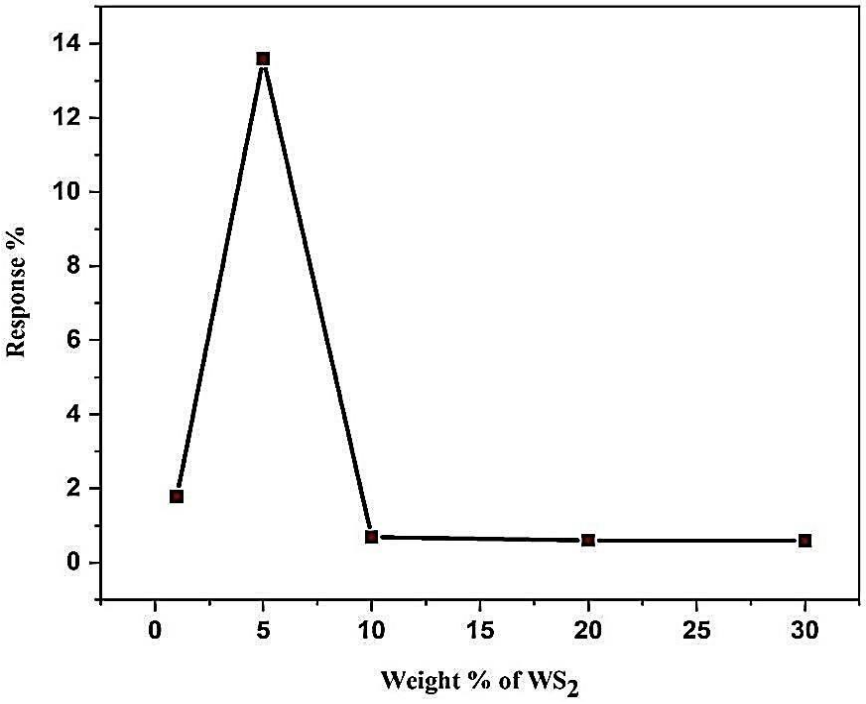

Figure 4.17 Response values of PPy/WS_2 (1 wt%, 5 wt%, 10 wt%, 20 wt% and 30 wt%) nanocomposites sensors at 100 ppm ammonia.

Ra values for PPy/WS_2 at different weight% is predicted in **Figure 4.18**.

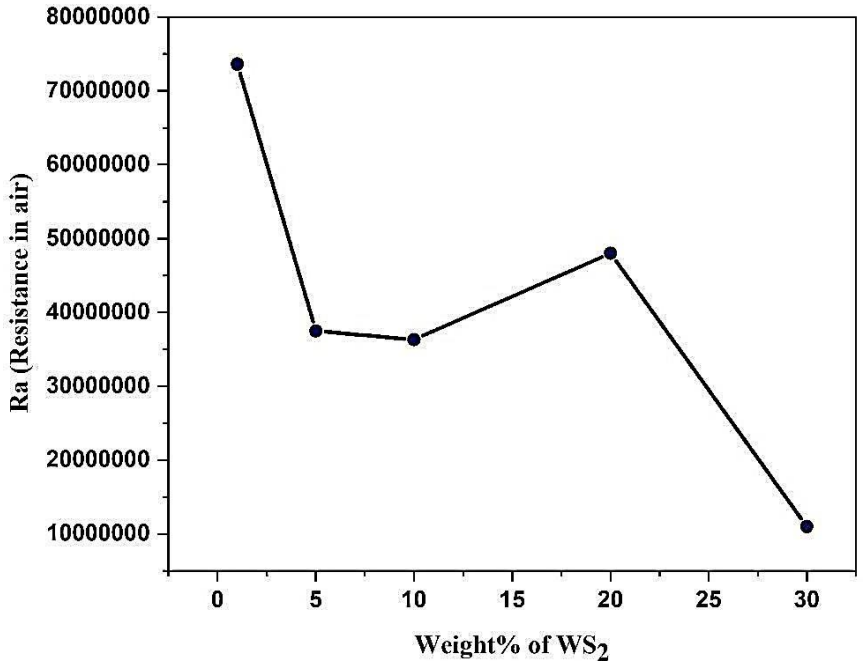

Figure 4.18 R_a values of PPy/WS_2 (1 wt%, 5 wt%, 10 wt%, 20 wt% and 30 wt%) nanocomposites sensors.

The response values under different operating temperature for in-situ synthesized PPy/WS_2 at 100 ppm NH_3 is shown in **Figure 4.19**. The response values decrease with increasing temperature. For conducting polymers, the desorption rate increases with temperature while the adsorption rate decreases which could be attributed to reduced response.

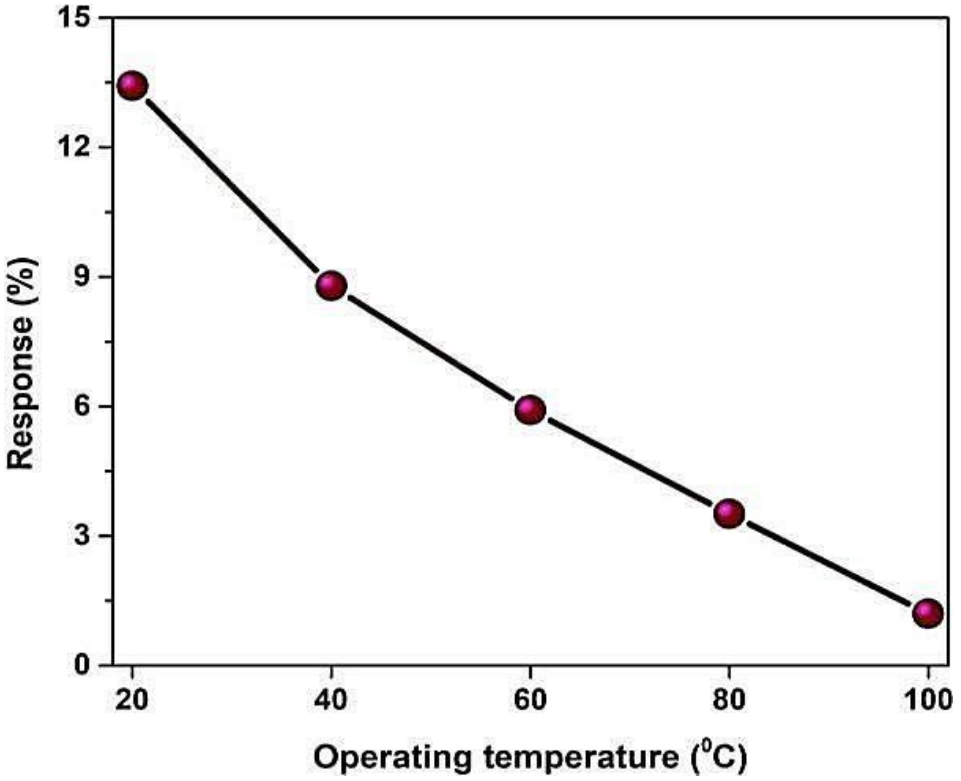

Figure 4.19 Response variation under various operating temperatures

In comparison with pure PPy, which displays 5.39% response for 200 ppm NH_3. In comparison to other nanocomposite-based sensors, the PPy/WS_2- 5 wt% based sensor exhibited the highest response of 30.10% for 200 ppm NH_3. Furthermore, the gas sensor repeatability also plays a major role in gas sensing as it describes the ability of sensor to provide the same result under same circumstances over and over again under the same conditions. It also plays a key role in determining product reliability. The proposed PPy/WS_2 nanocomposite synthesized by in-situ method was examined for 6 consecutive cycles, as shown in **Figure 4.20 (a)**. The results reveal highly stable fluctuations values on exposure of 100 ppm NH_3 for 6 consecutive cycles with shifting between air and ammonia. On the other hand, selectivity was also examined for in-situ synthesized PPy/WS_2- 5 wt% nanocomposite by adding several gases including H_2, EtOH, CO, CO_2 and NH_3 at 28 ˚C. Selectivity provides information on the material specific response toward certain gas as shown in **Figure 4.20 (b)**. When compared to other gases, ammonia gas had the highest

response, which illustrates the highly selective nature of the proposed ammonia gas. As a result, the ammonia selectivity at 100 ppm is around 3.77, 2.27, 1.101, 3.004 for H_2, EtOH, CO and CO_2 respectively. **Figure 4.20 (c)** shows long-term stability of PPy/WS_2 sensor upon exposure to 100 ppm NH_3 gas. The response of the sensor was examined for 4 weeks and it is observed that there is no great variation over a long-term of four weeks. The gas sensor demonstrates reliable response even at low concentrations such as 50 ppm, highlighting its effectiveness in detecting trace amounts. This capability makes the gas sensor ideal for real-time monitoring of ammonia, offering early detection capabilities.

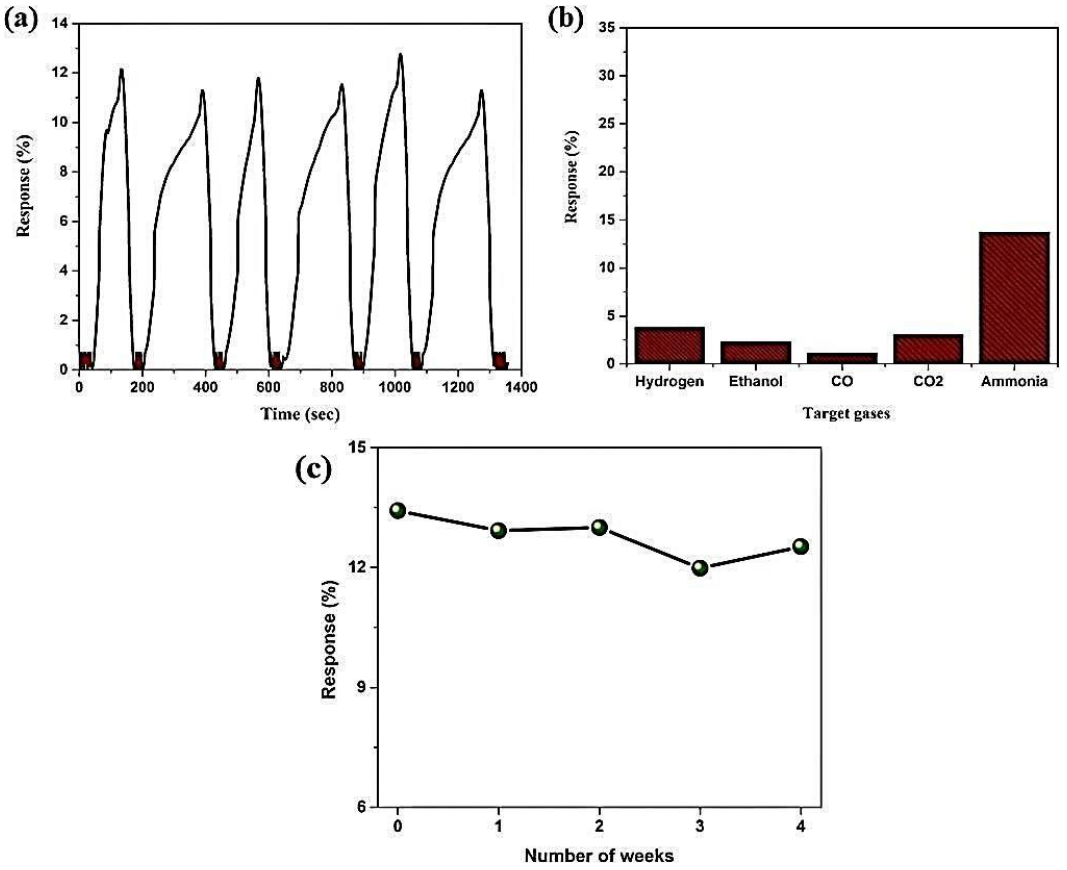

Figure 4.20 (a) Repeatability measurement of PPy/WS_2 – 5 wt% nanocomposite for consecutive 6 cycles of 100 ppm NH_3 (b) response values for 100 ppm H_2, EtOH, CO, CO_2 and NH_3 (c) long-term stability of sensor till 4 weeks.

Additionally, **Figure 4.21** shows response-recovery time of in-situ synthesized PPy/WS2-5 wt% nanocomposite of 51/79 sec.

.

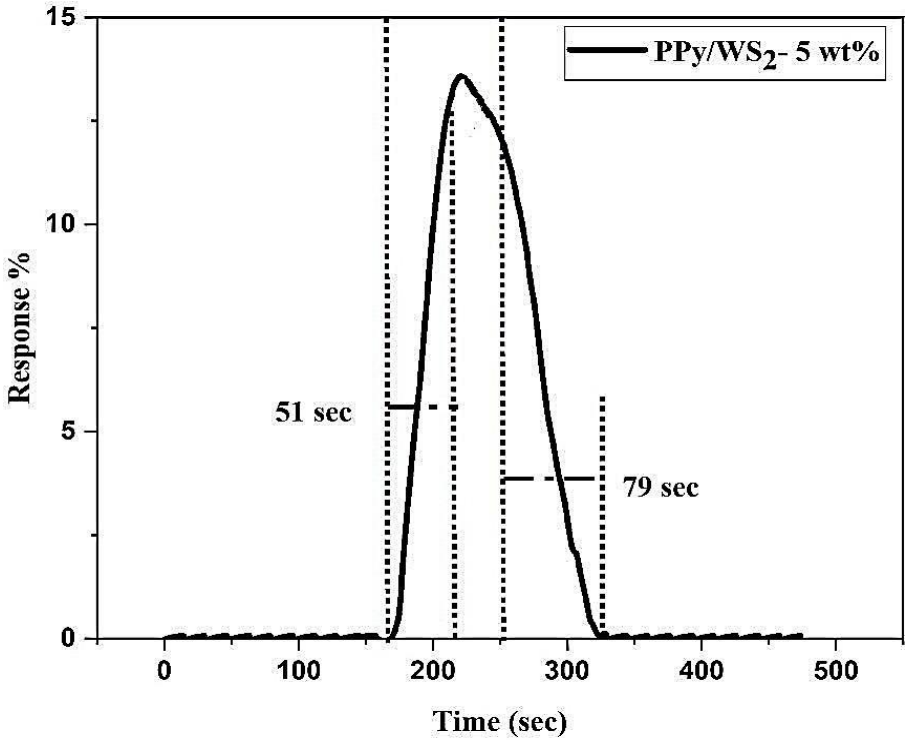

Figure 4.21 Response-recovery time on exposure of 100 ppm NH_3 for PPy/WS_2- 5 wt% nanocomposite.

4.2.6 Sensing mechanism

From the aforementioned experimental results, it can be observed that the PPy/WS_2 nanocomposite sensor has good ammonia-gas sensing properties at 28 ˚C suggesting PPy/WS_2 nanocomposite is an outstanding candidate material for ammonia detection. The potential ammonia-sensing mechanism is attributed to the synergistic effect of Polypyrrole and tungsten disulfide and special interactions at p-n heterojunction. **Figure 4.22 (a)** shows the role of PPy toward ammonia sensing. PPy is conducting p-type semiconductor that acquires proton to form N^+-H chemical bonds (protonation) due to in-situ oxidative polymerization. The ammonia molecules were absorbed on the surface of PPy when the sensor was exposed to ammonia gas and then interacts with PPy N-H group to produce NH_4^+ (ammonium ion) leading to an increase in the resistance of sensor. This reaction is described by the expression below:

$$NH_3\ (gas) + PPy\text{-}NH^+ \rightleftharpoons PPy + NH_4^+ \qquad (4.4)$$

The ammonium ion can undergo reversible decomposition into ammonia gas and a proton when the sensor is exposed to air. The synergistic effect of PPy/WS_2 binary nanomaterial is depicted in **Figure 4.22 (b)**. The synergistic action may be due to interaction between PPy and WS_2 which can weaken the filler-filler or polymer-polymer intramolecular and intermolecular interactions which leads to increase in the dispersion of WS_2 in PPy. Hence, the response of PPy to ammonia gas improves due to the presence of Polypyrrole and Tungsten disulfide. The oxygen containing surface defects of PPy and WS_2 produce covalent bonds when PPy is coated on their surfaces. Due to huge specific surface area of PPy and WS_2, there are now more contact sites with PPy which can result in significant increase in the number of ammonia gas adsorption sites. The nanocomposites integrated PPy and WS_2 serve as a conduction channel for charge transfer. Additionally, the swelling of PPy caused by NH_3 molecule adsorption may decrease the connectivity of nanocomposites and increase sensor resistance. Therefore, the synergistic combination of PPy/WS_2 yields much better sensing properties than that of PPy.

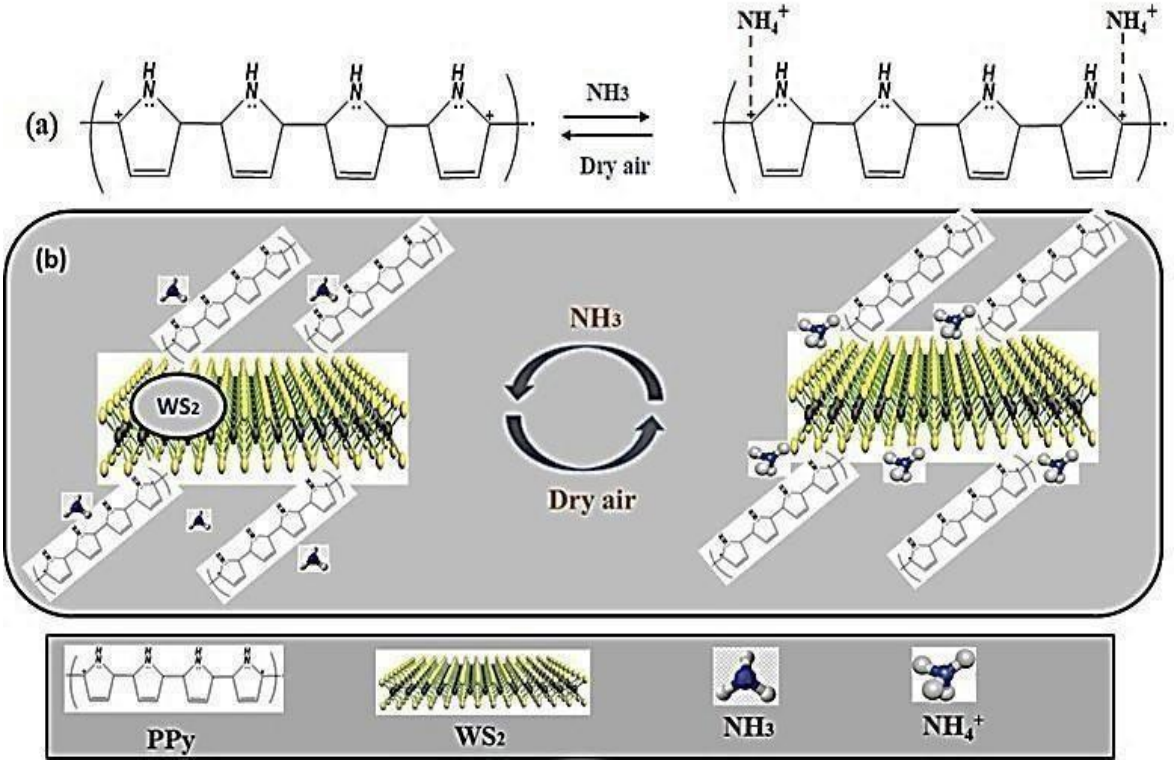

Figure 4.22 (a) The role of PPy for the ammonia-sensing (b) the synergistic effect of PPy/WS_2 binary nanomaterial.

The sensing performance of PPy/WS_2 nanocomposite was compared with other reported work, as shown in **Table 4.5**.

Table 4.5 Comparison of gas sensing performance of PPy based composites to NH_3.

Sensing material	Operating temp. (℃)	NH_3 Conc. (ppm)	Sensitivity (S%)	Response time (s)	Ref.
PPy/MoS_2	RT	1000	7%	60-70 s	[148]
PPy thin film	RT	100	0.4%	20 s	[41]
PPy/Ag_2S-CdS	RT	500	0.26%	20 s	[149]
PPy/Ag_2S NCs	RT	500	7.7%	20 s	[90]
Pd/PPy	RT	1000	58.9%	14 s	[50]

4.3 PPy/MoS_2 Nanocomposites

PPy/MoS_2 Nanocomposites were prepared with different MoS_2 content as given in **Table 4.6**. Before preparing nanocomposites pure PPy were kept fixed. The prepared

nanocomposites were characterized using XRD, FTIR and TEM techniques. The DC electrical conductivity was also measured using electrometer.

Table 4.6 Weight percentages of MoS_2 filler in PPy matrix

Sr No.	Weight %
1	1
2	5
3	10
4	20
5	30

4.3.1 Structural Study and Crystallinity Determination

To study the crystalline or amorphous nature of materials, we used the powder method of XRD patterns for pure MoS_2, pure PPy, and PPy/MoS_2 (1 wt%, 5 wt%, 10 wt%, 20 wt% and 30 wt%) nanocomposites. The XRD spectra of synthesized pure MoS_2, pure PPy and PPy/MoS_2 nanocomposites **(Figure 4.23)**.

In case of pure MoS_2, discernible peaks at $2\theta = 14.40°$, 32.63°, 34.67°, 35.87°, 39.45°, 49.76°, 58.20°, 60.77°, and 72.69° are observed (JCPDS file No. 37–1492), corresponding to the (0 0 2), (1 0 0), (1 0 1), (1 0 2), (1 0 3), (1 0 5), (1 1 0), (0 0 8) and (1 1 8) crystal planes of structured MoS_2 [150,151]. Pure PPy exhibits a broad spectrum within the 2θ range of 25-30°, indicative of the characteristic peak associated with amorphous like PPy [152]. PPy/MoS_2 (1 wt%, 5 wt%, 10 wt%, 20 wt% and 30 wt%) nanocomposites also shows the peak of pure PPy at $2\theta = 25\text{-}30°$. It seems to be more interesting that intensities of all peaks in nanocomposites are decreasing with the incorporation of filler in matrix PPy. The decrease in intensities show the interaction of MoS_2 filler with PPy matrix which are also in agreement with the results obtained from TEM study[153].

Applying Scherrer's method to analyze X-ray line broadening, the crystallite sizes of nanocomposites were determined by formula given in equation 4.5.

$$\boldsymbol{D = \frac{k\lambda}{Q\, cos\, \theta}} \qquad \textbf{(4.5)}$$

Where the symbol D, K, θ and β represent crystallite size, shape factor, diffraction angle, and FWHM (full width at half maximum), respectively.

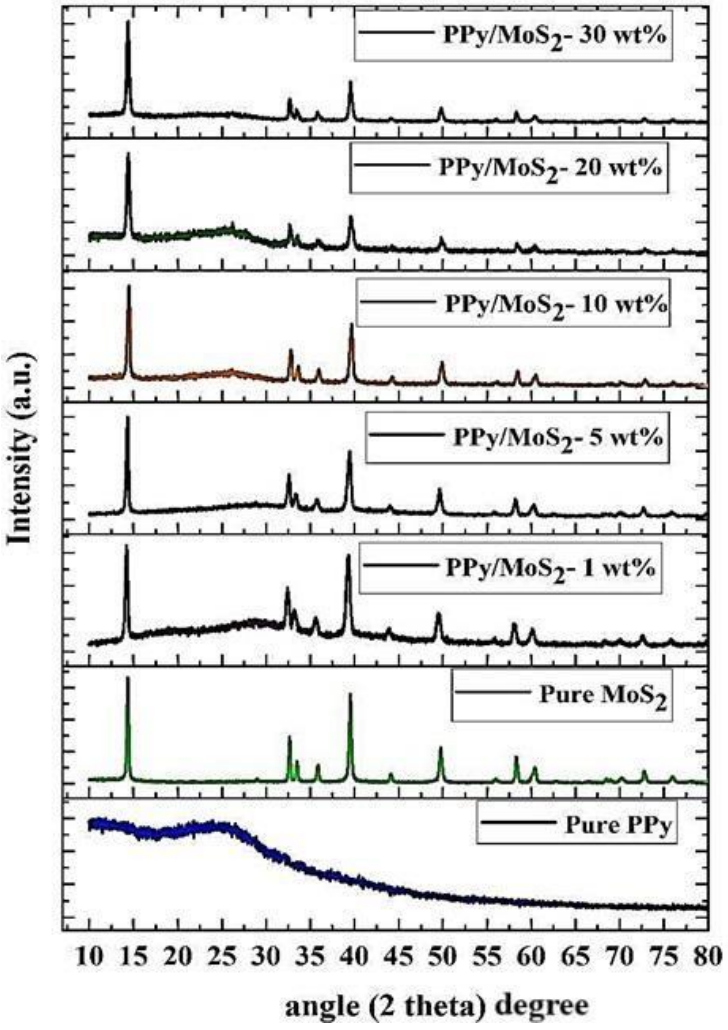

Figure 4.23 XRD spectra of pure PPy, pure MoS_2 and PPy/MoS_2 nanocomposites (1 wt%, 5 wt%, 10 wt%, 20 wt% and 30 wt%)

The calculated crystallite size of MoS_2 and its nanocomposite (002 plane) was found to be 36.39 nm (pure MoS_2), 28.58 nm (1 wt%), 24.26 nm (5 wt%), 23.92 nm (10 wt%), 22.92 nm (20 wt%), and 21.85 nm (30 wt%) as shown in **Table 4.7**.

Table 4.7 Calculations of crystallite size (T nm) of Pure MoS_2 and PPy/MoS_2 nanocomposites at different wt%.

Sample name	2θ (◦)	d-spacing (A◦)	FWHM (A◦)	β (Radian)	Cos θ (◦)	T (nm)
Pure MoS_2	14.34	6.10	0.234	0.0086	0.9998	36.39 nm
PPy/MoS_2- 1 wt%	14.20	6.10	0.280	0.0086	0.9998	28.58 nm
PPy/MoS_2- 5 wt%	14.29	6.09	0.329	0.0088	0.9998	24.26 nm
PPy/MoS_2-10 wt%	14.40	6.08	0.334	0.0090	0.9998	23.92 nm
PPy/MoS_2-20 wt%	14.42	6.09	0.366	0.0058	0.9998	22.92 nm
PPy/MoS_2-30 wt%	14.44	6.07	0.335	0.0060	0.9998	21.85 nm

4.3.2 Structural Study

Fourier transform infrared spectroscopy (FTIR) is employed to elucidate the functional groups of pure MoS_2, pure PPy and PPy/MoS_2 nanocomposites **(Figure 4.24)**.

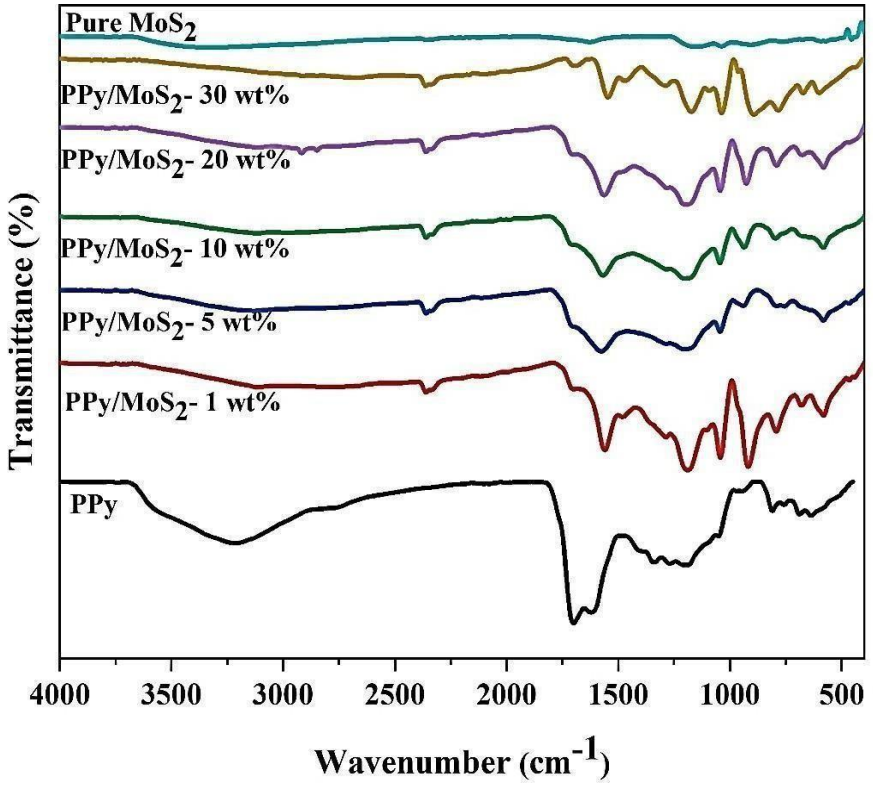

Figure 4.24 FT-IR spectra of pure PPy, pure MoS_2 and PPy/MoS_2 nanocomposites (1 wt%, 5 wt%, 10 wt%, 20 wt% and 30 wt%).

The main transmittance peaks of PPy are evident at 3225 cm^{-1} (O-H stretching) and 1709 cm^{-1} (C– C stretching vibrations) in the PPy ring. Additionally, the band at 1341 cm^{-1} (N-H bending), 1147 cm^{-1} and 1176 cm^{-1} (=C-H in-plane vibration), 1026 cm^{-1} (in-plane

deformation of C-H bond) and minor peaks below 1000 cm^{-1} indicate =C-H out-of-plane vibrations highlight Py polymerization [140,141,147,154].

Comparison of the FT-IR spectra of PPy nanocomposites with varying weight percentages of MoS_2 (1 wt%, 5 wt%, 10 wt%, 20 wt% and 30 wt%) reveals that the major characteristic peaks of PPy persist with slight shifts in some absorption frequencies. The spectra of nanocomposites corresponding to 1 wt% and 5 wt% of PPy/MoS_2 exhibits the absorption bands close to the absorption of neat PPy and with the highest absorption band above 1709 cm^{-1}, which is in agreement with the higher conductivity of these samples. This may be due to interaction of polymer chains of PPy deposited on the surface of MoS_2 nanoparticles. The spectra of the samples with PPy/MoS_2 (10 wt%, 20 wt% and 30 wt%) exhibit the lower absorption band observed above 1709 cm^{-1}. The shifting in peaks is probably due to the electrostatic forces between MoS_2 (negatively charged) and PPy (positively charged). In the spectra of this group of nanocomposites, we detect a small sharp peak of MoS_2. Apart from PPy peaks, bands at 620 cm^{-1} and 481 cm^{-1} are attributed to Mo-S stretching and S- S bond, indicating the embedding of MoS_2 in the PPy matrix [155]. These findings suggest interactions between PPy and MoS_2 in the nanocomposites.

4.3.3 Morphological analysis of PPy/MoS_2 Nanocomposites

To see the dispersion of MoS_2 in the matrix of PPy, Transmission Electron Microscopy (TEM) study was carried out. Therefore, the morphology of Pure MoS_2 and PPy/MoS_2- 5 wt% nanocomposite was done as shown in **Figure 4.25**.

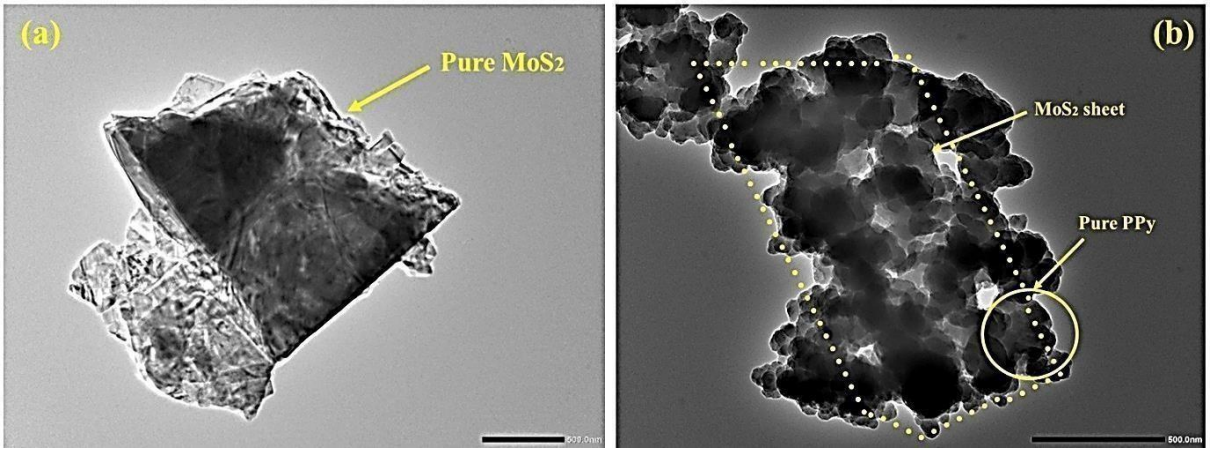

Figure 4.25 TEM images of (a) Pure MoS_2 (b) PPy/MoS_2 – 5 wt% nanocomposite

Figure 4.25 (a) shows that MoS_2 has sheet like 2D-structure. PPy has spherical like shape with multiple nanoparticles clustered together into agglomerates **(Figure 4.25 (b))**. As for

PPy/MoS_2- 5 wt%, a thin layer of PPy agglomerates was clearly observed which is very nicely dispersed on the MoS_2 sheets. This may due to the fact that MoS_2 as a supporting material provided abundant sites for heterogenous nucleation and uniform growth of PPy. Also, we can clearly see the PPy particles embedded with MoS_2 nanosheets form PPy/MoS_2 nanocomposites and some MoS_2 packed by PPy. The dispersion of filler in the matrix of PPy highlighted (**Figure 4.25 (b))** with a yellow colour and these results are in good agreement with the XRD results where the intensity of peak is going to decrease with the increment in wt% of filler.

4.3.4 Electrical Conductivity

The Direct Current (DC) electrical conductivity of PPy and PPy/MoS_2 nanocomposites were measured at room temperature using two probe method **(Figure 4.26)**. PPy and its nanocomposites show conductivities of 2.22 x 10^{-4} S/cm for pure PPy, 3.22 x 10^{-4} S/cm for PPy/MoS_2- 5 wt% and 0.68 x 10^{-4} S/cm for PPy/MoS_2- 10 wt%, respectively. The data indicates a noteworthy increase in the electrical conductivity of nanocomposites compared to PPy. Up to 1 V, the current-voltage characteristic plots for each nanocomposite exhibit ohmic behavior, transitioning to non-ohmic behaviour beyond that point. All plots demonstrate excellent linearity across a broad range of applied currents.

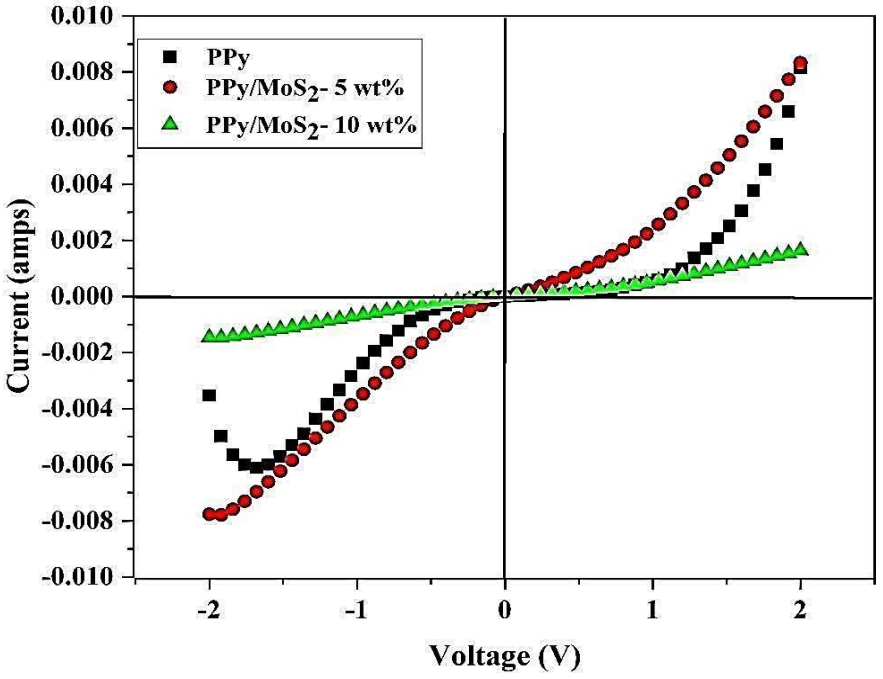

Figure 4.26 Current-voltage characteristics plot for pure PPy and PPy/MoS_2 nanocomposites (5 wt% and 10 wt%).

Upto 1V, the significant rise in electrical conductivity of PPy/MoS_2 -5 wt% can be attributed

to the initiation of a network between the MoS_2 filler and PPy matrix, through which charge carriers get a physical path to move [145]. It is suggested that MoS_2 acts as an effective electron acceptor while PPy serves as a competent electron donor. MoS_2 can serve as an effective conducting bridge connecting the conducting domains of PPy. Another reason for the high conductivity of PPy/MoS_2 -5 wt% may be the dispersion of MoS_2 in PPy which mutually improves the continuity of MoS_2 in the nanocomposites, as also confirmed by TEM images. [156]. At high voltage (beyond 1V) the breakage of bonds takes place, due to which charge carriers become free, so there is a sharp increase in electrical conductivity. The graph indicates that PPy nanocomposites containing 10 wt% of MoS_2 exhibit lower electrical conductivity. This can be attributed to both the low electrical conductivity of the filler and a reduced fraction of the PPy matrix. Another factor may be the heightened disorderliness within the nanocomposite, leading to a reduction in favorable localized sites. This disorderliness is likely a result of conformational changes in the PPy matrix [157].

4.3.5 Gas sensing properties

To illustrate the impact of varying loading ratios of MoS_2 on the gas sensing properties of PPy/ MoS_2 nanocomposites, a series of sensors with different MoS_2 loading ratios were examined for comparison. The sensor based on PPy, underwent sensing measurements for ammonia concentrations ranging from 10 to 100 ppm at room temperature. The results, presented in **Figure 4.27**, demonstrate that the PPy-based sensor exhibits a substantial response to increasing ammonia concentrations and yields an adequate response value even for a low concentration of NH_3 (10 ppm).

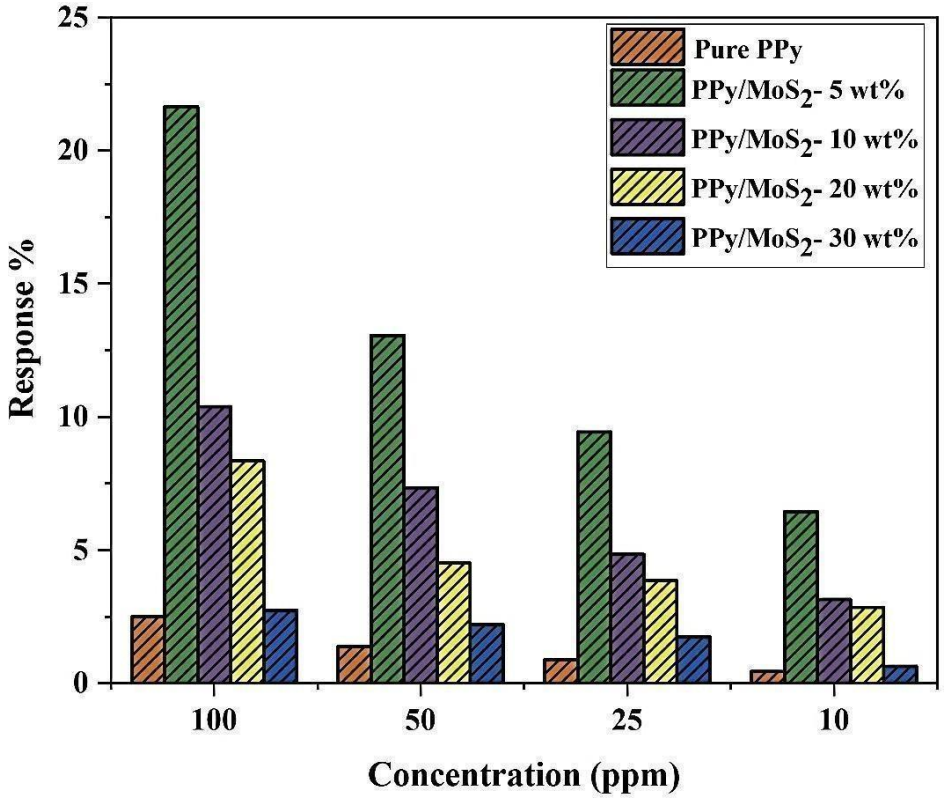

Figure 4.27 Comparison of sensitivities of pure PPy and PPy/MoS_2 (5 wt%, 10 wt%, 20 wt% and 30 wt%) nanocomposites for different concentrations of ammonia at room temperature.

Given that polypyrrole is a p-type material, its interaction with the reducing gas NH_3 induces a phenomenon of hole-electron recombination leading to a decrease in hole concentration and an increase in the resistance of PPy [158]. A notable increase in response is likely attributed to the substantial adsorption of target gas molecules at a concentration of 100 ppm. MoS_2 acknowledged for its exceptional electrical and chemical characteristics is considered a highly effective sensing material. As a result, the integration of MoS_2 into the PPy matrix is anticipated to improve the gas sensing properties. To explore this, gas sensing measurements were conducted on PPy/MoS_2 nanocomposites with varying weight percentages of MoS_2 ranging from 1 wt%, 5 wt%, 10 wt%, 20 wt%, 30 wt% for different concentrations of NH_3 at room temperature. PPy/MoS_2- 1 wt% do not show any response for gas sensing as there may be no interaction between PPy and MoS_2 due to low wt% of filler in the matrix PPy. The response of the in-situ polymerized PPy/MoS_2(5 wt%, 10 wt%, 20 wt% and 30 wt%) for corresponding NH_3 concentrations 10 ppm, 25 ppm, 50 ppm and 100 ppm is mentioned in **Table 4.8**.

Table 4.8 Response value for ammonia sensors presented in this work.

Sensing material	**Sensor response %**			
	100 ppm	**50 ppm**	**25 ppm**	**10 ppm**
PPy	2.5	1.39	0.89	0.45
PPy/MoS_2- 5 wt%	21.65	13.077	9.44	6.45
PPy/MoS_2- 10 wt%	10.39	7.35	4.85	3.15
PPy/MoS_2- 20 wt%	8.35	4.51	3.87	2.85
PPy/MoS_2- 30 wt%	2.75	2.21	1.76	0.65

Among the five sensors, in-situ polymerized PPy/MoS_2- 5 wt% sensor showed the highest response at 100 ppm concentration. The dynamic resistance curve of the PPy/MoS_2- 5 wt%, illustrated in **Figure 4.28 (a)**, depicts the resistance variation of sensors when exposed to different concentrations of NH_3 ranging from 10-100 ppm. The graph illustrates the p-type semiconducting nature of the sensors. Typically, the resistance of p-type semiconducting materials increases when exposed to reducing the concentration of NH_3 and decreases again in air atmosphere. Additionally in **Figure 4.28 (a)**, it is evident that the off-state terminal resistance (Ra) for the PPy/MoS_2- 5 wt% sensor is lower than that for pure PPy indicating a reduced band gap (Eg) resulting from the doping of MoS_2. However, the stability of air resistance (Ra) for both materials is slightly erratic, possibly attributed to the use of atmospheric air during the recovery process. The systematic response assessment of PPy/MoS_2- 5 wt% based sensor for various concentrations of ammonia is shown in **Figure 4.28 (b)**, demonstrating increase in sensor response to increasing ammonia concentration.
At higher concentration, the value of response is much higher due to the higher adsorption of target gas molecules on the surface of gas sensor. The results also demonstrate linear relation between the response values and ammonia concentration. As observed, the nanocomposite produced through the in-situ approach demonstrates superior sensing outcomes. This superiority can be attributed to a significant intertwining between the two materials and an increased abundance of adsorption sites on the surface of the prepared nanocomposites for target gas molecules. The PPy/MoS_2- 5 wt% sensor demonstrates a favourable response ranging from 2.75% to 21.65% for ammonia concentrations of 25 to 100 ppm at room temperature. The response of the gas sensor is directly correlated with the quantity of target gas molecules adsorbed on its surface. Notably, the gas sensor maintains an adequate response even at a low concentration of 10 ppm, underscoring its

capability for low-level detection. With its ability to detect low levels, the flexible gas sensor can be utilized for real-time monitoring of ammonia, serving as an early detection device. The response and recovery characteristics of PPy/MoS_2- 5 wt% nanocomposite-based sensor are shown in **Figure 4.28 (c).** The observed response/recovery time of PPy/MoS_2- 5 wt% nanocomposite was 340/680 sec.

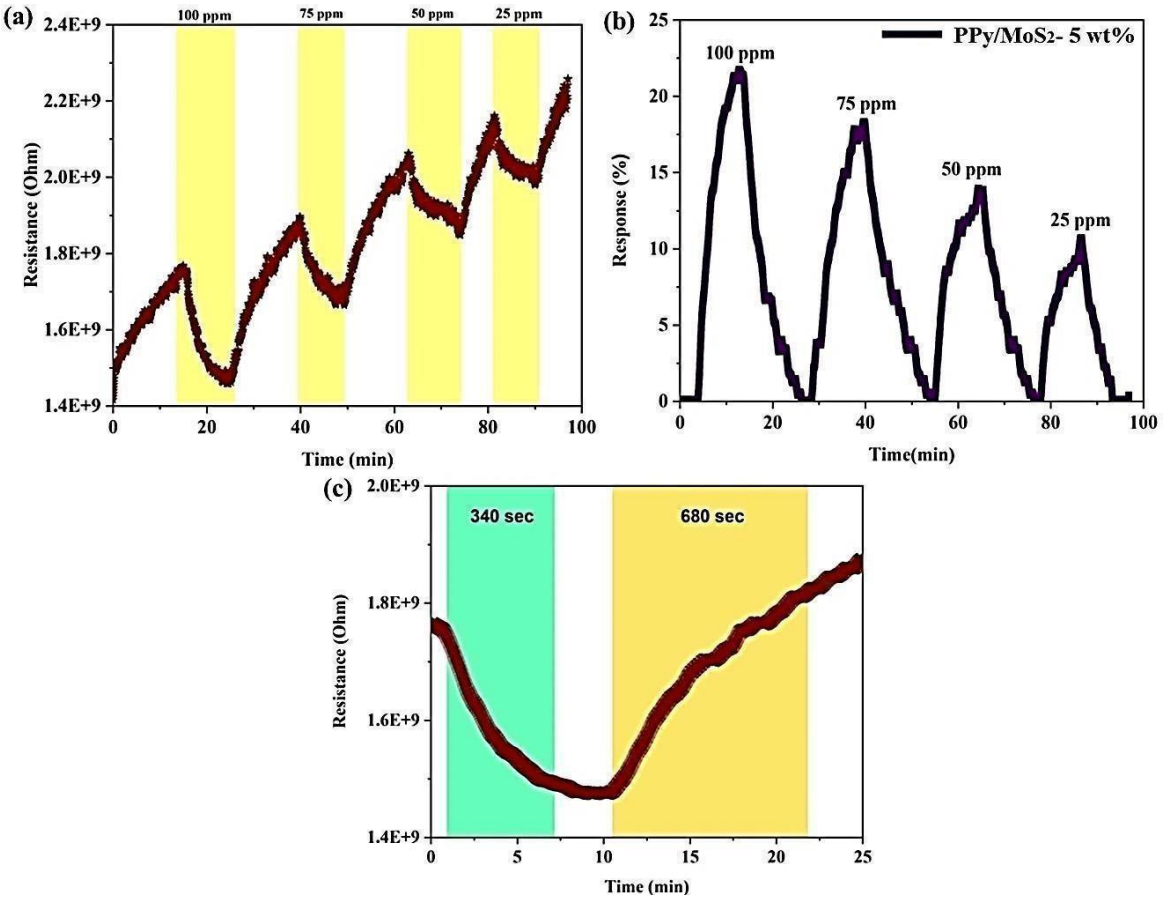

Figure 4.28 (a) Dynamic resistance curve for PPy/MoS_2- 5 wt% sensor for various concentration of NH_3 (b) Rapid response curve of PPy/MoS_2- 5 wt% for NH_3 concentration ranging from 25-100 ppm at RT (c) PPy/MoS_2- 5 wt% sample response and recovery times to 100 ppm of NH_3 at RT.

Moreover, stability and reproducibility were assessed to validate the accuracy of gas sensor for swiftly monitoring airborne ammonia leaks. The motivation behind fabricating the PPy/MoS_2- 5 wt% sensor is to achieve consistent response values even with repeated gas exposures. The repeatability is defined as the sensing material's capability of repeating similar characteristic behaviours when the same environment is repeated a number of times. Hence, the response of the PPy/MoS_2- 5 wt% nanocomposite was scrutinized across multiple sensing cycles at 100 ppm ammonia, as illustrated in **Figure 4.29 (a).** When

alternating between ammonia and air, the flexible sensor demonstrates good repeatability revealing highly stable fluctuations responses even after 5 consecutive sensing tests.

For the rapid monitoring of harmful gases in real time, reproducibility is the second factor that plays a critical role. For assessing reproducibility, the proposed sensor underwent continuous exposure to 100 ppm of NH_3 over a period of 21 days at regular intervals, as depicted in **Figure 4.29 (b)**. The outcomes indicate robust long-term durability even after the extended 21-day period. Furthermore, the baseline resistance exhibits negligible change even after 21 days indicating the sensor's commendable stability. Consequently, the fabricated PPy/MoS_2- 5 wt% sensor holds significant potential for the detection of ammonia in real-world applications. The selectivity characteristics of a gas sensor are crucial in practical applications, as they are directly linked to the sensor's response in diverse mixed gaseous environments. Therefore, the response of PPy/MoS_2- 5 wt% nanocomposite for different gases, including H_2, CO_2, C_2H_5OH, NO_2 and NH_3, was examined. The reason for selecting the mentioned gaseous analytes to assess selectivity is their prevalence in the environment and widespread use in daily life, potentially influencing the performance of the proposed ammonia sensor. As shown in **Figure 4.29 (c)** from all the gaseous analytes, the PPy/MoS_2- 5 wt% exhibited superior and highest response for ammonia gas. The maximal response for 100 ppm ammonia is 21.65, while the sensitivities for H_2, CO_2, C_2H_5OH and NO_2 were 1.55, 0.97, 2.67 and 5, respectively which are significantly lower than the response of NH_3. These findings indicate that the PPy/MoS_2- 5 wt% nanocomposite serves as a favourable material for the production of sensors designed to detect ammonia.

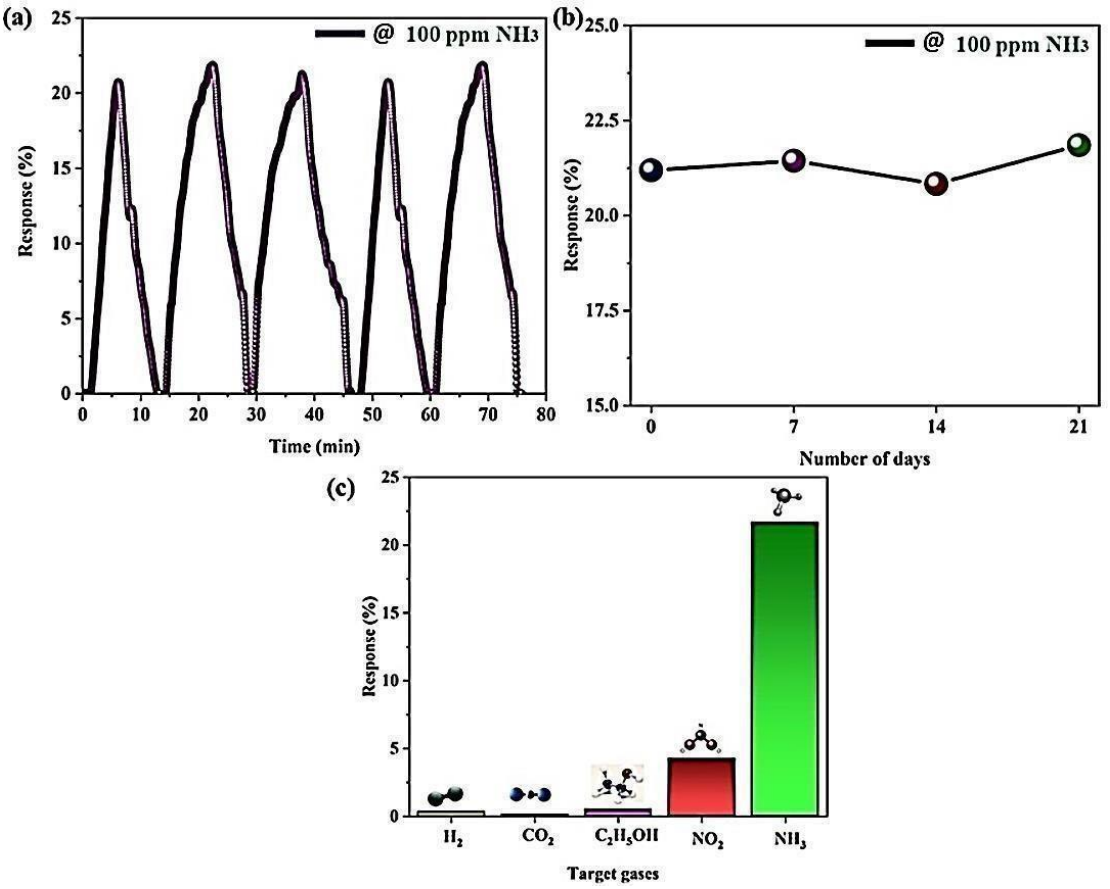

Figure 4.29 (a) Reproducibility assessment of PPy/MoS_2- 5 wt% sensor to 100 ppm of NH_3 with 5 continuous cycle at RT (b) Long term durability of PPy/MoS_2- 5 wt% sensor to 100 ppm of NH_3 at RT over 21 days (c) Response of the sensor based on PPy/MoS_2- 5 wt% to various gases at RT at 100 ppm.

4.3.6 Gas sensing mechanism

Based on the experimental findings mentioned above, it is evident that the PPy/MoS_2 nanocomposite sensor exhibits commendable sensing properties for ammonia gas at 28 °C. This suggests that the PPy/MoS_2 nanocomposite stands out as an excellent candidate material for detecting ammonia. The potential sensing mechanism for ammonia is attributed to the synergistic effects of polypyrrole and molybdenum disulfide, along with special interactions at the p-n heterojunction. The sensing analysis indicated that upon exposure to NH_3 gas, the resistance of the PPy/MoS_2- 5 wt% nanocomposite increased, aligning with the sensing characteristics of a p-type semiconductor. The hypothesized sensing mechanism of PPy to NH_3 involves the deprotonation/protonation process through adsorption/desorption of NH_3 on the composite surface as shown in **Figure 4.30 (a)**.

$PPy + NH_3 \longrightarrow PPy^0 + NH_4^+$ (adsorption) **(4.6)**

$PPy^0 + NH_4^+ \longrightarrow PPy^+ + NH_3$ (desorption) **(4.7)**

When the nanocomposites are placed in NH_3, the ammonia molecule is in contact with PPy/MoS_2- 5 wt%, and the nitrogen in ammonia loses an electron to the nitrogen in the main chain of the polymerization to form ammonium ion, which is similar to the process of de-doping (deprotonation), resulting in the change of resistance. While when the sensor is removed from NH_3 atmosphere and placed in the air again, its resistance will be fully or partially restored to its original state, thus achieving complete gas sensing response. Moreover, integrating PPy/MoS_2 into the PPy matrix has a substantial impact on both the structural and chemical properties of pure PPy contributing to the improvement of gas sensing characteristics. In addition, several other factors that may affect the response of PPy/MoS_2 nanocomposites to NH_3 sensing were also considered. Firstly, high electron mobility of MoS_2 contributes to the fast carrier transport of nanocomposites leading to better sensing behaviour. Secondly, the two-dimensional material MoS_2 has a large surface area, which is very conductive to the adsorption of ammonia molecules on the surface of the nanocomposites. Thirdly, the high gas sensing response may be related to synergistic effect of MoS_2 and PPy. The synergistic effect can be attributed to the interaction between PPy and MoS_2, potentially weakening filler-filler or polymer-polymer intramolecular and intermolecular interactions. This in turn enhances the dispersion of MoS_2 in PPy. Consequently, the response of PPy to ammonia gas improves due to the combined presence of polypyrrole and molybdenum disulfide. The oxygen-containing surface defects of PPy and MoS_2 result in covalent bonds when PPy is coated on their surfaces. The vast specific surface areas of PPy and MoS_2 provide more contact sites, significantly increasing the number of ammonia gas adsorption sites. The nanocomposites, integrating PPy and MoS_2, function as a conduction channel for charge transfer. Additionally, the adsorption of NH_3 molecules causing swelling in PPy may reduce the connectivity of nanocomposites and increase sensor resistance. Therefore, the synergistic combination of PPy/MoS_2 exhibits much improved sensing properties compared to PPy alone as depicted in **Figure 4.30 (b).** The work function for PPy is reported to be approximately 4.26 eV [159] while for MoS_2 it is ~ 4.3-4.5 eV[160] . This variance in work function causes electrons to migrate from the conduction band of MoS_2 towards PPy forming a Schottky barrier at the PPy/MoS_2 interface, as illustrated in **Figure 4.30 (c)**. This barrier is a key factor contributing to the increase in resistance in the presence of oxygen. Upon introducing NH_3 gas to the sensor,

the height of this Schottky barrier is decreased accompanied by a reduction in layer width. This leads to the release of electrons into the conduction band of MoS_2. This reduction enhances the response of PPy/MoS_2 samples when compared to the response observed in pure PPy samples. The sensing performance of PPy/MoS_2 nanocomposites in this research work have been compared with that of the reported works, and the comparison is presented in **Table 4.9**.

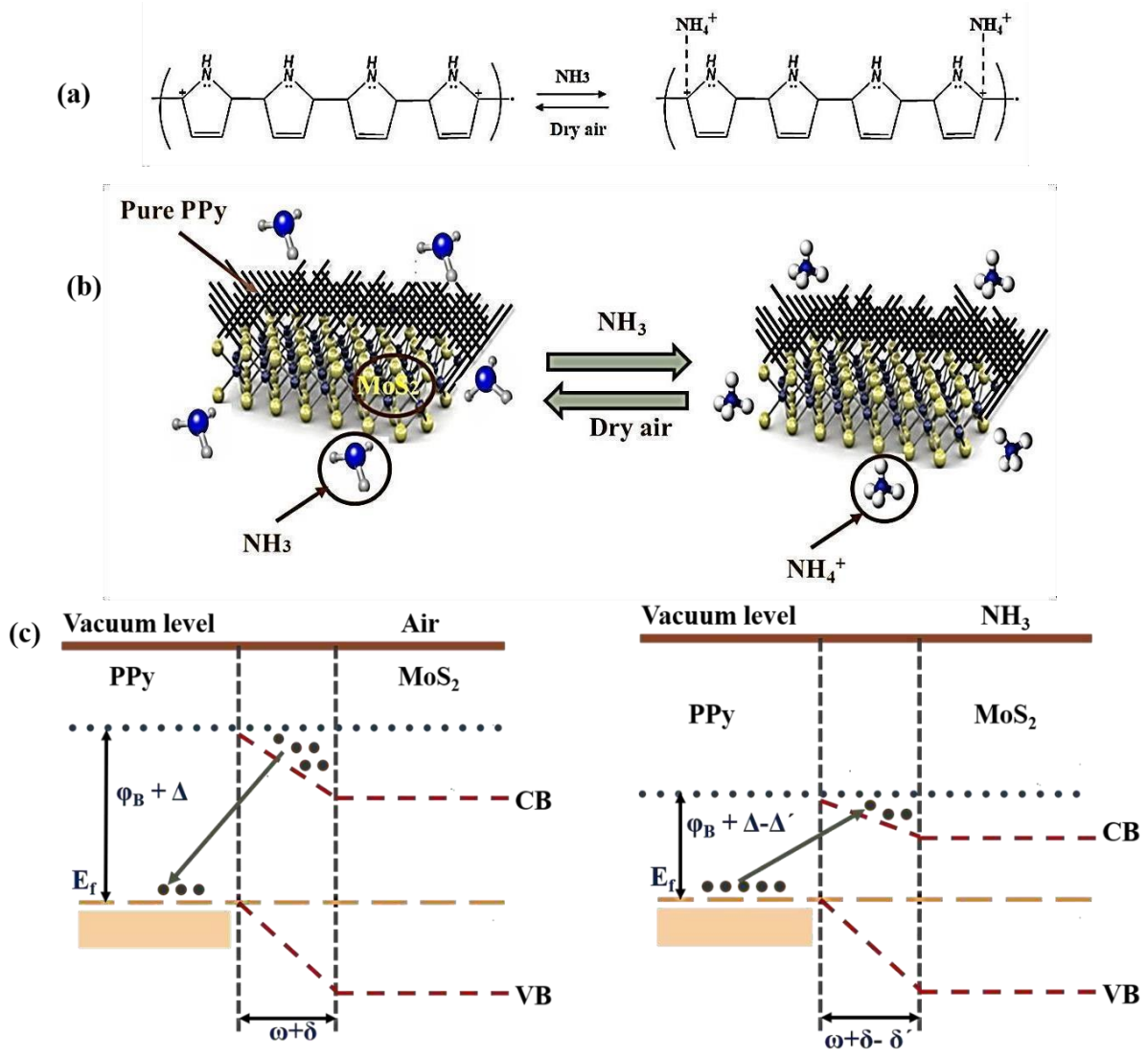

Figure 4.30 The role of PPy for ammonia sensing (a) Synergistic effect of PPy/MoS_2 binary nanocomposites(b) band diagram representation for PPy/MoS_2 in presence of Air and NH_3. (where ϕ_B and ware barrier height and depletion layer width at the interface between PPy/MoS_2 respectively, Δ and Δ' are the change in barrier height in presence of oxygen and NH_3 respectively, and δ & δ' are the change in depletion layer width in presence of oxygen and NH_3 respectively) (c).

Table 4.9 Comparison of sensor response of PPy/MoS_2 with those of reported sensors

Materials	Detection range	Response	Response and Recovery time	Reproducibility	Long-term stability	Selectivity	Temp.	Ref.
PPy/MoO_3	1 M, 0.5 M, 0.1 M	79.3% @ 1 M	20-20 sec	5 consecutive cycle	-	More selective to NH_3 than EtOH, CH_3OH, acetone, acetaldehyde, formaldehyde, toluene, benzene, chloroform and n-hexane	RT	[154]
PPy/Ag_2S NCs	100-500 ppm	7.7 @ 100 ppm	20-600 sec	-	-	-	RT	[149]
PPy/WS_2	50-200 ppm	30.10% @ 200 ppm	51-79 sec	6 consecutive cycle	4 weeks	More selective to NH_3 than Hydrogen, Ethanol, Carbon mono-oxide, Carbon dioxide	RT	[161]
PPy/rGO	33.2 ppm	7%	-	3 consecutive cycle	-	-	RT	[116]
PPy/SnO_2	1-200 ppm	15% @ 1 ppm	-	-	-	More selective to NH_3 than EtOH, ether, acetone, methanol, THF	RT	[162]

4.4 PPy/SnS_2 Nanocomposites

PPy/SnS_2 Nanocomposites were prepared with different SnS_2 content as given in **Table 4.10.** Before preparing nanocomposites pure PPy were kept fixed. The prepared nanocomposites were characterized using XRD, FTIR and TEM techniques.

Table 4.10 Weight percentages of SnS_2 filler in PPy matrix

Sr No.	Weight %
1	1
2	5
3	10
4	20
5	30

4.4.1 Structural Study

The XRD pattern of as synthesized SnS_2 product and PPy/SnS_2 (1 wt%, 5 wt%, 10 wt%, 20 wt% and 30 wt%) are shown in **Figure 4.31**. Pure PPy exhibits a broad spectrum within the 2θ range of 25-30°, indicative of the characteristic peak associated with amorphous like PPy [152]. The elevated background intensities observed in the XRD patterns may indicate the presence of amorphous substances within SnS_2. Products synthesized using EG as solvent exclusively exhibit characteristic XRD peaks corresponding to the hexagonal phase of SnS_2 (JCPDS card No.83-1705). Notably, no discernible peaks from impurity phases are detected, underscoring the high purity of the synthesized products.

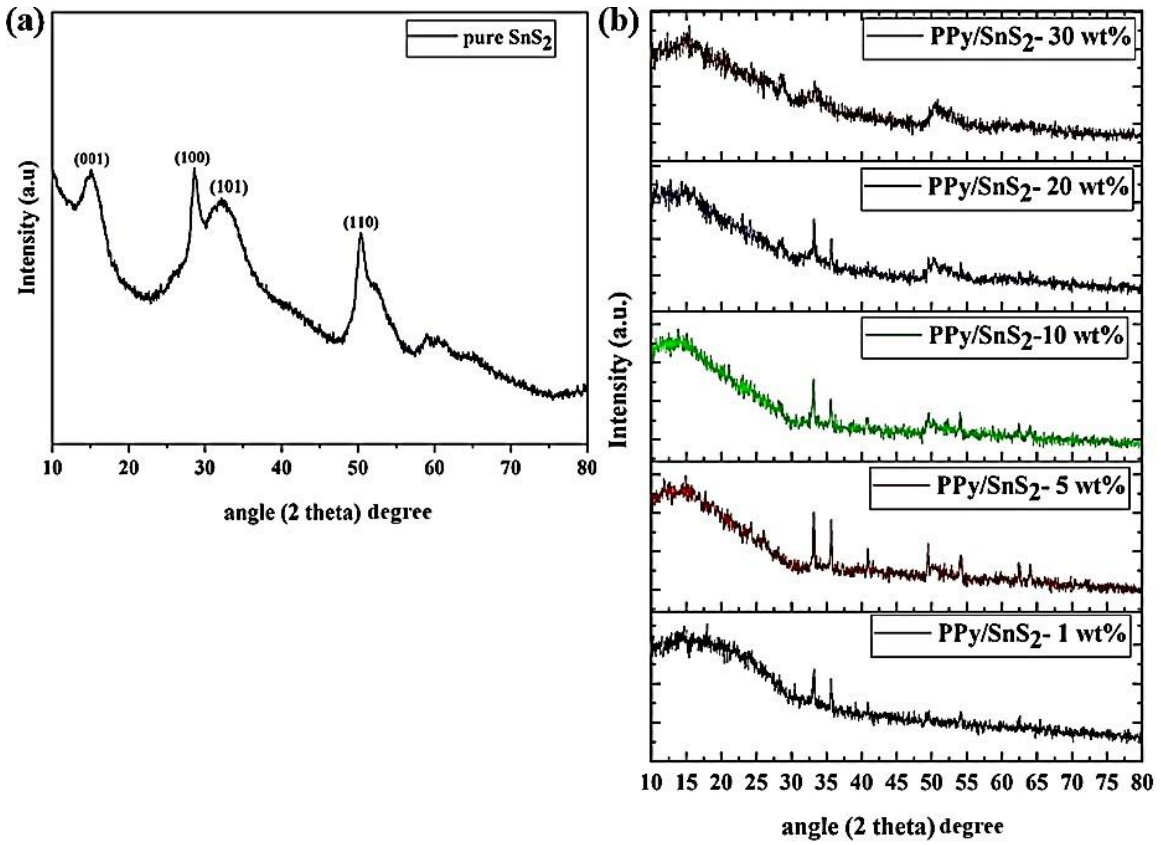

Figure 4.31 (a) XRD spectra of pure SnS_2 (b) XRD spectra of PPy/SnS_2 (1 wt%, 5 wt%, 10 wt%, 20 wt% and 30 wt%) nanocomposites.

In case of PPy/SnS_2 (1 wt%, 5 wt%, 10 wt%, 20 wt% and 30 wt%), comparison with standard data reveals deviations in diffraction peak intensities; specifically, the (001) and (100) peaks exhibit greater intensity than the standard pattern, while the intensity of the (101) peak is reduced and the (110) peak is absent [123]. The change in intensities indicates the interaction of Sns_2 filler and PPy matrix, aligning with findings from the TEM analysis.

4.4.2 FT-IR analysis

The FT-IR spectra of pure PPy, PPy/SnS_2 (1 wt%, 5 wt%, 10 wt%, 20 wt% and 30 wt%) nanocomposites and pure SnS_2 are shown in **Figure 4.32**. The prominent peaks observed in the transmittance spectrum of PPy are notable at 3225 cm^{-1} and 1709 cm^{-1}, corresponding to the N-H stretching and C=C stretching vibrations within the PPy ring, respectively. Additionally, the peak at 1341 cm^{-1} is attributed to the N-H bending vibration bond. Further, the peaks at 1147 cm^{-1} and 1176 cm^{-1} likely represent =C-H in-plane vibrations, while the peak at 1026 cm^{-1} signifies the in-plane deformation of the C-H bond within the pyrrole ring. Minor peaks below 1000 cm^{-1} are indicative of =C-H out of plane vibrations,

which further verify the polymerization of PPy [121,139–141]. The band at 551 cm^{-1} and 670 cm^{-1} correspond to Sn-S stretching and S-S bonds respectively [163]. Meanwhile, in the IR spectra of PPy/SnS_2 (1 wt%, 5 wt%, 10 wt%, 20 wt% and 30 wt%) nanocomposites and pure SnS_2, the intensities of diffraction peaks at 1000 cm^{-1}, 1176 cm^{-1} and 1709 cm^{-1} are significantly enhanced with a slight shift in frequency for PPy/SnS_2 nanocomposites at different weight percent indicating some interactions between PPy and SnS_2.

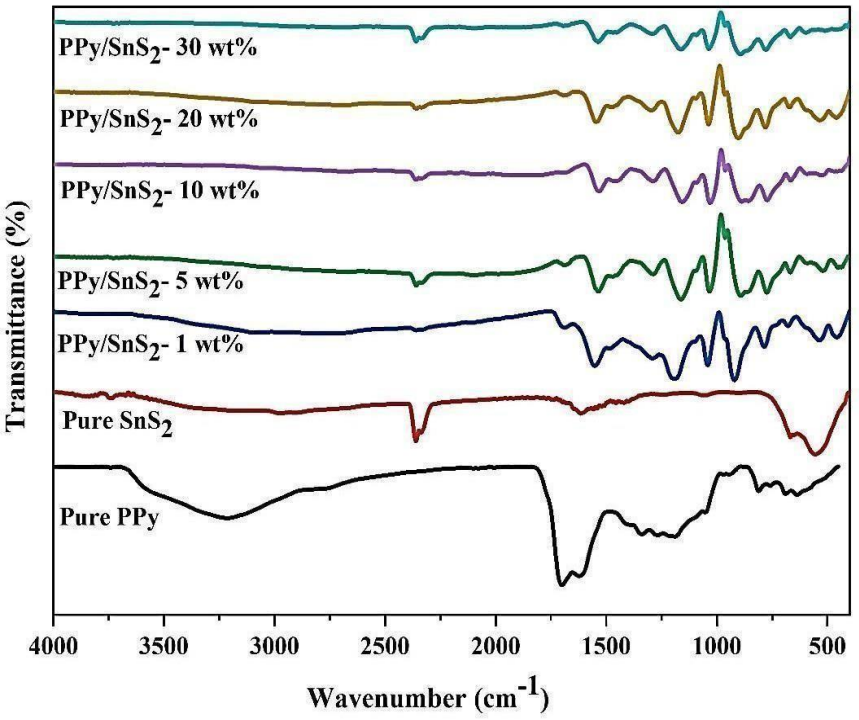

Figure 4.32 FT-IR spectra of pure PPy, pure SnS_2 and PPy/SnS_2 nanocomposites (1 wt%, 5 wt%, 10 wt%, 20 wt% and 30 wt%)

4.4.3 Morphological analysis of PPy/SnS_2 Nanocomposites

Transmission Electron Microscopy (TEM) analysis was conducted to observe the dispersion of SnS_2 within the PPy matrix. Consequently, the morphology of both Pure SnS_2 and PPy/SnS_2-5 wt% nanocomposite was examined, as depicted in **Figure 4.33**. In **Figure 4.33 (a)**, SnS_2 exhibit sheet like structure, while in **Figure 4.33 (b)**, dispersion of PPy particles can be seen in sheets for PPy/SnS_2 – 5 wt% nanocomposite. This phenomenon is likely attributed to SnS_2 acting as a supportive material providing abundant sites for heterogenous nucleation.

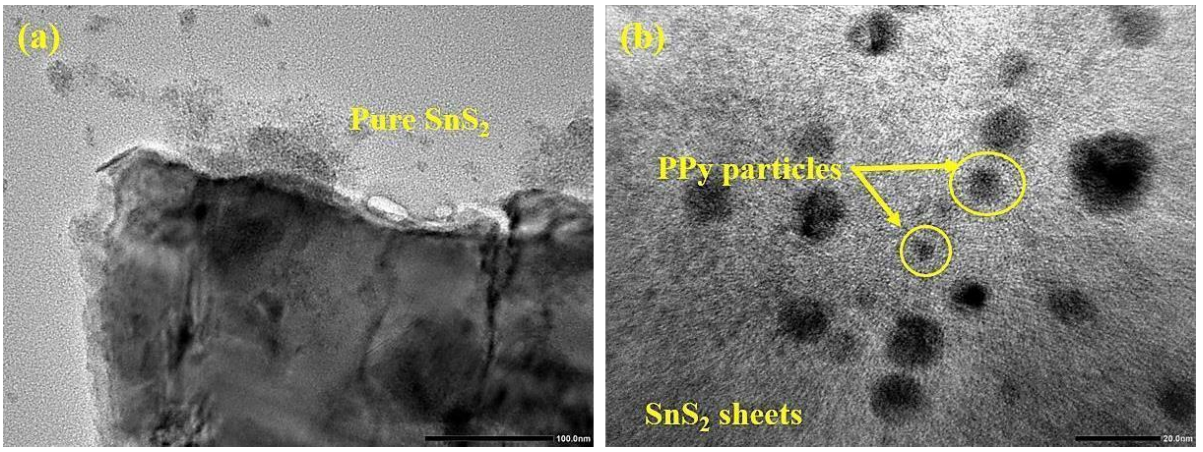

Figure 4.33 TEM images of (a) Pure SnS_2 (b) PPy/SnS_2 – 5 wt% nanocomposite

The dispersion of PPy as matrix is highlighted with yellow colour in the filler of SnS_2 confirming the presence of nanocomposite.

4.4.4 Gas sensing properties

To study the effect of different loading ratio of SnS_2 on the gas sensing performance of PPy/SnS_2 nanocomposites, we examined a range of sensors with different SnS_2 loading ratios for comparative analysis. The prepared PPy/SnS_2 based sensor was employed to conduct sensing assessments across ammonia concentrations ranging from 25 to 100 ppm at room temperature as illustrated in **Figure 4.34.** The findings reveal that PPy-based sensor displays a significant response to rising ammonia concentrations yielding an adequate response even at low NH_3 concentrations (25 ppm).

As PPy is known to be a p-type material, its interaction with the reducing gas NH_3 induces a phenomenon of hole-electron recombination, thereby causing a decrease in hole concentration and an increase in the resistance of PPy [45]. A notable rise in response is expected due to the substantial adsorption of target gas molecules at a concentration of 100 ppm. Recognized for its exceptional electrical and chemical characteristics, SnS_2 is considered highly effective as a sensing material. Consequently, the incorporation of SnS_2 into the PPy matrix is anticipated to enhance the gas sensing properties. To investigate this, gas sensing measurements were conducted on PPy/SnS_2 nanocomposites with varying weight percentages of SnS_2 (1 wt%, 5 wt%, 10 wt%, 20 wt% and 30 wt%) for different concentrations of NH_3 at room temperature. Out of the five sensors tested, the in-situ polymerized PPy/SnS_2-5 wt% sensor demonstrated the most substantial response when exposed to a concentration of 100 ppm.

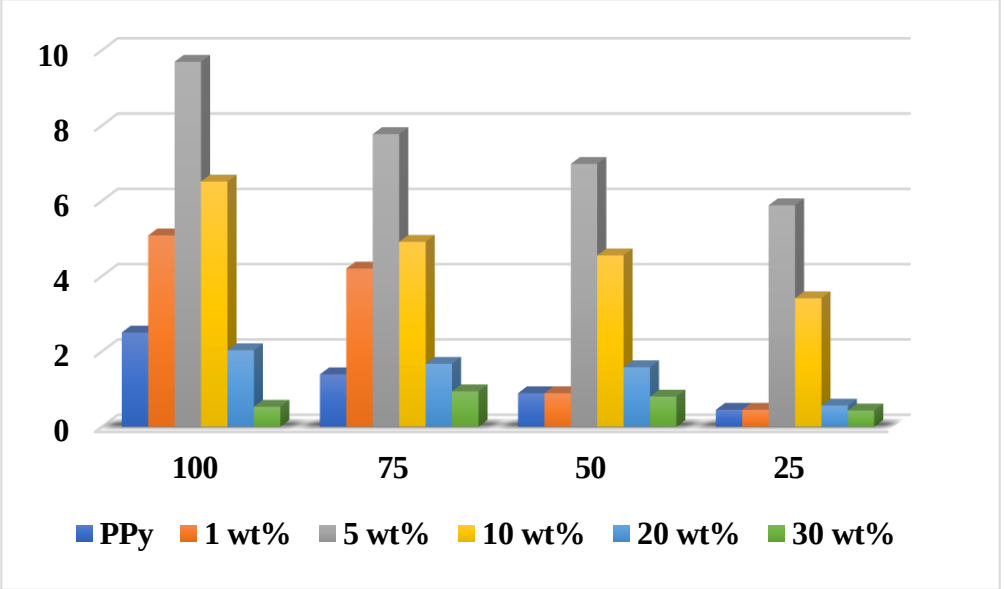

Figure 4.34 Comparison of sensitivities of pure PPy and PPy/SnS_2 (1 wt%, 5 wt%, 10 wt%, 20 wt% and 30 wt%) nanocomposites for different concentrations of ammonia at room temperature.

The systematic evaluation of the PPy/SnS_2-5 wt% based sensor's response to various concentrations of NH_3 is illustrated in **Figure 4.35**, depicting an increase in sensor response with rising NH_3 concentration. At higher concentrations, the response value notably escalates due to enhanced adsorption of target gas molecules on the sensor surface. Furthermore, the results exhibit a linear relationship between response values and NH_3 concentration. It's noteworthy that the nanocomposite fabricated via the in-situ method exhibits superior sensing performance. This superiority can be attributed to the substantial intertwining between the two materials and an increased abundance of adsorption sites on the nanocomposite surface for target gas molecules.

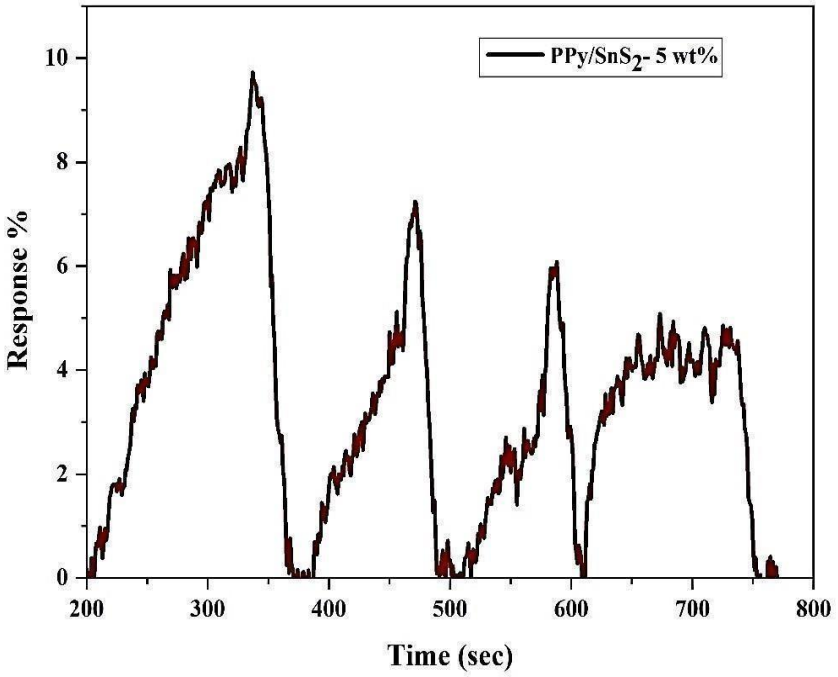

Figure 4.35 Rapid response curve of PPy/SnS_2- 5 wt% for NH_3 concentration ranging from 25-100 ppm at RT.

The PPy/SnS_2-5 wt% sensor showcases a favorable response ranging from 5.88% to 9.69% for NH_3 concentrations of 25 to 100 ppm at room temperature. The sensor's response is directly linked to the quantity of target gas molecules adsorbed on its surface. Notably, the flexible nature of the gas sensor maintains an adequate response even at low concentrations such as 10 ppm, highlighting its capability for detecting low levels. Given its ability to detect low concentrations, the flexible gas sensor holds potential for real-time NH_3 monitoring, serving as an early detection device.

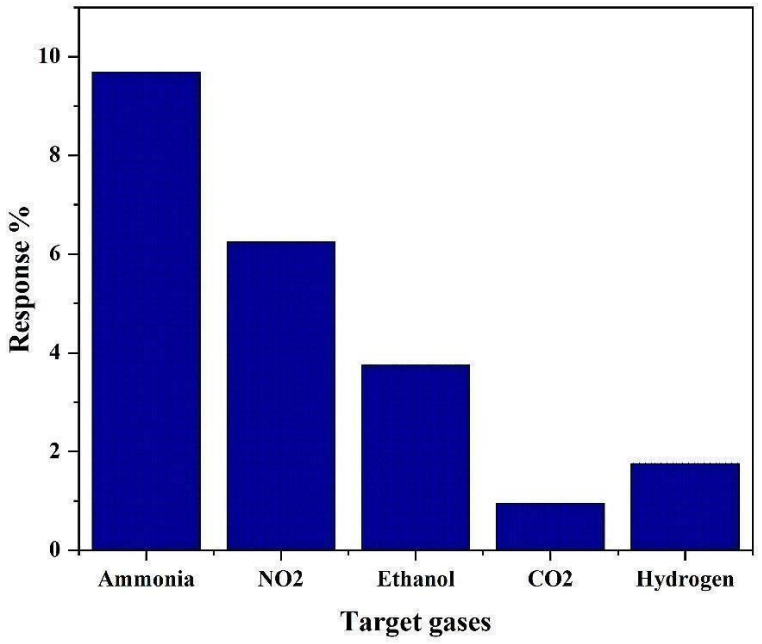

Figure 4.36 Response of the sensor based on PPy/SnS_2- 5 wt% to various gases at RT at 100 ppm.

Figure 4.36 demonstrates selectivity, revealing the material's distinct response to specific gases. Among them, ammonia exhibited the most pronounced response compared to others, indicating the exceptional selectivity of the sensor toward ammonia gas. Consequently, at 100 ppm, the selectivity of ammonia stands at approximately 6.25, 3.75, 0.95, and 1.75 for NO_2, C_2H_5OH, CO_2, and H_2 respectively. With a reliable response at low concentrations like 10 ppm, this gas sensor excels at detecting trace amounts of ammonia. This makes it ideal for real-time monitoring, providing early warnings of potential ammonia leaks.

CHAPTER FIVE

Conclusion and Future perspectives

This chapter wraps up the synthesis and characterization of PPy powder using oxidants $FeCl_3$ and APS, as well as PPy with metal sulfides (WS_2, MoS_2, SnS_2) nanocomposites. The chapter delves into the overall results of the materials post-characterization, drawing upon findings from XRD analysis, FTIR spectroscopy, electrical measurements, and morphological studies. Additionally, it discusses the conclusions derived from gas sensing experiments conducted within this chapter.

CHAPTER FIVE Conclusion and Future perspectives

5.1 Conclusion

The research work on preparation of polypyrrole based metal sulfides nanocomposites for gas sensing has been successfully carried out. Based on the findings from XRD analysis, FTIR spectroscopy, electrical measurements, morphological studies and gas sensing measurements the following conclusions can be made.

- PPy powder have successfully synthesized via chemical oxidative polymerization method using oxidants $FeCl_3$ and APS. The prepared PPy were further dried named as PPy/$FeCl_3$ and PPy/APS.

- The distribution of particle size of PPy globular morphology with oxidants $FeCl_3$ and APS revealed the average particle size to be 448 nm and 240 nm for PPy/$FeCl_3$ and PPy/APS respectively.

- The electrical conductivity of PPy/$FeCl_3$ is high as compared to PPy/APS due to enhanced crystallinity of polymer which can be confirmed from XRD analysis.

- Among all synthesized PPy, PPy/$FeCl_3$ selected as oxidant for further preparing metal sulfides nanocomposites like WS_2, MoS_2 and SnS_2 with different filler loading at different wt% (1 wt%, 5 wt%, 10 wt%, 20 wt% and 30 wt%).

- In-situ polymerization have been preferred over chemical oxidative polymerization method for the synthesis of polypyrrole-metal sulfides as polymer forms directly at the interface between the matrix and reinforcing material resulting in better adhesion and homogeneity leading to improve in properties as well as overall performance of the composite.

- XRD of PPy/WS_2 (1 wt%, 5 wt%, 10 wt%, 20 wt% and 30 wt%) confirms the existence and predominance of crystalline WS_2 in the composite and broad peak of PPy, indicating the PPy-deposited WS_2 and its crystalline nature.

- TEM study reveals the confirmation of the 2D sheets like structure of WS_2 in the matrix of PPy However, the existence of PPy and WS_2 is clearly seen.

- In XRD analysis of PPy/MoS_2 nanocomposites, intensities of all peaks in nanocomposites are decreasing with the incorporation of filler in matrix PPy. The decrease in intensities show the interaction of MoS_2 filler with PPy matrix which are also in agreement with the results obtained from TEM study.

- XRD analysis of PPy/SnS_2 (1 wt%, 5 wt%, 10 wt%, 20 wt% and 30 wt%), comparison with standard data reveals deviations in diffraction peak intensities; specifically, the (001) and (100) peaks exhibit greater intensity than the standard pattern, while the intensity of the (101) peak is reduced and the (110) peak is absent. The change in intensities indicates the interaction of Sns_2 filler and PPy matrix, aligning with findings from the TEM analysis.

- In-situ synthesized PPy/WS_2- 5 wt% nanocomposite exhibit response values of 3.04–30.10% for different concentrations of ammonia ranging over 50–200 ppm which is higher than PPy/Ag_2S-CdS (0.26%) and PPy thin film (0.4%). Lower response value leads to limited sensitivity, detection range and may not be suitable for applications requiring precise measurements. The possible mechanism of superior sensing properties of PPy/WS_2 was suggested to be due to synergistic effect of two materials.

- The optimized PPy/MoS_2- 5 wt% based gas sensor demonstrates improved sensing characteristics (21.65% for 100 ppm) with good response and recovery times of 340s and 680s, respectively. It also shows a high response towards NH_3 compared with pure PPy. In addition, high repeatability and long-term stability of prepared nanocomposites have also been observed over a concentration range of 10-200 ppm. Ahmad and their coworkers also reported on PPy/MoS_2 nanocomposites for NH_3 sensing, which had a good response time of 60-70 seconds. The described work was limited by a high detection range of 300-1000 ppm. Additionally, the % response, repeatability and long-term stability of the PPy/MoS_2 nanocomposite were not disclosed. Also, the author failed to disclose the tuning of nanocomposites at different ratios that could be helpful in maximizing the performance of PPy/MoS_2 nanocomposites for sensing.

- The PPy/SnS_2-5 wt% sensor showcases a favorable response ranging from 5.88% to 9.69% for NH_3 concentrations of 25 to 100 ppm at room temperature. The sensor's response is directly linked to the quantity of target gas molecules adsorbed on its surface.

- Limit of detection for ammonia gas sensors vary depending on the type of sensor. These polypyrrole based metal sulfides sensors offer detection in the range of ppm. The gas sensor demonstrates reliable response at low concentrations such as 50 ppm, 25 ppm and 10 ppm for PPy/WS_2, PPy/MoS_2 and PP/SnS_2 nanocomposites respectively, highlighting its effectiveness in detecting trace amounts. This capability makes the gas sensor ideal for real time monitoring of ammonia, offering early detection capabilities.

- Metal sulfides often possess unique 2D structures with larger surface areas compared to metal oxides. This larger surface area provides more active sites for gas molecule adsorption, leading to increased sensitivity. Metal sulfides can form stronger chemical bonds with certain target gases, resulting in a more significant change in electrical conductivity and, thus, a higher sensitivity. Some metal sulfides operate at lower temperatures compared to metal oxides, reducing power consumption and extending the sensor’s life.

5.2 Future perspectives

Based on the present study, the following work on PPy and PPy nanocomposites (WS_2, MoS_2 and SnS_2) could be done in future.

- By conducting humidity and other gas sensing studies with TMD-based composites, researchers can gain insights into the fundamental mechanisms governing sensor performance and explore novel strategies for improving sensor sensitivity and selectivity. These efforts can ultimately lead to the development of more efficient and reliable sensors for a wide range of practical applications.
- Such PPy based nanocomposites (WS_2, MoS_2 and SnS_2) can also be tested for LPG sensing.
- Density Functional Theory (DFT) calculations of PPy based nanocomposites (WS_2, MoS_2 and SnS_2) can be done in future as it helps in predicting how materials interact with gas molecules, provides information about charge transfer and band alignment at the surface.

Bibliography

[1] H. Kawasaki, T. Ueda, Y. Suda, T. Ohshima, Properties of metal doped tungsten oxide thin films for NOx gas sensors grown by PLD method combined with sputtering process, Sensors Actuators, B Chem. 100 (2004) 266–269. https://doi.org/10.1016/j.snb.2003.12.052.

[2] N. Yamazoe, N. Miura, Environmental gas sensing, Sensors Actuators B. Chem. 20 (1994) 95–102. https://doi.org/10.1016/0925-4005(93)01183-5.

[3] W.Y. Yi, K.M. Lo, T. Mak, K.S. Leung, Y. Leung, M.L. Meng, A survey of wireless sensor network based air pollution monitoring systems, Sensors (Switzerland). 15 (2015) 31392–31427. https://doi.org/10.3390/s151229859.

[4] R. Balint, N.J. Cassidy, S.H. Cartmell, Conductive polymers: Towards a smart biomaterial for tissue engineering, Acta Biomater. 10 (2014) 2341–2353. https://doi.org/10.1016/j.actbio.2014.02.015.

[5] S. Bhadra, D. Khastgir, N.K. Singha, J.H. Lee, Progress in preparation, processing and applications of polyaniline, Prog. Polym. Sci. 34 (2009) 783–810. https://doi.org/10.1016/j.progpolymsci.2009.04.003.

[6] C. Bora, S.K. Dolui, Interfacial synthesis of polypyrrole/graphene composites and investigation of their optical, electrical and electrochemical properties, Polym. Int. 63 (2014) 1439–1446. https://doi.org/10.1002/pi.4635.

[7] X. Lu, W. Zhang, C. Wang, T.C. Wen, Y. Wei, One-dimensional conducting polymer nanocomposites: Synthesis, properties and applications, Prog. Polym. Sci. 36 (2011) 671–712. https://doi.org/10.1016/j.progpolymsci.2010.07.010.

[8] F. Yan, G. Xue, F. Wan, A flexible giant magnetoresistance sensor prepared completely by electrochemical synthesis, J. Mater. Chem. 12 (2002) 2606–2608. https://doi.org/10.1039/b206896f.

[9] Y. Liu, Y. Chu, L. Yang, Adjusting the inner-structure of polypyrrole nanoparticles through microemulsion polymerization, Mater. Chem. Phys. 98 (2006) 304–308. https://doi.org/10.1016/j.matchemphys.2005.09.025.

[10] P.G. Su, X.C. Chai, Room-Temperature ppb-Level H_2S Gas Sensors Based on Ag Nanowire/Hollow PPy Nanotube Nanocomposites, Chemosensors. 10 (2022). https://doi.org/10.3390/chemosensors10080305.

[11] M.T. Ramesan, V. Santhi, In situ synthesis, characterization, conductivity studies of polypyrrole/silver doped zinc oxide nanocomposites and their application for ammonia gas sensing, J. Mater. Sci. Mater. Electron. 28 (2017) 18804–18814. https://doi.org/10.1007/s10854-017-7830-5.

[12] N. Mermilliod, J. Tanguy, F. Petiot, A Study of Chemically Synthesized Polypyrrole as Electrode Material for Battery Applications, J. Electrochem. Soc. 133 (1986) 1073–1079. https://doi.org/10.1149/1.2108788.

[13] N.A.J.M. Sommerdijk, R.J.M. Nolte, A. Kros, Conducting polymers with confined dimensions: Track-etch membranes for amperometric biosensor applications, Adv. Mater. 14 (2002) 1779–1782. https://doi.org/10.1002/1521-4095(20021203)14:23<1779::AID-ADMA1779>3.0.CO;2-T.

[14] K. Jurewicz, S. Delpeux, V. Bertagna, F. Béguin, E. Frackowiak, Supercapacitors from nanotubes/polypyrrole composites, Chem. Phys. Lett. 347 (2001) 36–40. https://doi.org/10.1016/S0009-2614(01)01037-5.

[15] J. Wang, C.O. Too, D. Zhou, G.G. Wallace, Novel electrode substrates for rechargeable lithium/polypyrrole batteries, J. Power Sources. 140 (2005) 162–167. https://doi.org/10.1016/j.jpowsour.2004.08.040.

[16] A. Joshi, S.A. Gangal, S.K. Gupta, Ammonia sensing properties of polypyrrole thin films at room temperature, Sensors Actuators, B Chem. 156 (2011) 938–942. https://doi.org/10.1016/j.snb.2011.03.009.

[17] A. Yussuf, M. Al-Saleh, S. Al-Enezi, G. Abraham, Synthesis and Characterization of Conductive Polypyrrole: The Influence of the Oxidants and Monomer on the Electrical, Thermal, and Morphological Properties, Int. J. Polym. Sci. 2018 (2018). https://doi.org/10.1155/2018/4191747.

[18] Z. Huang, S. Hu, N. Zhang, X. Chen, D. Chen, Q. Jin, X. Jian, Effect of volume ratio of acetonitrile to water on the morphology and property of polypyrrole prepared by chemical oxidation method, Polym. Eng. Sci. 52 (2012) 1600–1605.

https://doi.org/10.1002/pen.23101.

[19] Y. Tao, J. Li, A. Xie, S. Li, P. Chen, L. Ni, Y. Shen, Supramolecular self-assembly of three-dimensional polyaniline and polypyrrole crystals, Chem. Commun. 50 (2014) 12757–12760. https://doi.org/10.1039/c4cc05559d.

[20] A. Joshi, S.A. Gangal, S.K. Gupta, Ammonia sensing properties of polypyrrole thin films at room temperature, Sensors Actuators, B Chem. 156 (2011) 938–942. https://doi.org/10.1016/j.snb.2011.03.009.

[21] M. Das, S. Roy, Polypyrrole and associated hybrid nanocomposites as chemiresistive gas sensors: A comprehensive review, Mater. Sci. Semicond. Process. 121 (2021) 105332. https://doi.org/10.1016/j.mssp.2020.105332.

[22] F. Khadem, M. Pishvaei, M. Salami-Kalajahi, F. Najafi, Morphology control of conducting polypyrrole nanostructures via operational conditions in the emulsion polymerization, J. Appl. Polym. Sci. 134 (2017). https://doi.org/10.1002/app.44697.

[23] M.N. Norizan, M.H. Moklis, S.Z. Ngah Demon, N.A. Halim, A. Samsuri, I.S. Mohamad, V.F. Knight, N. Abdullah, Carbon nanotubes: Functionalisation and their application in chemical sensors, RSC Adv. 10 (2020) 43704–43732. https://doi.org/10.1039/d0ra09438b.

[24] A. Eftekhari, Tungsten dichalcogenides (WS_2, WSe_2, and WTe_2): Materials chemistry and applications, J. Mater. Chem. A. 5 (2017) 18299–18325. https://doi.org/10.1039/c7ta04268j.

[25] B.L. Li, J. Wang, H.L. Zou, S. Garaj, C.T. Lim, J. Xie, N.B. Li, D.T. Leong, Low-Dimensional Transition Metal Dichalcogenide Nanostructures Based Sensors, Adv. Funct. Mater. 26 (2016) 7034–7056. https://doi.org/10.1002/adfm.201602136.

[26] T.H. Kim, Y.H. Kim, S.Y. Park, S.Y. Kim, H.W. Jang, Two-dimensional transition metal disulfides for chemoresistive gas sensing: Perspective and challenges, Chemosensors. 5 (2017). https://doi.org/10.3390/chemosensors5020015.

[27] Q.H. Wang, K. Kalantar-Zadeh, A. Kis, J.N. Coleman, M.S. Strano, Electronics and optoelectronics of two-dimensional transition metal dichalcogenides, Nat. Nanotechnol. 7 (2012) 699–712. https://doi.org/10.1038/nnano.2012.193.

[28] I. Song, C. Park, H.C. Choi, Synthesis and properties of molybdenum disulphide:

From bulk to atomic layers, RSC Adv. 5 (2015) 7495–7514. https://doi.org/10.1039/c4ra11852a.

[29] X.J. Zhou, A.J. Harmer, N.F. Heinig, K.T. Leung, Parametric study on electrochemical deposition of copper nanoparticles on an ultrathin polypyrrole film deposited on a gold film electrode, Langmuir. 20 (2004) 5109–5113. https://doi.org/10.1021/la0497301.

[30] D. Kumar, R.C. Sharma, Advances in conductive polymers, Eur. Polym. J. 34 (1998) 1053–1060. https://doi.org/10.1016/S0014-3057(97)00204-8.

[31] T. V. Vernitskaya, O.N. Efimov, Polypyrrole: A conducting polymer (synthesis, properties, and applications), Usp. Khim. 66 (1997) 502–505. https://doi.org/10.1070/rc1997v066n05abeh000261.

[32] P.M. Beadle, S.P. Armes, Synthesis and characterization of novel polypyrrole colloids, Synth. Met. 55 (1993) 1114–1118. https://doi.org/10.1016/0379-6779(93)90209-F.

[33] D.D. Ateh, H.A. Navsaria, P. Vadgama, Polypyrrole-based conducting polymers and interactions with biological tissues, J. R. Soc. Interface. 3 (2006) 741–752. https://doi.org/10.1098/rsif.2006.0141.

[34] F.Z. Tebizi-Tighilt, F. Zane, N. Belhaneche-Bensemra, S. Belhousse, S. Sam, N.E. Gabouze, Electrochemical gas sensors based on polypyrrole-porous silicon, Appl. Surf. Sci. 269 (2013) 180–183. https://doi.org/10.1016/j.apsusc.2012.10.080.

[35] J.N. Barisci, G.G. Wallace, M.K. Andrews, A.C. Partridge, P.D. Harris, Conducting polymer sensors for monitoring aromatic hydrocarbons using an electronic nose, Sensors Actuators, B Chem. 84 (2002) 252–257. https://doi.org/10.1016/S0925-4005(02)00033-3.

[36] J. Yadong, W. Tao, W. Zhiming, L. Dan, C. Xiangdong, X. Dan, Study on the NH3-gas sensitive properties and sensitive mechanism of polypyrrole, Sensors Actuators, B Chem. 66 (2000) 280–282. https://doi.org/10.1016/S0925-4005(00)00342-7.

[37] H. Tai, Y. Jiang, G. Xie, J. Yu, M. Zhao, Self-assembly of TiO_2/polypyrrole nanocomposite ultrathin films and application for an NH_3 gas sensor, Int. J. Environ. Anal. Chem. 87 (2007) 539–551. https://doi.org/10.1080/03067310701272954.

[38] M. Brie, R. Turcu, C. Neamtu, S. Pruneanu, The effect of initial conductivity and doping anions on gas sensitivity of conducting polypyrrole films to NH_3, Sensors Actuators, B Chem. 37 (1996) 119–122. https://doi.org/10.1016/S0925-4005(97)80125-6.

[39] K.J. Dunst, K. Cysewska, P. Kalinowski, P. Jasiński, Polypyrrole based gas sensor for ammonia detection, IOP Conf. Ser. Mater. Sci. Eng. 104 (2016). https://doi.org/10.1088/1757-899X/104/1/012028.

[40] S.T. Navale, A.T. Mane, M.A. Chougule, R.D. Sakhare, S.R. Nalage, V.B. Patil, Highly selective and sensitive room temperature NO_2 gas sensor based on polypyrrole thin films, Synth. Met. 189 (2014) 94–99. https://doi.org/10.1016/j.synthmet.2014.01.002.

[41] T. Patois, J.B. Sanchez, F. Berger, J.Y. Rauch, P. Fievet, B. Lakard, Ammonia gas sensors based on polypyrrole films: Influence of electrodeposition parameters, Sensors Actuators, B Chem. 171–172 (2012) 431–439. https://doi.org/10.1016/j.snb.2012.05.005.

[42] I. Lähdesmäki, A. Lewenstam, A. Ivaska, A polypyrrole-based amperometric ammonia sensor, Talanta. 43 (1996) 125–134. https://doi.org/10.1016/0039-9140(95)01713-5.

[43] O.S. Kwon, J.Y. Hong, S.J. Park, Y. Jang, J. Jang, Resistive gas sensors based on precisely size-controlled polypyrrole nanoparticles: Effects of particle size and deposition method, J. Phys. Chem. C. 114 (2010) 18874–18879. https://doi.org/10.1021/jp1083086.

[44] X. Tang, J.P. Raskin, N. Kryvutsa, S. Hermans, O. Slobodian, A.N. Nazarov, M. Debliquy, An ammonia sensor composed of polypyrrole synthesized on reduced graphene oxide by electropolymerization, Sensors Actuators, B Chem. 305 (2020). https://doi.org/10.1016/j.snb.2019.127423.

[45] S.T. Navale, A.T. Mane, M.A. Chougule, R.D. Sakhare, S.R. Nalage, V.B. Patil, Highly selective and sensitive room temperature NO_2 gas sensor based on polypyrrole thin films, Synth. Met. 189 (2014) 94–99. https://doi.org/10.1016/j.synthmet.2014.01.002.

[46] Tai, Y. Jiang, G. Xie, J. Yu, M. Zhao, Self-assembly of TiO_2/polypyrrole nanocomposite ultrathin films and application for an NH_3 gas sensor, Int. J. Environ. Anal. Chem. 87 (2007) 539–551. https://doi.org/10.1080/03067310701272954.

[47] L. Groenendaal, F. Jonas, D. Freitag, H. Pielartzik, J.R. Reynolds, Poly(3,4-ethylenedioxythiophene) and its derivatives: past, present, and future, Adv. Mater. 12 (2000) 481–494. https://doi.org/10.1002/(SICI)1521-4095(200004)12:7<481::AID-ADMA481>3.0.CO;2-C.

[48] P.G. Su, C.P. Wang, Flexible humidity sensor based on TiO_2 nanoparticles-polypyrrole-poly-[3-(methacrylamino)propyl] trimethyl ammonium chloride composite materials, Sensors Actuators, B Chem. 129 (2008) 538–543. https://doi.org/10.1016/j.snb.2007.09.011.

[49] A. Singh, Z. Salmi, N. Joshi, P. Jha, A. Kumar, H. Lecoq, S. Lau, M.M. Chehimi, D.K. Aswal, S.K. Gupta, Photo-induced synthesis of polypyrrole-silver nanocomposite films on N-(3-trimethoxysilylpropyl)pyrrole-modified biaxially oriented polyethylene terephthalate flexible substrates, RSC Adv. 3 (2013) 5506–5523. https://doi.org/10.1039/c3ra22981e.

[50] L. Hong, Y. Li, M. Yang, Fabrication and ammonia gas sensing of palladium/polypyrrole nanocomposite, Sensors Actuators, B Chem. 145 (2010) 25–31. https://doi.org/10.1016/j.snb.2009.11.057.

[51] L. Hong, Y. Li, M. Yang, Fabrication and ammonia gas sensing of palladium/polypyrrole nanocomposite, Sensors Actuators, B Chem. 145 (2010) 25–31. https://doi.org/10.1016/j.snb.2009.11.057.

[52] X. Yang, L. Li, F. Yan, Polypyrrole/silver composite nanotubes for gas sensors, Sensors Actuators, B Chem. 145 (2010) 495–500. https://doi.org/10.1016/j.snb.2009.12.065.

[53] P. Song, Q. Wang, Z. Yang, Ammonia gas sensor based on PPy/$ZnSnO_3$ nanocomposites, Mater. Lett. 65 (2011) 430–432. https://doi.org/10.1016/j.matlet.2010.10.087.

[54] J. Jang, J. Bae, Carbon nanofiber/polypyrrole nanocable as toxic gas sensor, Sensors Actuators, B Chem. 122 (2007) 7–13. https://doi.org/10.1016/j.snb.2006.05.002.

[55] K. Jlassi, S. Mallick, H. Mutahir, Z. Ahmad, F. Touati, Synthesis of in situ photoinduced halloysite-polypyrrole@silver nanocomposite for the potential application in humidity sensors, Nanomaterials. 10 (2020) 1–14. https://doi.org/10.3390/nano10071426.

[56] S.K. Mahadeva, S. Yun, J. Kim, Flexible humidity and temperature sensor based on cellulose-polypyrrole nanocomposite, Sensors Actuators, A Phys. 165 (2011) 194–199. https://doi.org/10.1016/j.sna.2010.10.018.

[57] R. Najjar, S. Nematdoust, A resistive-type humidity sensor based on polypyrrole and ZnO nanoparticles: hybrid polymers vis-a-vis nanocomposites, RSC Adv. 6 (2016) 112129–112139. https://doi.org/10.1039/C6RA24002J.

[58] N. V. Blinova, J. Stejskal, M. Trchová, J. Prokeš, M. Omastová, Polyaniline and polypyrrole: A comparative study of the preparation, Eur. Polym. J. 43 (2007) 2331–2341. https://doi.org/10.1016/j.eurpolymj.2007.03.045.

[59] K. Kojima, T. Yamauchi, M. Shimomura, S. Miyauchi, Covalent immobilization of glucose oxidase on poly[1-(2-carboxyethyl)pyrrole] film for glucose sensing, Polymer (Guildf). 39 (1998) 2079–2082. https://doi.org/10.1016/S0032-3861(97)00531-4.

[60] X.G. Li, A. Li, M.R. Huang, Y. Liao, Y.G. Lu, Efficient and scalable synthesis of pure polypyrrole nanoparticles applicable for advanced nanocomposites and carbon nanoparticles, J. Phys. Chem. C. 114 (2010) 19244–19255. https://doi.org/10.1021/jp107435b.

[61] A.L. Sharma, R. Singhal, A. Kumar, Rajesh, K.K. Pande, B.D. Malhotra, Immobilization of glucose oxidase onto electrochemically prepared poly(aniline-co-fluoroaniline) films, J. Appl. Polym. Sci. 91 (2004) 3999–4006. https://doi.org/10.1002/app.13553.

[62] G.A. Grijalva-Bustamante, A.G. Evans-Villegas, T. Del Castillo-Castro, M.M. Castillo-Ortega, R. Cruz-Silva, F. Huerta, E. Morallón, Enzyme mediated synthesis of polypyrrole in the presence of chondroitin sulfate and redox mediators of natural origin, Mater. Sci. Eng. C. 63 (2016) 650–656. https://doi.org/10.1016/j.msec.2016.03.042.

[63] A. Kausaite-Minkstimiene, V. Mazeiko, A. Ramanaviciene, A. Ramanavicius, Evaluation of chemical synthesis of polypyrrole particles, Colloids Surfaces A Physicochem. Eng. Asp. 483 (2015) 224–231. https://doi.org/10.1016/j.colsurfa.2015.05.008.

[64] B. Lakard, G. Herlem, S. Lakard, A. Antoniou, B. Fahys, Urea potentiometric biosensor based on modified electrodes with urease immobilized on polyethylenimine films, Biosens. Bioelectron. 19 (2004) 1641–1647. https://doi.org/10.1016/j.bios.2003.12.035.

[65] W.J. Sung, Y.H. Bae, A glucose oxidase electrode based on polypyrrole with polyanion/PEG/enzyme conjugate dopant, Biosens. Bioelectron. 18 (2003) 1231–1239. https://doi.org/10.1016/S0956-5663(03)00091-5.

[66] T. Nakaminami, S.I. Ito, S. Kuwabata, H. Yoneyama, Uricase-catalyzed oxidation of uric acid using an artificial electron acceptor and fabrication of amperometric uric acid sensors with use of a redox ladder polymer, Anal. Chem. 71 (1999) 1928–1934. https://doi.org/10.1021/ac981168u.

[67] A. Ramanavicius, A. Kausaite, A. Ramanaviciene, J. Acaite, A. Malinauskas, Redox enzyme - glucose oxidase - initiated synthesis of polypyrrole, Synth. Met. 156 (2006) 409–413. https://doi.org/10.1016/j.synthmet.2005.12.018.

[68] M.R. Nabid, A.A. Entezami, A novel method for synthesis of water-soluble polypyrrole with horseradish peroxidase enzyme, J. Appl. Polym. Sci. 94 (2004) 254–258. https://doi.org/10.1002/app.20882.

[69] K. Won, Y.H. Kim, E.S. An, Y.S. Lee, B.K. Song, Horseradish peroxidase-catalyzed polymerization of cardanol in the presence of redox mediators, Biomacromolecules. 5 (2004) 1–4. https://doi.org/10.1021/bm034325u.

[70] R. Bouldin, S. Ravichandran, A. Kokil, R. Garhwal, S. Nagarajan, J. Kumar, F.F. Bruno, L.A. Samuelson, R. Nagarajan, Synthesis of polypyrrole with fewer structural defects using enzyme catalysis, Synth. Met. 161 (2011) 1611–1617. https://doi.org/10.1016/j.synthmet.2011.05.026.

[71] Z. Deljoo Kojabad, S.A. Shojaosadati, Chemical synthesis of polypyrrole nanostructures: Optimization and applications for neural microelectrodes, Mater.

Des. 96 (2016) 378–384. https://doi.org/10.1016/j.matdes.2016.02.045.

[72] R. Jain, N. Jadon, A. Pawaiya, Polypyrrole based next generation electrochemical sensors and biosensors: A review, TrAC Trends Anal. Chem. 97 (2017) 363–373. https://doi.org/https://doi.org/10.1016/j.trac.2017.10.009.

[73] H.K. Chitte, G.N. Shinde, N. V. Bhat, V.E. Walunj, Synthesis of Polypyrrole Using Ferric Chloride (FeCl₃) as Oxidant Together with Some Dopants for Use in Gas Sensors, J. Sens. Technol. 01 (2011) 47–56. https://doi.org/10.4236/jst.2011.12007.

[74] M. Omastová, M. Trchová, J. Kovářová, J. Stejskal, Synthesis and structural study of polypyrroles prepared in the presence of surfactants, Synth. Met. 138 (2003) 447–455. https://doi.org/10.1016/S0379-6779(02)00498-8.

[75] S. Khamlich, F. Barzegar, Z.Y. Nuru, J.K. Dangbegnon, A. Bello, B.D. Ngom, N. Manyala, M. Maaza, Polypyrrole/graphene nanocomposite: High conductivity and low percolation threshold, Synth. Met. 198 (2014) 101–106. https://doi.org/10.1016/j.synthmet.2014.10.004.

[76] N. Hassanzadeh, H. Omidvar, S.H. Tabaian, Chemical synthesis of high density and long polypyrrole nanowire arrays using alumina membrane and their hydrogen sensing properties, Superlattices Microstruct. 51 (2012) 314–323. https://doi.org/10.1016/j.spmi.2011.12.001.

[77] S.A. Waghuley, S.M. Yenorkar, S.S. Yawale, S.P. Yawale, Application of chemically synthesized conducting polymer-polypyrrole as a carbon dioxide gas sensor, Sensors Actuators, B Chem. 128 (2008) 366-373. https://doi.org/10.1016/j.snb.2007.06.023.

[78] X. Chen, J. -P Issi, J. Devaux, D. Billaud, Chemically oxidized polypyrrole: Influence of the experimental conditions on its electrical conductivity and morphology, Polym. Eng. Sci. 35 (1995) 642–647. https://doi.org/10.1002/pen.760350803.

[79] K. Malook, H. Khan, M. Shah, Ammonia sensing behavior of polypyrrole-bimetallic oxide composites, Polym. Compos. 41 (2020) 2610–2615. https://doi.org/10.1002/pc.25559.

[80] Z. Jun, W. Shurong, X. Mijuan, W. Yan, X. Huijuan, Z. Shoumin, G. Xianzhi, W. Shihua, Polypyrrole-coated SnO_2 hollow spheres and their application for ammonia sensor, J. Phys. Chem. C. 113 (2009) 1662–1665. https://doi.org/10.1021/jp8096633.

[81] D.S. Dhawale, R.R. Salunkhe, U.M. Patil, K. V. Gurav, A.M. More, C.D. Lokhande, Room temperature liquefied petroleum gas (LPG) sensor based on p-polyaniline/n-TiO_2 heterojunction, Sensors Actuators, B Chem. 134 (2008) 988–992. https://doi.org/10.1016/j.snb.2008.07.003.

[82] X.W. Lou, L.A. Archer, Z. Yang, Hollow micro-/nanostructures: Synthesis and applications, Adv. Mater. 20 (2008) 3987–4019. https://doi.org/10.1002/adma.200800854.

[83] X.L. Li, T.J. Lou, X.M. Sun, Y.D. Li, Highly sensitive WO_3 hollow-sphere gas sensors, Inorg. Chem. 43 (2004) 5442–5449. https://doi.org/10.1021/ic049522w.

[84] M. Tiemann, Porous metal oxides as gas sensors, Chem. - A Eur. J. 13 (2007) 8376–8388. https://doi.org/10.1002/chem.200700927.

[85] Y. Qin, B. Zhang, Z. Zhang, Combination of PPy with three-dimensional rGO to construct bioinspired nanocomposite for NH_3-sensing enhancement, Org. Electron. 70 (2019) 240–245. https://doi.org/10.1016/j.orgel.2019.04.023.

[86] J. Sun, X. Shu, Y. Tian, Z. Tong, S. Bai, R. Luo, D. Li, C.C. Liu, Facile preparation of polypyrrole-reduced graphene oxide hybrid for enhancing NH_3 sensing at room temperature, Sensors Actuators, B Chem. 241 (2017) 658–664. https://doi.org/10.1016/j.snb.2016.10.047.

[87] C. Mahajan, P. Chaudhari, S. Mishra, RGO–MWCNT–ZnO based polypyrrole nanocomposite for ammonia gas sensing, J. Mater. Sci. Mater. Electron. 29 (2018) 8039–8048. https://doi.org/10.1007/s10854-018-8810-0.

[88] G. Kiani, A. Nourizad, R. Nosrati, In-situ Chemical Synthesis of Polypyrrole/Silver Nanocomposite for the Use as a Room Temperature Ammonia Gas Sensor, Fibers Polym. 19 (2018) 2188–2194. https://doi.org/10.1007/s12221-018-8097-z.

[89] M.T. Ramesan, Synthesis, characterization, and conductivity studies of polypyrrole/copper sulfide nanocomposites, J. Appl. Polym. Sci. 128 (2013) 1540–

1546. https://doi.org/10.1002/app.38304.

[90] B. Yeole, T. Sen, D. Hansora, S. Mishra, Electrical and Gas Sensing Behaviour of Polypyrrole / silver Sulphide Nanocomposites, J. Appl. Polym. Sci. 4 (2017) 10–20. https://doi.org/10.12691/ajst-4-1-2.

[91] C. Li, J.H. Hsieh, Y.T. Lee, Fabrication and structural characterization of plasma polymerized polypyrrole thin film, Surf. Coatings Technol. 320 (2017) 206–212. https://doi.org/10.1016/j.surfcoat.2017.01.049.

[92] J.L. Yagüe, N. Agulló, S. Borrós, Plasma polymerization of polypyrrole-like films on nanostructured surfaces, Plasma Process. Polym. 5 (2008) 433–443. https://doi.org/10.1002/ppap.200700139.

[93] A. Dhillon, A. Kaur, A.K. Srivastava, D.K. Avasthi, Experimental investigations of semi-crystalline plasma polymerized polypyrrole for surface coating, Prog. Org. Coatings. 69 (2010) 396–401. https://doi.org/10.1016/j.porgcoat.2010.08.002.

[94] L. Geng, Y. Zhao, X. Huang, S. Wang, S. Zhang, W. Huang, S. Wu, The preparation and gas sensitivity study of polypyrrole/zinc oxide, Synth. Met. 156 (2006) 1078–1082. https://doi.org/10.1016/j.synthmet.2006.06.019.

[95] S.R. Nalage, A.T. Mane, R.C. Pawar, C.S. Lee, V.B. Patil, Polypyrrole–NiO hybrid nanocomposite films: highly selective, sensitive, and reproducible NO_2 sensors, Ionics (Kiel). 20 (2014) 1607–1616. https://doi.org/10.1007/s11581-014-1122-3.

[96] K.H. An, S.Y. Jeong, H.R. Hwang, Y.H. Lee, Enhanced sensitivity of a gas sensor incorporating single-walled carbon nanotube-polypyrrole nanocomposites, Adv. Mater. 16 (2004) 1005–1009. https://doi.org/10.1002/adma.200306176.

[97] W.-K. Jang, J.-M. Yun, H.-I. Kim, Y.-S. Lee, Improvement in ammonia gas sensing behavior by polypyrrole/multi-walled carbon nanotubes composites, Carbon Lett. 13 (2012) 88–93. https://doi.org/10.5714/cl.2012.13.2.088.

[98] S.G. Bachhav, D.R. Patil, Synthesis and Characterization of Polyaniline- Multiwalled Carbon Nanotube Nanocomposites and Its Electrical Percolation Behavior, Am. J. Mater. Sci. 5 (2015) 90–95. https://doi.org/10.13140/RG.2.1.2131.5924.

[99] S.B. Kondawar, S.P. Agrawal, S.H. Nimkar, H.J. Sharma, P.T. Patil, Conductive

polyaniline-tin oxide nanocomposites for ammonia sensor, Adv. Mater. Lett. 3 (2012) 393–398. https://doi.org/10.5185/amlett.2012.6361.

[100] D.C. Tiwari, P. Atri, R. Sharma, Sensitive detection of ammonia by reduced graphene oxide/polypyrrole nanocomposites, Synth. Met. 203 (2015) 228–234. https://doi.org/10.1016/j.synthmet.2015.02.026.

[101] W. De Lin, H.M. Chang, R.J. Wu, Applied novel sensing material graphene/polypyrrole for humidity sensor, Sensors Actuators, B Chem. 181 (2013) 326–331. https://doi.org/10.1016/j.snb.2013.02.017.

[102] S.K. Shukla, C.S. Kushwaha, A. Shukla, G.C. Dubey, Integrated approach for efficient humidity sensing over zinc oxide and polypyrole composite, Mater. Sci. Eng. C. 90 (2018) 325–332. https://doi.org/10.1016/j.msec.2018.04.054.

[103] N. Gaikwad, S. Bhanoth, P. V. More, G.H. Jain, P.K. Khanna, Chemically designed Pt/PPy nano-composite for effective LPG gas sensor, Nanoscale. 6 (2014) 2746–2751. https://doi.org/10.1039/c3nr05375j.

[104] H. Shokry Hassan, A.B. Kashyout, I. Morsi, A.A.A. Nasser, H. Abuklill, Development of polypyrrole coated copper nanowires for gas sensor application, Sens. Bio-Sensing Res. 5 (2015) 50–54. https://doi.org/10.1016/j.sbsr.2015.07.004.

[105] Y. Wang, A. Liu, Y. Han, T. Li, Sensors based on conductive polymers and their composites: a review, Polym. Int. 69 (2020) 7–17. https://doi.org/10.1002/pi.5907.

[106] T.N. Ly, S. Park, Highly sensitive ammonia sensor for diagnostic purpose using reduced graphene oxide and conductive polymer, Sci. Rep. 8 (2018) 1–12. https://doi.org/10.1038/s41598-018-36468-z.

[107] J. Zhang, X. Liu, S. Wu, H. Xu, B. Cao, One-pot fabrication of uniform polypyrrole/Au nanocomposites and investigation for gas sensing, Sensors Actuators, B Chem. 186 (2013) 695–700. https://doi.org/10.1016/j.snb.2013.06.063.

[108] P.G. Su, S.L. Liao, Fabrication of a flexible H_2 sensor based on Pd nanoparticles modified polypyrrole films, Mater. Chem. Phys. 170 (2016) 180–185. https://doi.org/10.1016/j.matchemphys.2015.12.037.

[109] S.S. Barkade, D. V. Pinjari, A.K. Singh, P.R. Gogate, J.B. Naik, S.H. Sonawane, M. Ashokkumar, A.B. Pandit, Ultrasound assisted miniemulsion polymerization for

preparation of polypyrrole-zinc oxide (PPy/ZnO) functional latex for liquefied petroleum gas sensing, Ind. Eng. Chem. Res. 52 (2013) 7704–7712. https://doi.org/10.1021/ie301698g.

[110] B. Yeole, T. Sen, D.P. Hansora, S. Mishra, Effect of electrical properties on gas sensitivity of polypyrrole/cds nanocomposites, J. Appl. Polym. Sci. 132 (2015). https://doi.org/10.1002/app.42379.

[111] M. Baruah, S. Kalra, B. Kalra, Primordial prevention of atherosclerotic vascular disease: Preventing the "pre-event," J. Med. Nutr. Nutraceuticals. 4 (2015) 61. https://doi.org/10.4103/2278-1870.162169.

[112] S. Seema, M.V.N.A. Prasad, Studies on DC conductivity and LPG sensing behaviour of nanostructured polypyrrole-CeO_2 composites, AIP Conf. Proc. 1989 (2018). https://doi.org/10.1063/1.5047737.

[113] G.T. Lamdhade, K.B. Raulkar, S.S. Yawale, S.P. Yawale, Fabrication of multilayer SnO_2–ZnO–PPy sensor for ammonia gas detection, Indian J. Phys. 89 (2015) 1025–1030. https://doi.org/10.1007/s12648-015-0676-x.

[114] H.A. Khorami, A. Eghbali, M. Keyanpour-Rad, M.R. Vaezi, M. Kazemzad, Ammonia sensing properties of (SnO_2-ZnO)/polypyrrole coaxial nanocables, J. Mater. Sci. 49 (2014) 685–690. https://doi.org/10.1007/s10853-013-7749-z.

[115] P.G. Su, Y.T. Peng, Fabrication of a room-temperature H_2S gas sensor based on PPy/WO_3 nanocomposite films by in-situ photopolymerization, Sensors Actuators, B Chem. 193 (2014) 637–643. https://doi.org/10.1016/j.snb.2013.12.027.

[116] W.K. Jang, J. Yun, H. Il Kim, Y.S. Lee, Improvement of ammonia sensing properties of polypyrrole by nanocomposite with graphitic materials, Colloid Polym. Sci. 291 (2013) 1095–1103. https://doi.org/10.1007/s00396-012-2832-6.

[117] X. Tang, D. Lahem, J.P. Raskin, P. Gérard, X. Geng, N. André, M. Debliquy, A Fast and Room-Temperature Operation Ammonia Sensor Based on Compound of Graphene with Polypyrrole, IEEE Sens. J. 18 (2018) 9088–9096. https://doi.org/10.1109/JSEN.2018.2869203.

[118] M.T. Ramesan, V. Santhi, Synthesis, characterization, conductivity and sensor application study of polypyrrole/silver doped nickel oxide nanocomposites,

Compos. Interfaces. 25 (2018) 725–741. https://doi.org/10.1080/09276440.2018.1439626.

[119] Y. Li, M. Jiao, M. Yang, In-situ grown nanostructured ZnO via a green approach and gas sensing properties of polypyrrole/ZnO nanohybrids, Sensors Actuators, B Chem. 238 (2017) 596–604. https://doi.org/10.1016/j.snb.2016.07.089.

[120] B. Yeole, T. Sen, D. Hansora, S. Mishra, Gas Sensing Behaviour of Polypyrrole/silver Sulphide Nanocomposites, Am. J. Sens. Technol. 4 (2017) 10–20. https://doi.org/10.12691/ajst-4-1-2.

[121] H.K. Chitte, N. V. Bhat, M.A. V. Gore, G.N. Shind, Synthesis of Polypyrrole Using Ammonium Peroxy Disulfate (APS) as Oxidant Together with Some Dopants for Use in Gas Sensors, Mater. Sci. Appl. 02 (2011) 1491–1498. https://doi.org/10.4236/msa.2011.210201.

[122] S. Nor, A. Baharin, N.H. Hashim, I. Najwa, M. Norsham, S. Shahabuddin, Optimization of Tungsten Disulfide / Polypyrrole Composite as Photocatalyst in Sunlight-Asissted Photodegradation of Methylene Blue in Aqueous Solution, Res. Sq. (2021) 1–18. https://doi.org/10.1016/j.mssp.2021.010.

[123] G. Zhang, X. Du, Y. Wang, H. Wang, W. Wang, Z. Fu, Controllable synthesis of SnS2 nanostructures with high adsorption and photocatalytic activities, Mater. Sci. Semicond. Process. 64 (2017) 77–84. https://doi.org/10.1016/j.mssp.2017.03.010.

[124] M. Vinitha, G. Velraj, Synthesis and characteristic studies on pure and nano silver oxide-doped polypyrrole for supercapacitor application, J. Mater. Sci. Mater. Electron. 33 (2022) 6627–6635. https://doi.org/10.1007/s10854-022-07837-2.

[125] R.D. Sakhare, Y.H. Navale, S.T. Navale, V.B. Patil, Investigation of structural, morphological and electrical properties of nanocomposite based on SnO_2 nanoparticles filled polypyrrole matrix, J. Mater. Sci. Mater. Electron. 28 (2017) 11132–11141. https://doi.org/10.1007/s10854-017-6900-z.

[126] J. Kopecká, D. Kopecký, M. Vrňata, P. Fitl, J. Stejskal, M. Trchová, P. Bober, Z. Morávková, J. Prokeš, I. Sapurina, Polypyrrole nanotubes: Mechanism of formation, RSC Adv. 4 (2014) 1551–1558. https://doi.org/10.1039/c3ra45841e.

[127] A.M.R. Ramírez, M.A. Gacitúa, E. Ortega, F.R. Díaz, M.A. del Valle,

Electrochemical in situ synthesis of polypyrrole nanowires, Electrochem. Commun. 102 (2019) 94–98. https://doi.org/10.1016/j.elecom.2019.04.007.

[128] Z. Bekkar Djelloul Sayah, A. Mekki, F. Delaleux, O. Riou, J.F. Durastanti, Response Surface Methodology as a Powerful Tool for the Synthesis of Polypyrrole-Doped Organic Sulfonic Acid and the Optimization of its Thermoelectric Properties, J. Electron. Mater. 48 (2019) 3662–3675. https://doi.org/10.1007/s11664-019-07124-7.

[129] C. Wang, M. Yang, L. Liu, Y. Xu, X. Zhang, X. Cheng, S. Gao, Y. Gao, L. Huo, One-step synthesis of polypyrrole/Fe_2O_3 nanocomposite and the enhanced response of NO_2 at low temperature, J. Colloid Interface Sci. 560 (2020) 312–320. https://doi.org/10.1016/j.jcis.2019.10.076.

[130] H. Farrokhi, O. Khani, F. Nemati, M. Jazirehpour, Synthesis and investigation of microwave characteristics of polypyrrole nanostructures prepared via self-reactive flower-like MnO_2 template, Synth. Met. 215 (2016) 142–149. https://doi.org/10.1016/j.synthmet.2016.02.016.

[131] Z. Qi, P.G. Pickup, Size Control of Polypyrrole Particles, Chem. Mater. 9 (1997) 2934–2939. https://doi.org/10.1021/cm970280q.

[132] A.A. Yadav, S.B. Kulkarni, C.D. Lokhande, Synthesis and characterization of polypyrrole thin film by MW-CBD method for NH_3 gas sensor, Polym. Bull. 75 (2018) 4547–4553. https://doi.org/10.1007/s00289-018-2282-5.

[133] N. Othman, Z.A. Talib, A. Kassim, A.H. Shaari, J.Y.C. Liew, Electrical Properties of Polypyrrole Conducting Polymer at Various Dopant Concentrations, Malaysian J. Fundam. Appl. Sci. 5 (2014) 1–6. https://doi.org/10.11113/mjfas.v5n1.284.

[134] A.K. Mishra, Conducting Polymers: Concepts and Applications, J. At. Mol. Condens. Nano Phys. 5 (2018) 159–193. https://doi.org/10.26713/jamcnp.v5i2.842.

[135] S. Majumdar, K. Sarmah, D. Mahanta, A Simple Route to Prepare Polypyrrole-Coated Filter Papers via Vapor Phase Polymerization and Their Gas Sensing Application, ACS Appl. Polym. Mater. 2 (2020) 1933–1942. https://doi.org/10.1021/acsapm.0c00147.

[136] I. Sapurina, Y. Li, E. Alekseeva, P. Bober, M. Trchová, Z. Morávková, J. Stejskal,

Polypyrrole nanotubes: The tuning of morphology and conductivity, Polymer (Guildf). 113 (2017) 247–258. https://doi.org/10.1016/j.polymer.2017.02.064.

[137] R.H. Santim, H.A. de Aquino, J.A. Malmonge, Fabrication of polypyrrole nanoparticles using microemulsion polymerization for diferent Py/APS/SDS molar ratios, Mater. Sci. Forum. 869 (2016) 391–395. https://doi.org/10.4028/www.scientific.net/MSF.869.391.

[138] S. Nosheen, M. Irfan, F. Habib, S.Z. Abbas, B. Waseem, F. Iftikhar, B. Soomro, A.K. Aziz, Synthesis and Characterization of Polypyrrole Synthesized via Different Routes, Bull. Mater. Sci. 9 (2020) 1630–1633. https://doi.org/10.1155/2020/481633

[139] A. Sunilkumar, S. Manjunatha, T. Machappa, B. Chethan, Y.T. Ravikiran, A tungsten disulphide–polypyrrole composite-based humidity sensor at room temperature, Bull. Mater. Sci. 42 (2019) 1–5. https://doi.org/10.1007/s12034-019-1955-5.

[140] A. Yussuf, M. Al-Saleh, S. Al-Enezi, G. Abraham, Synthesis and Characterization of Conductive Polypyrrole: The Influence of the Oxidants and Monomer on the Electrical, Thermal, and Morphological Properties, Int. J. Polym. Sci. 2018 (2018). https://doi.org/10.1155/2018/4191747.

[141] A. Afzal, F.A. Abuilaiwi, A. Habib, M. Awais, S.B. Waje, M.A. Atieh, Polypyrrole/carbon nanotube supercapacitorsTechnological advances and challenges, J. Power Sources. 352 (2017) 174–186. https://doi.org/10.1016/j.jpowsour.2017.03.128.

[142] N. Sakhuja, S. Member, R.K. Jha, M. Ieee, N. Bhat, Tungsten Disulphide nanosheets for high performance chemiresistive Ammonia gas sensor, IEEE 19 (2019) 11767-11774. https://doi.org/10.1109/ICSENS.2018.8589916.

[143] A. Sunilkumar, S. Manjunatha, Y.T. Ravikiran, M. Revanasiddappa, M. Prashantkumar, T. Machappa, AC conductivity and dielectric studies in polypyrrole wrapped tungsten disulphide composites, Polym. Bull. 79 (2022) 1391–1407. https://doi.org/10.1007/s00289-021-03552-w.

[144] B.H. Xu, B.Z. Lin, Z.J. Chen, X.L. Li, Q.Q. Wang, Preparation and electrical conductivity of polypyrrole/WS_2 layered nanocomposites, J. Colloid Interface Sci.

330 (2009) 220–226. https://doi.org/10.1016/j.jcis.2008.10.033.

[145] K. Shimakawa, Electrical transport properties, World Sci. Ref. Amorph. Mater. Struct. Prop. Model. Main Appl. (In 3 Vol. (2020) 177–202. https://doi.org/10.1142/9789811215575_0007.

[146] S. Manjunatha, T. Machappa, A. Sunilkumar, Y.T. Ravikiran, Tungsten disulfide: an efficient material in enhancement of AC conductivity and dielectric properties of polyaniline, J. Mater. Sci. Mater. Electron. 29 (2018) 11581–11590. https://doi.org/10.1007/s10854-018-9255-1.

[147] S.D. Lawaniya, N. Meena, S. Kumar, Y. Yu, K. Awasthi, Effect of MWCNTs incorporation into polypyrrole (PPy) on ammonia sensing at room temperature, IEEE 23 (2022) 1–8. https://doi.org/10.1109/JSEN.2022.3224165.

[148] S. Ahmad, I. Khan, A. Husain, A. Khan, A.M. Asiri, Properties of Polypyrrole / MoS_2 Nanocomposite, Polymers (Basel) 12 (2020) 1–13. https://doi.org/10.3390/polym12123047.

[149] B. Yeole, T. Sen, D. Hansora, S. Mishra, Polypyrrole/metal sulphide hybrid nanocomposites: Synthesis, characterization and room temperature gas sensing properties, Mater. Res. 19 (2016) 999–1007. https://doi.org/10.1590/1980-5373-MR-2015-0502.

[150] D. Zhang, C. Jiang, Y. Sun, Room-temperature high-performance ammonia gas sensor based on layer-by-layer self-assembled molybdenum disulfide/zinc oxide nanocomposite film, J. Alloys Compd. 698 (2017) 476–483. https://doi.org/10.1016/j.jallcom.2016.12.222.

[151] D.H. Youn, J.W. Jang, J.Y. Kim, J.S. Jang, S.H. Choi, J.S. Lee, Fabrication of graphene-based electrode in less than a minute through hybrid microwave annealing, Sci. Rep. 4 (2014) 05492. https://doi.org/10.1038/srep05492.

[152] Y. Sood, H. Mudila, A. Katoch, P.E. Lokhande, D. Kumar, A. Sharma, A. Kumar, Eminence of oxidants on structural–electrical property of Polypyrrole, J. Mater. Sci. Mater. Electron. 34 (2023). https://doi.org/10.1007/s10854-023-10834-8.

[153] H. Mao, Y. Fu, H. Yang, S. Zhang, J. Liu, S. Wu, Q. Wu, T. Ma, X.M. Song, Structure-activity relationship toward electrocatalytic nitrogen reduction of MoS_2

growing on polypyrrole/graphene oxide affected by pyridinium-type ionic liquids, Chem. Eng. J. 425 (2021). https://doi.org/10.1016/j.cej.2021.131769.

[154] M.U. Shariq, A. Husain, M. Khan, A. Ahmad, Synthesis and characterization of polypyrrole/molybdenum oxide composite for ammonia vapour sensing at room temperature, Polym. Compos. 29 (2021) S989–S999. https://doi.org/10.1177/09673911211036589.

[155] L. Gai, Y. Zhao, G. Song, Q. An, Z. Xiao, S. Zhai, Z. Li, Construction of core-shell PPy@MoS_2 with nanotube-like heterostructures for electromagnetic wave absorption: Assembly and enhanced mechanism, Compos. Part A Appl. Sci. Manuf. 136 (2020). https://doi.org/10.1016/j.compositesa.2020.105965.

[156] A. Kumar, V. Kumar, M. Kumar, K. Awasthi, Synthesis and characterization of hybrid PANI/MWCNT nanocomposites for EMI applications, Polym. Compos. 39 (2018) 3858–3868. https://doi.org/10.1002/pc.24418.

[157] Z. Yang, H. Guo, W. You, Z. Wu, L. Yang, M. Wang, R. Che, Compressible and flexible PPy@MoS_2/C microwave absorption foam with strong dielectric polarization from 2D semiconductor intermediate sandwich structure, Nanoscale. 13 (2021) 5115–5124. https://doi.org/10.1039/d0nr08794g.

[158] D. Zhang, Z. Wu, P. Li, X. Zong, G. Dong, Y. Zhang, Facile fabrication of polyaniline/multi-walled carbon nanotubes/molybdenum disulfide ternary nanocomposite and its high-performance ammonia-sensing at room temperature, Sensors Actuators, B Chem. 258 (2018) 895–905. https://doi.org/10.1016/j.snb.2017.11.168.

[159] R.N. Bulakhe, S. V. Patil, P.R. Deshmukh, N.M. Shinde, C.D. Lokhande, Fabrication and performance of polypyrrole (Ppy)/TiO_2 heterojunction for room temperature operated LPG sensor, Sensors Actuators, B Chem. 181 (2013) 417–423. https://doi.org/10.1016/j.snb.2013.01.056.

[160] S.Y. Lee, U.J. Kim, J. Chung, H. Nam, H.Y. Jeong, G.H. Han, H. Kim, H.M. Oh, H. Lee, H. Kim, Y.G. Roh, J. Kim, S.W. Hwang, Y. Park, Y.H. Lee, Large Work Function Modulation of Monolayer MoS_2 by Ambient Gases, ACS Nano. 10 (2016) 6100–6107. https://doi.org/10.1021/acsnano.6b01742.

[161] Y. Sood, S.D. Lawaniya, H. Mudila, K. Awasthi, A. Kumar, Polypyrrole-Tungsten disulphide 2D nanocomposites for ammonia sensing, Sensors Actuators B Chem. 394 (2023) 134298. https://doi.org/10.1016/j.snb.2023.134298.

[162] Y. Li, H. Ban, M. Yang, Highly sensitive NH_3 gas sensors based on novel polypyrrole-coated SnO_2 nanosheet nanocomposites, Sensors Actuators, B Chem. 224 (2016) 449–457. https://doi.org/10.1016/j.snb.2015.10.078.

[163] A. Joseph, C.R. Anjitha, A. Aravind, P.M. Aneesh, Structural, optical and magnetic properties of SnS_2 nanoparticles and photo response characteristics of p-Si/n-SnS_2 heterojunction diode, Appl. Surf. Sci. 528 (2020). https://doi.org/10.1016/j.apsusc.2020.146977.

List of Publications from this Research Work

1. Yuvika Sood, Harish Mudila, Akash Katoch, P. E. Lokhande, Deepak Kumar, Ajit Sharma, and Anil Kumar. "Eminence of oxidants on structural–electrical property of Polypyrrole. *Journal of Materials Science: Materials in Electronics* 34, no. 18 **(2023)**: 1401. https://doi.org/10.1007/s10854-023-10834-8
2. Yuvika Sood, Shiv Dutta Lawaniya, Harish Mudila, Kamlendra Awasthi, and Anil Kumar. "Polypyrrole-Tungsten disulphide 2D nanocomposites for ammonia sensing. *Sensors and Actuators B: Chemical* 394 **(2023)**: 134298. https://doi.org/10.1016/j.snb.2023.134298
3. Yuvika Sood, Varsha S. Pawar, Harish Mudila, and Anil Kumar. "A review on synthetic strategies and gas sensing approach for polypyrrole-based hybrid nanocomposites. *Polymer Engineering & Science* 61, no. 12 **(2021):** 2949-2973. https://doi.org/10.1002/pen.25822.
4. Yuvika Sood, Varsha S. Pawar, Harish Mudila, and Anil Kumar Influence of Polypyrrole Morphology on Gas Sensing. In Journal of Physics: Conference Series (Vol. 2267, No. 1, p. 012050). IOP Publishing, **(2022)**, https://doi.org/ 10.1088/1742-6596/2267/1/012050.
5. Yuvika Sood, Shiv Dutta Lawaniya, Harish Mudila, Akash Katoch, Kamlendra Awasthi, and Anil Kumar. Ultra-High Performance of PPy/MoS_2 2D Nanocomposites for Ammonia Sensing. *Sensors and Actuators B: Chemical* 417 **(2024):** 136165. https://doi.org/10.1016/j.snb.2024.136165.

Other Publications

1. Yuvika Sood, Himanshu Kapoor, Pankaj Chamoli, Harish Mudila, Anil Kumar. Hydrogel Nanocomposites for Waste Water Treatment. **Book Chapter**. *Springer Nature*. ***(*2024)** (Under Review)
2. Yuvika Sood, Kartika Singh, Harish Mudila, P.E. Lokhande, Lakhveer Singh, Deepak Kumar, Anil Kumar, Nabisab Mujawar Mubarak, Mohammad Hadi Dehghani. Insights into properties, synthesis and emerging applications of polypyrrole-based composites, and future prospective: A review. *Heliyon* 10 **(2024):** e33643. https://doi.org/10.1016/j.heliyon.2024.e33643.

3. Yuvika Sood, Harish Mudila, Pankaj Chamoli, Parveen Saini, Anil Kumar. Exploring the efficacy and future potential of polypyrrole/metal oxide nanocomposites for electromagnetic interference shielding: a review. *Material Horizon* 11**(2024):** 4256**.** 10.1039/D4MH00594E.

4. Yuvika Sood, P.E. Lokhande, Vishal Kadam, Chaitali Jagtap, Harish Mudila, Udayabhaskar Rednam, Deepak Kumar, Anil Kumar, Nanocomposites combining 2D WS_2 and 1D Polyaniline for enhanced high-performance Supercapacitors, *Journal of Alloys and Compounds* **(2024)**:176006. https://doi.org/10.1016/j.jallcom.2024.176006.

5. Raeesah Islam, Yuvika Sood, Harish Mudila, Anil Ohlan, Anil Kumar, Microwave absorbing properties of polypyrrole-based 2D nanocomposites, *Journal of Material Chemistry A* **(2024):** 31004. https://doi.org/10.1039/D4TA05676K

List of Conferences Attended

1. Presented Oral Talk presentation on Polypyrrole based Hybrid Nanocomposites for Gas Sensor in 4th International Conference on Soft Materials (ICSM 2021) held at MNIT Jaipur during December 13-18, 2021.
2. Presented Poster presentation on Influence of Polypyrrole Morphology on Gas Sensing Properties in 3rd International Conference on Recent Advances in Fundamental and Applied Sciences (RAFAS 2021) held at Lovely Professional University, Phagwara during June 25-26,2021.
3. Presented Poster presentation on Structural – Property correlation of Polypyrrole – Tungsten disulfide composites in 1st International Conference on "Innovations in Applied Science and Engineering" (ICIASE 2022) held at NIT Jalandhar during May 18-19, 2022.
4. Presented Flash talk and poster presentation on Polypyrrole- Tungsten disulfide Hybrid Nanocomposite Fabricated for Gas Sensing in 5th International Conference on Soft Materials (ICSM 2022) held at MNIT Jaipur during December 11-16, 2022.